UNCLASSIFIED

AD NUMBER

AD472608

NEW LIMITATION CHANGE

TO

Approved for public release, distribution
unlimited

FROM

Distribution authorized to U.S. Gov't.
agencies and their contractors;
Administrative/Operational Use; Sep 1965.
Other requests shall be referred to Air
Force Weapons Lab., Kirtland AFB, NM
87117.

AUTHORITY

Air Force Weapons Lab ltr dtd 1 Jun 1972

SECURITY

MARKING

The classified or limited status of this report applies
to each page, unless otherwise marked.
Separate page printouts MUST be marked accordingly.

DYNAMIC STRESSES IN A THICK ELASTIC CYLINDER SUBJECT TO TRANSIENT PRESSURE LOADINGS

Volume I: Theoretical Analysis and Discussion of Results

Hyman Garnet
Jacques Crouzet-Pascal
Gabriel Isakson
Allan Pifko

Grumman Aircraft Engineering Corporation
Bethpage, N. Y.
Contract AF29(601)-5993

TECHNICAL REPORT NO. AFWL-TR-65-20, Vol. I

September 1965

AIR FORCE WEAPONS LABORATORY
Research and Technology Division
Air Force Systems Command
Kirtland Air Force Base
New Mexico

DDC
OCT 28 1965
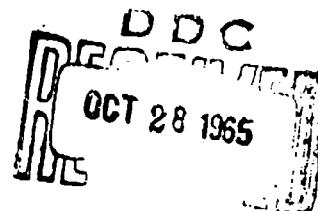
Research and Technology Division
AIR FORCE WEAPONS LABORATORY
Air Force Systems Command
Kirtland Air Force Base
New Mex co

DYNAMIC STRESSES IN A THICK ELASTIC CYLINDER
SUBJECT TO TRANSIENT PRESSURE LOADINGS

Volume I: Theoretical Analysis and Discussion of Results

Hyman Garnet
Jacques Crouzet-Pascal
Gabriel Isakson
Allan Pifko

Grumman Aircraft Engineering Corporation
Bethpage, N. Y.
Contract AF 29(601)-5993

TECHNICAL REPORT NO. AFWL-TR-65-20, Vol. I.

FOREWORD

The report is presented in two volumes. Volume I is concerned with the theoretical analysis and discussion of the solution. Volume II, subtitled "Computer Program," presents a listing and discusses the details of the computer program

This report has been reviewed and is approved.

DWAYNE D. PIEPENBURG
1Lt   USAF
Project Officer

ROBERT E. CRAWFORD
Major   USAF
Deputy Chief,
Civil Engineering Branch
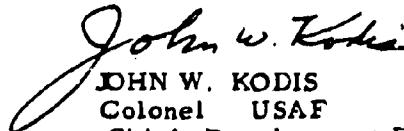
JOHN W. KODIS
Colonel   USAF
Chief, Development Division

ABSTRACT

The response of a hollow circular cylindrical shell of arbitrary thickness, in either an elastic or a viscoelastic medium, to transient dilatational and shear waves (and their s perposition) is presented. The solution is valid within the scope of the linear theory of elasticity or viscoelasticity. The technique for obtaining the solution relies upon 1) the construction of a train of incident pulses from steady-state components, where each pulse represents the time history of the transient stress in the incident wave, and 2) the existence of a physical mechanism that, between pulses, restores the disturbed particles of the cylinder and the surrounding medium to an unstrained state of rest.

The influence on the cylinder response of the following factors is discussed: liner thickness, cylinder-medium impedance mismatch, viscoelasticity in the medium, and incident wave form (step pulse, rectangular, triangular, linear rise-exponential decay).

CONTENTS

vii

LIST OF ILLUSTRATIONS

ix

LIST OF SYMBOLS

a	liner inner radius
A_p	complex constant of superposition in the series defining the incident waves, Eq. (3.1.6a) and (4.2.5)
A_{p1}, B_{p1}	constants of superposition associated with rigid body displacement in the series defining the dilatational and distortional solutions in the cylinder
A_{pn} A_{p0}	complex Fourier coefficient defined by Eqs. (3.1.15a, b) for incident dilatational wave and by Eqs. (4.2.16a) for incident shear wave
a_p	Fourier coefficients defining the incident wave form
b	liner outer radius
B_{pn} B_{p0}	complex Fourier coefficient defined by Eq. (3.1.15c) for incident dilatational wave and by Eq. (4.2.16b,c) for an incident shear wave
C_{p1}, D_{p1}	constants of superposition associated with rigid body displacement in the series defining the scattered dilatational and distortional solutions in the medium
C_{pn} C_{p0}	complex Fourier coefficient defined by Eq. (3.1.19a,b) for an incident dilatational wave and by Eq. (4.2.19a) for an incident shear wave
c_d, c_{dm}	speed of propagation of dilatational waves in the liner and medium respectively
c_t, c_{tm}	speed of propagation of shear waves in the liner and medium respectively
D_{pn} D_{p0}	complex Fourier coefficient defined by Eq. (3.1.19c) for an incident dilatational wave and by Eq. (4.2.19b,c) for an incident shear wave

e_{ij}	strain deviator
E, E_m	Young's modulus for the liner and medium respectively
h	liner thickness
$H_n^{(2)}$	Hankel function of the second kind of order n
J_n	Bessel functions of the first kind of order n
k_{p1}, k_{p2}, k_{p3}, k_{p4}	wave numbers for dilatational and shear waves in the liner and medium respectively
n, $\bar{n}$	integer, defining the Fourier expansion in the circumferential direction
p	summation integer in the representation of the incident wave form
P P'	viscoelastic linear operators defined in Eq. (3.4.4a)
P_1, ..., P_P P'_1, ..., P'_P	constant coefficients in the viscoelastic operators defined in Eqs. (3.4.5a,c)
q_1, q_2; q_3, q_4	nondimensional wave numbers for dilatational and shear waves in the liner and medium
$\bar{q}_3$, $\bar{q}_4$	real part of the nondimensional wave number for dilatational and shear wave respectively in a viscoelastic medium
$\tilde{q}_3$, $\tilde{q}_4$	imaginary part of the nondimensional wave number for dilatational and shear wave respectively in a viscoelastic medium
Q, Q'	linear operators defined in Eq. (3.4.4b)

$Q_1, \ldots, Q_Q$ $\Big\}$ $q_1', \ldots, q_Q'$ $\Big\}$	constant coefficients in the viscoelastic operators defined in Eq. (3.4.5b, d)
r	radial coordinate
R	mean radius of the liner
s_{ij}	stress deviator
t	time coordinate
t_0	rest time parameter, shown in Fig. 2a
$\bar{t}$	time coordinate with respect to the arrival of the incident wave ($\bar{t} = t - t_0$)
$t^*, \tilde{t}^*$	time at which rigid body displacements are removed for dilatational and shear wave respectively
T	half-period of the incident wave
u_r, u_θ	radial and circumferential displacement in the liner
u_x	displacement due to the incident dilatational wave
$\tilde{u}_r, \tilde{u}_\theta$	nondimensional radial and circumferential displacements $\left(\dfrac{2\mu u_x}{\sigma_0 b}, \dfrac{2\mu u_\theta}{\sigma_0 b}\text{ respectively}\right)$
x	reference coordinate for incident dilatational wave
$\bar{x}$	reference coordinate for incident shear wave
Y_n	Bessel function of the second kind
Y_s	deviatoric complex modulus

Y_ν	dilatational complex modulus
$\left.\begin{array}{l} Y_{\nu p}^{(1)} \\ Y_{sp}^{(1)} \end{array}\right\}$	real part of Y_ν and Y_s
$\left.\begin{array}{l} Y_{\nu p}^{(2)} \\ Y_{sp}^{(2)} \end{array}\right\}$	imaginary part of Y_ν and Y_s
$C_{ij,pn}$	matrix defined in Eq. (3.8.2)
$Z_{j,pn}$	column vector defined in Eq. (3.8.2)
$D_{i,pn}$	column vector defined in Eq. (3.8.2)
$\mathcal{C}_{ij,pn}$	matrix defined in Eq. (4.5.2)
$\zeta_{j,pn}$	column vector defined in Eq. (4.5.2)
$\mathcal{D}_{i,pn}$	column vector defined in Eq. (4.5.2)
$Z_{1,pn}, \ldots, Z_{6,pn}$	unknown constants of superposition in the series representation of the solutions in the cylinder and medium
β	ratio of inner to outer radius of the liner, $\beta = \dfrac{a}{b}$
γ	mass density of the liner
γ_m	mass density of the medium
Δ	duration of rectangular pulse
ϵ	parameter arising from the transformation of the incident wave form into polar coordinates and defined in Eqs. (3.1.12c) and (3.4.18)

$\bar{\epsilon}$, $\tilde{\epsilon}$	real and imaginary part of ϵ in a viscoelastic medium
ϵ_{xx}, ϵ_{yy}, ϵ_{zz} ϵ_{rr}, $\epsilon_{\theta\theta}$, $\epsilon_{r\theta}$	components of strain in Cartesian and polar coordinates respectively
θ	circumferential coordinate for dilatational wave
$\bar{\theta}$	circumferential coordinate for shear wave
λ, λ_m	Lamé constant for liner and medium respectively
$\bar{\lambda}$, $\tilde{\lambda}$	real and imaginary part of the complex Lamé modulus for a viscoelastic medium
μ, μ_m	shear modulus for liner and medium respectively
$\bar{\mu}$, $\tilde{\mu}$	real and imaginary part of the complex shear modulus, for viscoelastic medium
ν, ν_m	Poisson's ratio in the liner and medium respectively
ρ	nondimensional radial coordinate r/b
σ_0	amplitude of incident dilatational wave
σ_{xx}	direct stress in incident dilatational wave
σ_{rr}, $\sigma_{\theta\theta}$, $\sigma_{r\theta}$	polar coordinate components of the stress tensor associated with a dilatational incident wave
τ_{xy}	shear stress in incident distortional wave
τ_{rr}, $\tau_{\theta\theta}$, $\tau_{r\theta}$	polar coordinate components of the stress tensor associated with a distortional incident wave
τ_0	amplitude of incident shear wave

$1/\tau_1$	strain recovery time in uniaxial strain case
$1/\tau_2$	recovery time for shear strain
Φ, Φ_c, Φ_m	dilatational displacement potential functions
Ψ, Ψ_c, Ψ_{pn}	distortional displacement potential functions
ω_p	frequency parameter
$1/\Omega_1$	relaxation time for normal stress in uniaxial strain case
$1/\Omega_2$	relaxation time for shear stress
$(\ )^d$	superscript, denoting dilatational solutions in liner
$(\ )^B$	superscript, describing quantities at the liner medium interface
$(\ )^s$	superscript, denoting distortional solutions in the liner
$(\ )^{dm}$	superscript, denoting dilatational solutions in the medium
$(\ )^{sm}$	superscript, denoting distortional solutions in the medium

SECTION I

INTRODUCTION

Statement of the Problem and General Discussion

The study reported herein is concerned with the dynamic response of deep-buried protective installations subjected to stress waves resulting from nuclear explosions. As pointed out elsewhere, for example in Ref. 1, the actual problem is exceedingly complex. However, certain justifiable idealizations can be made, that lead to tractable formulations of the subject problem, the solution of which yields information on the principal effects in the actual problem. For example, the structure considered is a long thick isotropic elastic cylinder. The surrounding medium is regarded in two distinct phases of the study as either elastic or viscoelastic. It is assumed that the pressure front generated by the nuclear burst travels on the surface with superseismic velocity and thus can be considered to transmit plane seismic waves into the ground (Ref. 1). Because of the depth at which the structure is buried, the influence of Rayleigh waves is neglected. For the same reason, it is assumed that no appreciable influence is exerted on the peak response by reflections from the surface. Gravity stresses in the cylinder are not considered.

In view of the foregoing considerations, the idealized problem, which is the subject of the analytical and computational investigation described in this report, is that of determining the stresses and displacements in an infinitely long hollow cylinder of arbitrary thickness embedded in an infinite medium. The cylinder is enveloped by plane stress waves progressing in a direction perpendicular to its axis (see Fig. 1). The problem is thus one of plane strain. The cylinder is elastic, homogeneous, and isotropic. The surrounding medium is homogeneous and isotropic, and in two separate and distinct phases of the analysis is considered to be either elastic or viscoelastic. The plane waves impinging on the cylinder are, in succession, dilatational and distortional (Fig. 1). An analysis is developed to account for an arbitrary pressure-time history of the incoming waves.

Computations have been carried out for the following wave forms: 1) a step pulse; 2) a rectangular wave; 3) a triangular wave; and 4) a linear rise-exponential decay wave form.

1

SECTION II

DISCUSSION OF ANALYSIS

Two limiting cases of the present problem have been studied by a number of investigators. The diffraction of a stress wave by a cylindrical cavity in an infinite medium is examined in Refs. 2, 3, 4, and 5. Using thin shell theory to describe the behavior of the liner, Ref. 6 treats the problem of the diffraction of a stress wave by a thin cylindrical liner in an elastic medium.

In the foregoing references, transform or related integral techniques are employed to obtain solutions. Such techniques, however, if applied to the present problem, where the cylinder must be analyzed within the scope of the theory of elasticity (since it is considered to be of arbitrary thickness), would lead to formidable difficulties in the inversion process.

The method utilized in the current analysis circumvents these difficulties. It consists of devising a solution to the transient problem from a superposition of appropriate steady-state solutions to the wave equation. Its success stems from: 1) the capability of constructing a train of pulses from steady-state sinusoidal components (Fig. 2a) where each pulse represents with sufficient accuracy the time history of the transient stress in the incident wave; 2) the existence of a mechanism which, between pulses, restores the disturbed particles of the cylinder and the surrounding medium to an unstrained state of rest. Physically, in the present problem, this mechanism is provided by the continuous radiation of energy from the excited cylinder through the surrounding medium outward to infinity. Mathematically, it is implied by solutions of the field equations that enforce continuity of stresses and displacements between the cylinder and the embedding medium, and which at infinity represent outgoing, decaying waves. Thus, if time is measured from the moment of arrival of a pulse at the cylinder, the response will be identical to that excited by a transient loading having the time history of a single pulse. The validity of this technique is amply demonstrated in the present report.

The use of steady-state solutions to obtain a transient response has also been suggested by Ref. 8 for systems in which damping provides the mechanism for bringing the system to rest.

As will be seen, the present approach offers greater opportunity
to gain physical insight into the problem than do previous ap-
proaches. An additional point of departure in the present
approach concerns the number of circumferential modes chosen to
describe the deformation. All the afore-mentioned approaches
constrain the deformation by selecting in advance a fixed number
of modes to apply to all material points and at all times of the
response. In the present analysis, the accuracy with which the
solution is required to converge determines the number of modes
selected. This number is permitted to vary with both the
material point being considered and the time at which its re-
sponse is calculated. Thus, within the limitations of a Fourier
series representation at the initial discontinuity, the present
method should, in general, be more accurate. This will be shown
to be especially the case during the early part of the response.

The dynamic response of the cylinder is determined by ob-
taining separately and subsequently combining several distinct
component parts, each of which is a solution of the wave equation
in either the cylinder or the surrounding infinite medium. These
are the stresses and displacements associated with: 1) the inci-
dent wave; 2) the transmitted and reflected waves in the cylinder;
and 3) the scattered waves in the surrounding medium. The fore-
going components must be combined so that the inner surface of
the cylinder is traction free, and at the outer surface the normal
stresses in the radial direction, the shear stresses in the cir-
cumferential direction, and the displacements in the cylinder are
continuous with the corresponding quantities in the medium.

3

SECTION III

SOLUTION FOR AN INCIDENT DILATATIONAL PLANE WAVE

1. Stresses and Displacements Applied to the Cylinder by an Incident Dilatational Plane Wave in an Elastic Medium

The Cartesian coordinate system in which the incident plane dilatational wave is described is illustrated in Fig. 3a. The disturbance is assumed to be traveling in the negative x-direction. The equation governing the propagation of the wave (which depends only on the space coordinate x and time coordinate t) is given by Ref. 9 as

$$\frac{\partial^2 \Phi}{\partial x^2} - \frac{1}{c_{dm}^2} \frac{\partial^2 \Phi}{\partial t^2} = 0 , \tag{3.1.1}$$

where Φ is a displacement potential defined as follows:

$$u_x = \frac{\partial \Phi}{\partial x} , \quad u_y = 0 \tag{3.1.2}$$

$$u_z = 0 ,$$

and the pertinent stresses are given by

$$\sigma_{xx} = (\lambda_m + 2\mu_m) \frac{\partial^2 \Phi}{\partial x^2} , \tag{3.1.3}$$

$$\sigma_{yy} = \lambda_m \frac{\partial^2 \Phi}{\partial x^2} . \tag{3.1.4}$$

The quantities u_x, u_y, u_z, σ_{xx}, and σ_{yy} are ⋯ ments and stresses in Cartesian coordinates, λ_m an⋯ ne Lamé constants of the medium, c_{dm} is the spe⋯ ⋯ation of dilatational waves in the elastic medium an⋯ ⋯ y

4

$$c_{dm} = \sqrt{\frac{\lambda_m + 2\mu_m}{\gamma_m}} \,, \qquad\qquad (3.1.5)$$

and γ_m is the mass density.

A steady state solution of (3.1.1) is

$$\Phi = \sum_{p=1}^{\infty} A_p \, e^{i[k_{p3}(x-b) + \omega_p t]} \qquad\qquad (3.1.6a)$$

where the frequency ω_p is given by

$$\omega_p = \frac{p\pi}{T} \qquad\qquad (3.1.6b)$$

and

$$k_{p3} = \frac{\omega_p}{c_{dm}} \,. \qquad\qquad (3.1.6c)$$

Also, T is an arbitrary time interval and the A_p are complex constants of superposition that will be expressed in terms of the Fourier coefficients defining the incoming wave form.

For our purpose, we represent the incident stress wave σ_{xx}, (see Fig. 2) in the form

$$\sigma_{xx} = \sum_{p=1}^{\infty} a_p \, \sin \omega_p \left[\left(\frac{x-b}{c_{dm}} \right) + t \right] ; \qquad\qquad (3.1.7a)$$

or at $x = b$ as

$$\sigma_{xx} = \sum_{p=1}^{\infty} a_p \, \sin \omega_p t \,, \qquad\qquad (3.1.7b)$$

where the a_p are the coefficients defining the wave form over the arbitrary half period T.

5

$$a_p = \frac{2}{T} \int_0^T \sigma_{xx} \sin \omega_p t \, dt \qquad (3.1.7c)$$

An expression for σ_{xx} identical with (3.1.7a) is the real part of

$$\sigma_{xx} = \sum_{p=1}^{\infty} (-ia_p) \, e^{i[k_{p3}(x-b) + \omega_p t]} . \qquad (3.1.8)$$

From (3.1.3) and (3.1.6a),

$$\sigma_{xx} = -\sum_{p=1}^{\infty} (\lambda_m + 2\mu_m) k_{p3}^2 A_p \, e^{i[k_{p3}(x-b) + \omega_p t]} . \qquad (3.1.9)$$

Comparing (3.1.8) and (3.1.9), we obtain

$$A_p = \frac{ia_p}{(\lambda_m + 2\mu_m) k_{p3}^2} . \qquad (3.1.10)$$

Now, from (3.1.2), (3.1.6a), and (3.1.10) we can write

$$u_x = \sum_{p=1}^{\infty} \frac{-a_p}{(\lambda_m + 2\mu_m) k_{p3}} \, e^{i[k_{p3}(x-b) + \omega_p t]} , \qquad (3.1.11a)$$

or, noting (3.1.5) and (3.1.6c),

$$u_x = \sum_{p=1}^{\infty} \frac{-a_p}{\gamma_m c_{dm} \omega_p} \, e^{i[k_{p3}(x-b) + \omega_p t]} . \qquad (3.1.11b)$$

6

Since the cylinder boundaries are naturally defined by polar coordinates it will be more convenient to write the stresses and displacements associated with the incident wave in polar coordinates. Then

$$\sigma_{rr}^{B} = \sigma_{xx}(\cos^2\theta + \epsilon \sin^2\theta) \, , \tag{3.1.12a}$$

$$\sigma_{r\theta}^{B} = - \sigma_{xx}\left(\frac{1 - \epsilon}{2}\right) \sin 2\theta \, , \tag{3.1.12b}$$

where

$$\epsilon = \frac{\lambda_m}{\lambda_m + 2\mu_m} \, . \tag{3.1.12c}$$

Substituting (3.1.8) into (3.1.12) and setting $x = b \cos\theta$, we obtain the following expressions for the stresses applied to the boundary by the incident wave:

$$\sigma_{rr}^{B} = \sum_{p=1}^{\infty} \sigma_{r,p} \, e^{i\omega_p t} \, , \tag{3.1.13a}$$

$$\sigma_{r\theta}^{B} = - \sum_{p=1}^{\infty} \sigma_{r\theta,p} \, e^{i\omega_p t} \, , \tag{3.1.13b}$$

where

$$\sigma_{r,p} = (-ia_p)(\cos^2\theta + \epsilon \sin^2\theta) \, e^{iq_3(\cos\theta-1)} \, , \tag{3.1.13c}$$

$$\sigma_{r\theta,p} = (-ia_p)\left(\frac{1 - \epsilon}{2}\right) \sin 2\theta \, e^{iq_3(\cos\theta-1)} \, , \tag{3.1.13d}$$

7

with

$$q_3 = bk_{p3} = p\pi\left(\frac{p}{c_{dm}T}\right) .$$

(3.1.13e)

In anticipation of matching, later in the analysis, the tractions applied by the incident train of pulses with the cylinder stresses and stresses associated with scattered waves in the medium, we represent the stresses given by (3.1.13), and acting at the cylinder boundary, as the real part of

$$\sigma_{rr}^B = \sum_{p=1}^{\infty} \sum_{n=0}^{\infty} a_p A_{pn} \cos n\theta \, e^{i\omega_p t} ,$$

(3.1.14a)

$$\sigma_{r\theta}^B = \sum_{p=1}^{\infty} \sum_{n=1}^{\infty} a_p B_{pn} \sin n\theta \, e^{i\omega_p t} ,$$

(3.1.14b)

where the complex Fourier coefficients A_{pn} and B_{pn} are obtained by comparing (3.1.14) with (3.1.13). They are

$$A_{pn} = -\frac{2i}{\pi} \int_0^{\pi} (\cos^2\theta + \epsilon \sin^2\theta) \, e^{iq_3(\cos\theta-1)} \cos n\theta \, d\theta ,$$

(3.1.15a)

$$n \geq 1$$

$$A_{p0} = -\frac{i}{\pi} \int_0^{\pi} (\cos^2\theta + \epsilon \sin^2\theta) \, e^{iq_3(\cos\theta-1)} \, d\theta ,$$

(3.1.15b)

$$B_{pn} = \frac{i(1-\epsilon)}{\pi} \int_0^{\pi} e^{iq_3(\cos\theta-1)} \sin 2\theta \sin n\theta \, d\theta .$$

(3.1.15c)

8

These expressions, (3.1.15), are representable in terms of Bessel functions of a complex argument of the first kind and integral order n — as shown in Appendix B.

Conditions of continuity between the cylinder and surrounding medium require that we match displacements as well as appropriate stress components. The radial and tangential displacements in polar coordinates are related to the Cartesian coordinate displacement u_x as follows:

$$u_r = u_x \cos \theta \quad , \quad u_\theta = - u_x \sin \theta . \tag{3.1.16}$$

Substituting (3.1.11b) into (3.1.16) and setting $x = b \cos \theta$ leads to

$$u_r = \sum_{p=1}^{\infty} u_{r,p} \, e^{i\omega_p t} , \tag{3.1.17a}$$

$$u_\theta = \sum_{p=1}^{\infty} u_{\theta,p} \, e^{i\omega_p t} , \tag{3.1.17b}$$

where

$$u_{r,p} = - \frac{a_p \cos \theta \, e^{iq_3(\cos \theta - 1)}}{\gamma_m c_{dm} \omega_p} , \tag{3.1.17c}$$

$$u_{\theta,p} = \frac{a_p \sin \theta \, e^{iq_3(\cos \theta - 1)}}{\gamma_m c_{dm} \omega_p} , \tag{3.1.17d}$$

or alternatively,

$$u_{r,p} = - \frac{a_p k_{p3} \cos \theta \, e^{iq_3(\cos \theta - 1)}}{\gamma_m \omega_p^2} , \tag{3.1.17e}$$

9

$$u_{\theta,p} = \frac{a_p k_{p3} \sin \theta \; e^{iq_3(\cos \theta - 1)}}{\gamma_m \omega_p^2} . \tag{3.1.17f}$$

As with the stresses, we expand the displacements at the
boundary in the form

$$u_r^B = -\sum_{p=1}^{\infty} \sum_{n=0}^{\infty} \frac{a_p C_{pn}}{\gamma_m c_{dm} \omega_p} \cos n\theta \; e^{i\omega_p t} , \tag{3.1.18a}$$

$$u_\theta^B = \sum_{p=1}^{\infty} \sum_{n=1}^{\omega} \frac{a_p D_{pn}}{\gamma_m c_{dm} \omega_p} \sin n\theta \; e^{i\omega_p t} , \tag{3.1.18b}$$

where the complex Fourier coefficients C_{pn} and D_{pn} are
obtained by comparing (3.1.18) with (3.1.17). Thus,

$$C_{pn} = \frac{2}{\pi} \int_0^{\pi} e^{iq_3(\cos \theta - 1)} \cos \theta \cos n\theta \; d\theta , \tag{3.1.19a}$$
$$n \geq 1$$

$$C_{p0} = \frac{1}{\pi} \int_0^{\pi} e^{iq_3(\cos \theta - 1)} \cos \theta \; d\theta , \tag{3.1.19b}$$

$$D_{pn} = \frac{2}{\pi} \int_0^{\pi} e^{iq_3(\cos \theta - 1)} \sin \theta \sin n\theta \; d\theta . \tag{3.1.19c}$$

As in (3.1.15), the complex Fourier coefficients defined
by (3.1.19) are shown in Appendix B to be representable in terms
of Bessel functions of a complex argument.

10

2. General Solution of the Wave Equation in the Cylinder

The stresses and displacements generated in the elastic cylinder are presented in this section. The solution is constructed from dilatational and distortional displacement potential functions. Such solutions are discussed in Refs. 9 and 10 for example. The polar coordinate notation of Fig. 3 is used.

The nonvanishing strains are given in terms of the displacements (Ref. 9) as

$$\epsilon_{rr} = \frac{\partial u_r}{\partial r} \quad , \quad \epsilon_{\theta\theta} = \frac{1}{r}\frac{\partial u_\theta}{\partial \theta} + \frac{u_r}{r} \quad ,$$

(3.2.1)

$$\epsilon_{r\theta} = \frac{\partial u_\theta}{\partial r} - \frac{u_\theta}{r} + \frac{1}{r}\frac{\partial u_r}{\partial \theta} \quad .$$

The stress strain relations are

$$\sigma_{rr} = \lambda(\epsilon_{rr} + \epsilon_{\theta\theta}) + 2\mu\epsilon_{rr} \quad ,$$

$$\sigma_{\theta\theta} = \lambda(\epsilon_{rr} + \epsilon_{\theta\theta}) + 2\mu\epsilon_{\theta\theta} \quad ,$$

(3.2.2)

$$\sigma_{r\theta} = \mu\epsilon_{r\theta} \quad ,$$

where λ and μ are the Lamé constant and shear modulus, respectively, of the cylinder. The equations of equilibrium are

$$\gamma\frac{\partial^2 u_r}{\partial t^2} = \frac{\partial \sigma_{rr}}{\partial r} + \frac{1}{r}\frac{\partial \sigma_{r\theta}}{\partial \theta} + \frac{1}{r}(\sigma_{rr} - \sigma_{\theta\theta}) \quad ,$$

(3.2.3)

$$\gamma\frac{\partial^2 u_\theta}{\partial t^2} = \frac{\partial \sigma_{r\theta}}{\partial r} + \frac{1}{r}\frac{\partial \sigma_{\theta\theta}}{\partial \theta} + \frac{2}{r}\sigma_{r\theta} \quad .$$

11

Displacements u_r and u_θ, which satisfy (3.2.1) through (3.2.3) identically, and are associated with dilatational waves, are given by

$$u_r^d = \frac{\partial \Phi_c}{\partial r} \quad , \quad u_\theta^d = \frac{1}{r}\frac{\partial \Phi_c}{\partial \theta} \quad , \tag{3.2.4}$$

in which Φ_c, the displacement potential, is governed by the wave equation

$$\nabla^2 \Phi_c - \frac{1}{c_d^2}\frac{\partial^2 \Phi_c}{\partial t^2} = 0 \quad , \tag{3.2.5a}$$

where

$$\nabla^2 = \frac{\partial^2}{\partial r^2} + \frac{1}{r}\frac{\partial}{\partial r} + \frac{1}{r^2}\frac{\partial^2}{\partial \theta^2} \quad , \tag{3.2.5b}$$

and c_d, the speed of propagation of dilatational waves in the cylinder, is given by

$$c_d = \sqrt{\frac{\lambda + 2\mu}{\gamma}} \quad , \tag{3.2.5c}$$

where γ is the mass density of the cylinder.

When Eqs. (3.2.4) are introduced into the strain displacement relations (3.2.1), and these in turn into the stress strain relations (3.2.2), we obtain the stresses associated with dilatational waves, in terms of the displacement potential Φ, as follows

$$\sigma_{rr}^d = \lambda \nabla^2 \Phi_c + 2\mu \frac{\partial^2 \Phi_c}{\partial r^2} \quad ; \quad \sigma_{\theta\theta}^d = \lambda \nabla^2 \Phi_c + 2\mu \left(\frac{1}{r^2}\frac{\partial^2 \Phi_c}{\partial \theta^2} + \frac{1}{r}\frac{\partial \Phi_c}{\partial r}\right)$$

$$\tag{3.2.6}$$

$$\sigma_{r\theta}^d = 2\mu \frac{1}{r}\frac{\partial}{\partial \theta}\left(\frac{\partial \Phi_c}{\partial r} - \frac{\Phi_c}{r}\right) \quad .$$

12

A solution of (3.2.5a) may be written as

$$\Phi_c = \sum_{p=1}^{\infty} \left\{ \sum_{n=0}^{\infty} \left[Z_{1,pn} J_n(k_{p1}r) + Z_{2,pn} Y_n(k_{p1}r) \right] \cos n\theta \right\} e^{i\omega_p t}$$

(3.2.7)

$$+ \sum_{p=1}^{\infty} A_{p1} r \cos \theta \; ,$$

where: 1) $k_{p1} = \omega_p/c_d$; 2) the series $\displaystyle\sum_{p=1}^{\infty} A_{p1} r \cos \theta$ consists of a superposition of solutions to (3.2.5) that correspond to rigid body displacement; 3) the $J_n(z)$ and $Y_n(z)$ are Bessel functions of the first and second kind, respectively, of integral order n; and 4) the $Z_{1,pn}$ and $Z_{2,pn}$ are complex constants of super-position to be determined from the boundary conditions.

A bar is placed over the integer n in certain subsequent terms for the following reason: In the analysis to follow, the potential functions will be differentiated with respect to the circumferential coordinate, θ, and also the radial coordinate, r. Differentiation with respect to θ introduces the integer n as a factor directly into the expressions for the stresses. Dif-ferentiation with respect to r, and subsequent use of the Bessel function recursion relations, also introduces the integer n into the stress and displacement expressions. It will be convenient to identify the origin of the integer n because the solutions for the cylinder and for the scattered response in the medium, appropriate for incoming shear waves, can be obtained from the corresponding solutions for incoming dilatational waves by: 1) interchanging $\sin n\theta$ and $\cos n\theta$; and 2) setting $\bar{n} = -n$. In the case of the dilatational wave, we simply set $\bar{n} = n$.

It will be noted that Φ_c is constructed by a superposition of steady state solutions of the form

$$\varphi_p = \sum_{n=0}^{\infty} \left[Z_{1,pn} J_n(k_{p1}r) + Z_{2,pn} Y_n(k_{p1}r) \right] \cos n\theta \; e^{i\omega_p t} \; , \qquad (3.2.8)$$

13

and a solution describing rigid body displacements. Such solutions have been used to solve the steady state problems reported in Refs. 11 and 12. The use of steady state solutions to construct the solution to a transient problem has already been discussed.

It is shown in Ref. 13 that the derivatives of the Bessel functions may be expressed as

$$J_n'(z) = \frac{n}{z} J_n(z) - J_{n+1}(z) , \qquad (3.2.9a)$$

$$J_n''(z) = \left[\frac{n(n-1)}{z^2} - 1\right] J_n(z) + \frac{1}{z} J_{n+1}(z) , \qquad (3.2.9b)$$

and similar relations for the derivatives of $Y_n(z)$.

As mentioned in the text preceding Eq. (3.2.8), and as can be seen in Eqs. (3.2.9), the recursion relations for the derivatives of the Bessel functions introduce the integer n into the stress and displacement expressions. Introducing Eq. (3.2.7) into Eqs. (3.2.4) and (3.2.6), making use of relations (3.2.9a and b), and defining a nondimensional radial coordinate as

$$\rho = \frac{r}{b} , \qquad (3.2.9c)$$

and a nondimensional wave number as

$$q_1 = bk_{p1} , \qquad (3.2.9d)$$

we can write the expressions for the displacements and stresses as

$$u_r^d = \frac{1}{b} \sum_{p=1}^{\infty} \sum_{n=0}^{\infty} q_1\left\{Z_{1,pn}\left(\frac{n}{q_1\rho} J_n(q_1\rho) - J_{n+1}(q_1\rho)\right)\right.$$

$$\left. + Z_{2,pn}\left(\frac{n}{q_1\rho} Y_n(q_1\rho) - Y_{n+1}(q_1\rho)\right)\right\}\cos n\theta \ e^{i\omega_p t} \qquad (3.2.10a)$$

$$+ \sum_{p=1}^{\infty} A_{p1}\cos \theta ,$$

14

$$u_\theta^d = -\frac{1}{b} \sum_{p=i}^{\infty} \sum_{n=i}^{\infty} \frac{\bar{n}}{\rho} \left\{ z_{1,pn} J_n(q_1\rho) + z_{2,pn} Y_n(q_1\rho) \right\} \sin n\theta \ e^{i\omega_p t}$$

(3.2.10b)

$$- \sum_{p=1}^{\infty} A_{p1} \sin \theta \ ,$$

$$\sigma_{rr}^d = -\frac{1}{b^2} \sum_{p=1}^{\infty} \sum_{n=0}^{\infty} q_1^2 \left\{ z_{1,pn} \left[\left\{ \lambda - 2\mu \left(\frac{n(n-1)}{(q_1\rho)^2} - 1 \right) \right\} J_n(q_1\rho) \right. \right.$$

$$\left. - \frac{2\mu}{q_1\rho} J_{n+1}(q_1\rho) \right]$$

(3.2.10c)

$$+ z_{2,pn} \left[\left\{ \lambda - 2\mu \left(\frac{n(n-1)}{(q_1\rho)^2} - 1 \right) \right\} Y_n(q_1\rho) \right.$$

$$\left. \left. - \frac{2\mu}{q_1\rho} Y_{n+1}(q_1\rho) \right] \right\} \cos n\theta \ e^{i\omega_p t} \ ,$$

$$\sigma_{\theta\theta}^d = -\frac{1}{b^2} \sum_{p=1}^{\infty} \sum_{n=0}^{\infty} \left\{ z_{1,pn} \left[\left\{ \lambda q_1^2 + \frac{2\mu n(n-1)}{\rho^2} \right\} J_n(q_1\rho) \right. \right.$$

$$\left. + 2\mu \frac{q_1}{\rho} J_{n+1}(q_1\rho) \right]$$

(3.2.10d)

$$+ z_{2,pn} \left[\left\{ \lambda q_1^2 + \frac{2\mu n(n-1)}{\rho^2} \right\} Y_n(q_1\rho) \right.$$

$$\left. \left. + 2\mu \frac{q_1}{\rho} Y_{n+1}(q_1\rho) \right] \right\} \cos n\theta \ e^{i\omega_p t} \ ,$$

15

$$
\sigma_{r\theta}^{d} = \frac{2\mu}{b^2} \sum_{p=1}^{\infty} \sum_{n=1}^{\infty} \frac{\bar{n}}{\rho^2} \Big\{ z_{1,pn} \Big[q_1\rho J_{n+1}(q_1\rho) - (n-1)J_n(q_1\rho) \Big]
$$

$$\text{(3.2.10e)}$$

$$
+ z_{2,pn} \Big[q_1\rho Y_{n+1}(q_1\rho) - (n-1)Y_n(q_1\rho) \Big] \Big\} \sin n\theta \, e^{i\omega_p t} ,
$$

where the superscript d has been used to designate the contribution from the dilatational solution. The contribution from the distortional, or shear wave solution, will now be discussed.

A representation of the displacements u_r and u_θ associated with shear waves is

$$
u_r^s = \frac{1}{r} \frac{\partial \Psi_c}{\partial \theta} \quad , \quad u_\theta^s = - \frac{\partial \Psi_c}{\partial r} ,
$$

$$\text{(3.2.11)}$$

in which the displacement potential, Ψ_c, is governed by the wave equation

$$
\nabla^2 \Psi_c - \frac{1}{c_t^2} \frac{\partial^2 \Psi_c}{\partial t^2} = 0 ,
$$

$$\text{(3.2.12a)}$$

where c_t, the speed of propagation of shear waves in the cylinder, is given by

$$
c_t = \sqrt{\frac{\mu}{\gamma}} .
$$

$$\text{(3.2.12b)}$$

When Eqs. (3.2.11) are introduced into the strain displacement relations (3.2.1) and these in turn into the stress strain relations (3.2.2), we obtain the stresses associated with shear waves in terms of the displacement potential Ψ_c:

$$
\sigma_{rr}^s = 2\mu \frac{\partial}{\partial r}\Big[\frac{1}{r} \frac{\partial \Psi_c}{\partial \theta} \Big] \quad , \quad \sigma_{\theta\theta}^s = - \sigma_{rr}^s ,
$$

$$\text{(3.2.13)}$$

$$
\sigma_{r\theta}^s = \mu \Big[- r \frac{\partial}{\partial r}\Big[\frac{1}{r} \frac{\partial \Psi_c}{\partial r} \Big] + \frac{1}{r^2} \frac{\partial^2 \Psi_c}{\partial \theta^2} \Big] .
$$

16

A solution of (3.2.12a) may be written as

$$\Psi_c = \sum_{p=1}^{\infty} \left\{ \sum_{n=1}^{\infty} \left[Z_{3,pn} J_n(k_{p2}r) + Z_{4,pn} Y_n(k_{p2}r) \right] \sin n\theta \right\} e^{i\omega_p t}$$

(3.2.14)

$$+ \sum_{p=1}^{\infty} B_{p1} r \sin \theta ,$$

where: 1) $k_{p2} = \omega_p / c_t$; 2) the series $\sum_{p=1}^{\infty} B_{p1} r \sin \theta$ consists of a superposition of solutions to (3.2.12) that corresponds to rigid body displacements; and 3) the $Z_{3,pn}$ and $Z_{4,pn}$ are complex constants to be determined from the boundary conditions.

As in the dilatational solution, Ψ_c is constructed from a superposition of steady-state solutions of the form

$$\psi_p = \sum_{n=1}^{\infty} \left[Z_{3,pn} J_n(k_{p2}r) + Z_{4,pn} Y_n(k_{p2}r) \right] \sin n\theta \, e^{i\omega_p t} ,$$

(3.2.15)

and a solution corresponding to rigid body displacements.

When Eq. (3.2.14) is substituted into Eqs. (3.2.11) and (3.2.13), and the relations in (3.2.9a and b) and the quantity defined in (3.2.9c) are introduced along with

$$q_2 = b k_{p2} ,$$

(3.2.16)

we have finally the following expressions for the displacements and stresses associated with the shear wave solution:

17

$$u_r^s = \frac{1}{b} \sum_{p=1}^{\infty} \sum_{n=0}^{\infty} \frac{\bar{n}}{\rho} \left\{ Z_{3,pn} J_n(q_2\rho) + Z_{4,pn} Y_n(q_2\rho) \right\} \cos n\theta \ e^{i\omega_p t}$$

$$(3.2.17a)$$

$$+ \sum_{p=1}^{\infty} B_{p1} \cos \theta \ ,$$

$$u_\theta^s = -\frac{1}{b} \sum_{p=1}^{\infty} \sum_{n=1}^{\infty} q_2 \left\{ Z_{3,pn} \left[\frac{n}{q_2\rho} J_n(q_2\rho) - J_{n+1}(q_2\rho) \right] \right.$$

$$\left. + Z_{4,pn} \left[\frac{n}{q_2\rho} Y_n(q_2\rho) - Y_{n+1}(q_2\rho) \right] \right\} \sin n\theta \ e^{i\omega_p t} \qquad (3.2.17b)$$

$$- \sum_{p=1}^{\infty} B_{p1} \sin \theta \ ,$$

$$\sigma_{rr}^s = \frac{2\mu}{b^2} \sum_{p=1}^{\infty} \sum_{n=0}^{\infty} \frac{\bar{n}}{\rho^2} \left\{ Z_{3,pn} \left[(n-1) J_n(q_2\rho) - q_2\rho J_{n+1}(q_2\rho) \right] \right.$$

$$(3.2.17c)$$

$$\left. + Z_{4,pn} \left[(n-1) Y_n(q_2\rho) - q_2\rho Y_{n+1}(q_2\rho) \right] \right\} \cos n\theta \ e^{i\omega_p t}$$

$$\sigma_{\theta\theta}^s = - \sigma_{rr}^s \ , \qquad\qquad (3.2.17d)$$

18

$$\sigma_{r\theta}^s = -\frac{\mu}{b^2} \sum_{p=1}^{\infty} \sum_{n=1}^{\infty} q_2^2 \Bigg\{ Z_{3,pn} \Bigg[\left(\frac{2n(n-1)}{(q_2\rho)^2} - 1 \right) J_n(q_2\rho) $$

$$+ \frac{2}{q_2\rho} J_{n+1}(q_2\rho) \Bigg]$$

$$+ Z_{4,pn} \Bigg[\left(\frac{2n(n-1)}{(q_2\rho)^2} - 1 \right) Y_n(q_2\rho)$$

$$+ \frac{2}{q_2\rho} Y_{n+1}(q_2\rho) \Bigg] \Bigg\} \sin n\theta \; e^{i\omega_p t} \; .$$

(3.2.17e)

3. Solution of the Wave Equation for Scattered Waves in the Surrounding Medium

As in the cylinder, the solution in the surrounding infinite medium may be constructed from two displacement potentials, one dilatational, the other distortional. However, in addition it is required that at infinity these solutions represent outgoing, decaying waves.

After c_d is replaced by c_{dm} (the dilatational wave velocity in the medium), the dilatational potential, namely a solution of (3.2.5a) that meets the requirements at infinity, may be taken as

$$\Phi_m = \sum_{p=1}^{\infty} \sum_{n=0}^{\infty} Z_{5,pn} H_n^{(2)}(k_{p3}r) \cos n\theta \; e^{i\omega_p t} + \sum_{p=1}^{\infty} C_{p1} r \cos \theta \; , \quad (3.3.1)$$

where 1) $k_{p3} = \dfrac{\omega_p}{c_{dm}}$; 2) $H_n^{(2)} = J_n(z) - iY_n(z)$

are Hankel functions of the second kind; 3) the $Z_{5,pn}$ are complex constants of superposition to be determined from the

19

boundary conditions; and 4) the series $\sum\limits_{p=1}^{\infty} C_{p1}$, $r \cos \theta$ consists of solutions associated with rigid body displacements.

Substituting Eq. (3.3.1) into Eqs. (3.2.4) and (3.2.6) and introducing Eqs. (3.2.9a and b) and the definition (3.2.9c) along with the definition $q_3 \sim bk_{p3}$, we obtain the following expressions for displacements and stresses:

$$u_r^{dm} = \frac{1}{b} \sum_{p=1}^{\infty} \sum_{n=0}^{\infty} \left\{ z_{5,pn}\left[\frac{n}{\rho} J_n(q_3\rho) - q_3 J_{n+1}(q_3\rho)\right] \right.$$

$$\left. - i\bar{z}_{5,pn}\left[\frac{n}{\rho} Y_n(q_3\rho) - q_3 Y_{n+1}(q_3\rho)\right]\right\} \cos n\theta \; e^{i\omega_p t} \tag{3.3.2a}$$

$$+ \sum_{p=1}^{\infty} C_{p1} \cos \theta ,$$

$$u_\theta^{dm} = -\frac{1}{b} \sum_{p=1}^{\infty} \sum_{n=1}^{\infty} \left\{ z_{5,pn}\left[\frac{\bar{n}}{\rho} J_n(q_3\rho)\right] - i\bar{z}_{5,pn}\left[\frac{\bar{n}}{\rho} Y_n(q_3\rho)\right]\right\} \sin n\theta \; e^{i\omega_p t}$$

$$\tag{3.3.2b}$$

$$- \sum_{p=1}^{\infty} C_{p1} \sin \theta ,$$

$$\sigma_{rr}^{dm} = -\frac{1}{b^2} \sum_{p=1}^{\infty} \sum_{n=0}^{\infty} q_3^2 \left\{ z_{5,pn}\left[\left\{\lambda_m - 2\mu_m\left(\frac{n(n-1)}{(q_3\rho)^2} - 1\right)\right\} J_n(q_3\rho)\right.\right.$$

$$\left. - \frac{2\mu_m}{(q_3\rho)} J_{n+1}(q_3\rho)\right] - i\bar{z}_{5,pn}\left[\left\{\lambda_m - 2\mu_m\left(\frac{n(n-1)}{(q_3\rho)^2} - 1\right)\right\} Y_n(q_3\rho)\right.$$

$$\tag{3.3.2c}$$

$$\left.\left. - \frac{2\mu_m}{(q_3\rho)} Y_{n+1}(q_3\rho)\right]\right\} \cos n\theta \; e^{i\omega_p t} ,$$

20

$$\sigma_{r\theta}^{dm} = \frac{2\mu_m}{b^2} \sum_{p=1}^{\infty} \sum_{n=1}^{\infty} \frac{\bar{n}}{\rho^2} \left\{ Z_{5,pn} \left[(q_3\rho) J_{n+1}(q_3\rho) - (n-1) J_n(q_3\rho) \right] \right.$$

<div align="right">(3.3.2d)</div>

$$\left. - i Z_{5,pn} \left[(q_3\rho) Y_{n+1}(q_3\rho) - (n-1) Y_n(q_3\rho) \right] \right\} \sin n\theta \; e^{i\omega_p t} ,$$

where, as already cited,

$$q_3 = b k_{p3} . \tag{3.3.2e}$$

After c_t is replaced by c_{tm} (the distortional wave velocity in the medium), the distortional displacement potential for the medium, namely, a solution of (3.2.12a) that meets the requirements at infinity, may be taken as

$$\Psi_m = \sum_{p=1}^{\infty} \sum_{n=1}^{\infty} Z_{6,pn} H_n^{(2)}(k_{p4} r) \sin n\theta \; e^{i\omega_p t} + \sum_{p=1}^{\infty} D_{p1} r \sin \theta , \tag{3.3.3}$$

where: 1) $k_{p4} = \omega_p / c_{tm}$; 2) the series $\sum D_{p1} r \sin \theta$ consists of solutions associated with rigid body displacements; and 3) the $Z_{6,pn}$ are complex constants of superposition to be determined from the boundary conditions.

The displacements and stresses associated with Ψ_m are obtained by substituting (3.3.3) into equations of the form (3.2.11) and (3.2.13), and introducing (3.2.9a-c). Thus

$$u_r^{sm} = \frac{1}{b} \sum_{p=1}^{\infty} \sum_{n=0}^{\infty} \frac{\bar{n}}{\rho} \left\{ Z_{6,pn} \left[J_n(q_4\rho) \right] \right.$$

<div align="right">(3.3.4a)</div>

$$\left. - i Z_{6,pn} \left[Y_n(q_4\rho) \right] \right\} \cos n\theta \; e^{i\omega_p t} + \sum_{p=1}^{\infty} D_{p1} \cos \theta ,$$

$$u_\theta^{sm} = -\frac{1}{b} \sum_{p=1}^{\infty} \sum_{n=1}^{\infty} \left\{ Z_{6,pn} \left[\frac{n}{\rho} J_n(q_4\rho) - q_4 J_{n+1}(q_4\rho) \right] \right.$$

$$\left. - i Z_{6,pn} \left[\frac{n}{\rho} Y_n(q_4\rho) - q_4 Y_{n+1}(q_4\rho) \right] \right\} \sin n\theta \ e^{i\omega_p t} \qquad (3.3.4b)$$

$$- \sum_{p=1}^{\infty} D_{p1} \sin\theta \ ,$$

$$\sigma_{rr}^{sm} = \frac{2\mu_m}{b^2} \sum_{p=1}^{\infty} \sum_{n=0}^{\infty} \frac{\bar{n}}{\rho^2} \left\{ Z_{6,pn} \left[(n-1)J_n(q_4\rho) - q_4\rho J_{n+1}(q_4\rho) \right] \right.$$

$$\qquad\qquad (3.3.4c)$$

$$\left. - i Z_{6,pn} \left[(n-1)Y_n(q_4\rho) - q_4\rho Y_{n+1}(q_4\rho) \right] \right\} \cos n\theta \ e^{i\omega_p t} \ ,$$

$$\sigma_{r\theta}^{sm} = -\frac{\mu_m}{b^2} \sum_{p=1}^{\infty} \sum_{n=1}^{\infty} q_4^2 \left\{ Z_{6,pn} \left[\left\{ \frac{2n(n-1)}{(q_4\rho)^2} - 1 \right\} J_n(q_4\rho) \right. \right.$$

$$\left. + \frac{2}{q_4\rho} J_{n+1}(q_4\rho) \right] \qquad\qquad (3.3.4d)$$

$$\left. - i Z_{6,pn} \left[\left\{ \frac{2n(n-1)}{(q_4\rho)^2} - 1 \right\} Y_n(q_4\rho) + \frac{2}{q_4\rho} Y_{n+1}(q_4\rho) \right] \right\} \sin n\theta \ e^{i\omega_p t} \ ,$$

where

$$q_4 = bk_{p4} \ . \qquad\qquad (3.3.4e)$$

22

4. Correspondence Between Elastic and Viscoelastic Field Equations

Viscoelastic problems are very often formulated on the basis of an analogy with corresponding elastic problems. In general, the procedure consists of replacing the elastic parameters by expressions involving linear operators that contain the viscoelastic properties of the material being considered. In the case of steady-state problems, the operator expressions reduce to algebraic functions containing the frequency as well as viscoelastic properties (see, for example, Ref. 14). For the sake of completeness, we will review the procedure, following, for the most part, Ref. 14. The linear strain displacement relations, referred to Cartesian axes (x_1, x_2, x_3), are

$$\epsilon_{ij} = \tfrac{1}{2}(u_{i,j} + u_{j,i}) \qquad i,j = 1, 2, 3 . \qquad (3.4.1a)$$

The elastic stress strain law is

$$\sigma_{ij} = \lambda \delta_{ij} \epsilon_{kk} + 2\mu \epsilon_{ij} . \qquad (3.4.1b)$$

The equilibrium equation is

$$\sigma_{ij,j} - \gamma \frac{\partial^2 u_i}{\partial t^2} = 0 . \qquad (3.4.2)$$

In Eqs. (3.4.1), and in what follows, $i,j = 1, 2, 3$; repeated indices indicate summation over all the possible values of the index; commas denote differentiation with respect to the Cartesian coordinate associated with the index following the comma, and δ_{ij} is the Kronecker delta ($\delta_{ij} = 0$ when $i \neq j$, $\delta_{ij} = 1$ when $i = j$).

The stress deviator, s_{ij}, and the strain deviator, e_{ij}, are defined as

$$s_{ij} = \sigma_{ij} - \tfrac{1}{3}\delta_{ij}\sigma_{kk} , \qquad (3.4.3a)$$

$$e_{ij} = \epsilon_{ij} - \tfrac{1}{3}\delta_{ij}\epsilon_{kk} . \qquad (3.4.3b)$$

The creep laws are written as

$$P s_{ij} = Q e_{ij} \, , \tag{3.4.4a}$$

$$P' \sigma_{kk} = Q' \epsilon_{kk} \, , \tag{3.4.4b}$$

where P, Q, P', and Q' are linear operators with constant coefficients and are defined as follows:

$$P = P_0 + P_1 \frac{\partial}{\partial t} + \ldots + P_p \frac{\partial^p}{\partial t^p} \, , \tag{3.4.5a}$$

$$Q = Q_0 + Q_1 \frac{\partial}{\partial t} + \ldots + Q_k \frac{\partial^k}{\partial t^k} \, , \tag{3.4.5b}$$

$$P' = P_0' + P_1' \frac{\partial}{\partial t} + \ldots + P_n' \frac{\partial^n}{\partial t^n} \, , \tag{3.4.5c}$$

$$Q' = Q_0' + Q_1' \frac{\partial}{\partial t} + \ldots + Q_n' \frac{\partial^n}{\partial t^n} \, . \tag{3.4.5d}$$

The constants P_0, P_1, $\ldots$, Q_n' in these equations are determined on the basis of the viscoelastic model selected.

Since the present analysis utilizes solutions that are harmonic in time, we select displacements of the form

$$u_i = \bar{u}_i \, e^{i\omega t} \, , \tag{3.4.6a}$$

where barred quantities are dependent upon space coordinates only. From the representation (3.4.6a), it follows that

$$\epsilon_{ij} = \bar{\epsilon}_{ij} \, e^{i\omega t} \, , \quad \text{where} \quad \bar{\epsilon}_{ij} = \tfrac{1}{2}(\bar{u}_{i,j} + \bar{u}_{j,i}) \, , \tag{3.4.6b}$$

$$e_{ij} = \bar{e}_{ij} \, e^{i\omega t} \, , \quad \text{where} \quad \bar{e}_{ij} = \bar{\epsilon}_{ij} - \tfrac{1}{3}\delta_{ij}\bar{\epsilon}_{kk} \, , \tag{3.4.6c}$$

$$s_{ij} = \bar{s}_{ij} \, e^{i\omega t} \, , \quad \text{where} \quad \bar{s}_{ij} = \bar{\sigma}_{ij} - \tfrac{1}{3}\delta_{ij}\bar{\sigma}_{kk} \, , \tag{3.4.6d}$$

$$\sigma_{ij} = \bar{\sigma}_{ij} \, e^{i\omega t} \, . \tag{3.4.6e}$$

24

When Eqs. (3.4.6) are introduced into Eqs. (3.4.4), the creep laws become

$$P(i\omega)\bar{s}_{ij} = Q(i\omega)\bar{e}_{ij} \quad , \tag{3.4.7a}$$

$$P'(i\omega)\bar{\sigma}_{kk} = Q'(i\omega)\bar{\epsilon}_{kk} \quad , \tag{3.4.7b}$$

where now the symbols $P(i\omega)$, $Q(i\omega)$, $P'(i\omega)$, $Q'(i\omega)$ represent the polynomials in $(i\omega)$ that result when the operations defined by (3.4.5) are carried out, that is,

$$P(i\omega) = P_0 + (i\omega)P_1 + (i\omega)^2 P_2 + \ldots + (i\omega)^P P_p \quad , \tag{3.4.8}$$

etc.

If we define the following rational functions of $(i\omega)$,

$$Y_s = \frac{Q(i\omega)}{P(i\omega)} \quad \text{(deviatoric complex modulus)} \quad , \tag{3.4.9a}$$

$$Y_v = \frac{Q'(i\omega)}{P'(i\omega)} \quad \text{(dilatational complex modulus)} \quad , \tag{3.4.9b}$$

the creep laws (3.4.7) may be written as

$$\bar{s}_{ij} = Y_s \bar{e}_{ij} \quad , \tag{3.4.10a}$$

$$\bar{\sigma}_{kk} = Y_v \bar{\epsilon}_{kk} \quad . \tag{3.4.10b}$$

Then, combining Eqs. (3.4.10) with the definitions of the deviator amplitudes in Eqs. (3.4.6), gives

$$\bar{\sigma}_{ij} = \tfrac{1}{3}\delta_{ij}(Y_v - Y_s)\bar{\epsilon}_{kk} + Y_s \bar{\epsilon}_{ij} \quad . \tag{3.4.11}$$

25

Comparison of Eq. (3.4.11) with the elastic stress strain law, Eq. (3.4.1b), indicates that the elastic field equations (and corresponding solutions) may be employed in viscoelastic problems provided that the elastic modulii λ and μ are replaced by the corresponding viscoelastic modulii λ_v and μ_v, respectively, where

$$\lambda_v = \tfrac{1}{3}(Y_v - Y_s) \, , \qquad\qquad (3.4.12a)$$

$$\mu_v = \tfrac{1}{2}Y_s \, . \qquad\qquad (3.4.12b)$$

It is to be noted that λ_v and μ_v are, in general, complex, and are functions of the frequency, ω, and the parameters that define the viscoelastic model.

The viscoelastic equivalents λ_v and μ_v must replace their elastic counterparts wherever they occur. This substitution is necessary not only where λ_m and μ_m appear explicitly, but also in those parameters in which they are implied, namely, k_{p3} or k_{p4} and ϵ. In what follows, the subscript v will be dropped, and a subscript m will be used to distinguish the medium from the liner.

For convenience of reference we rewrite the dependence of these parameters on λ_m and μ_m:

$k_{p3} = \omega_p/c_{dm}$ [see Eq. (3.1.6c)], which may be put into the nondimensional form

$$q_3 = bk_{p3} \qquad\qquad \text{[see Eq. (3.3.2e)]} \, ,$$

$$\epsilon = \lambda_m/(\lambda_m + 2\mu_m) \qquad \text{[see Eq. (3.1.12c)]},$$

$$k_{p4} = \omega_p/c_{tm} \, ,$$

$$\left. \begin{array}{c} \\ \\ \\ \\ \\ \\ \end{array} \right\} \qquad (3.4.13)$$

or, in the nondimensional form

$$q_4 = bk_{p4} \, .$$

We now introduce (3.4.12) into (3.4.13). Recalling that Y_v and Y_s are rational functions of the pure imaginary variable $i\omega$, and that the frequency ω depends upon the index of summation p, (i.e., $\omega_p = p\pi/T$) we write

$$Y_v(i\omega_p) = Y_{vp}^{(1)} + iY_{vp}^{(2)} ,$$

$$Y_s(i\omega_p) = Y_{sp}^{(1)} + iY_{sp}^{(2)} ,$$

(3.4.14)

where

$$Y_{vp}^{(1)} \quad , \quad Y_{vp}^{(2)} \quad , \quad Y_{sp}^{(1)} \quad , \quad Y_{sp}^{(2)}$$

are real, and the subscript p is used to indicate dependence on the index of summation. In addition, we let

$$Y_p^{(1)} = Y_{vp}^{(1)} + 2Y_{sp}^{(1)} ,$$

$$Y_p^{(2)} = Y_{vp}^{(2)} + 2Y_{sp}^{(2)} .$$

(3.4.15)

Then, if we introduce (3.4.12) into (3.4.13), and take account of (3.4.14) and (3.4.15), we obtain the viscoelastic equivalents of k_{p3} and k_{p4} in nondimensional form (dropping the subscripts p, but keeping in mind the dependence on p), as follows:

$$q_3 = (bk_3) = \bar{q}_3 - i\tilde{q}_3 ,$$

(3.4.16a)

$$q_4 = (bk_4) = \bar{q}_4 - i\tilde{q}_4 ,$$

(3.4.16b)

27

where

$$\bar{q}_3 = \frac{\sqrt{\frac{3}{2}\,\gamma_m}\,b\omega_n}{\sqrt{Y_p^{(1)^2} + Y_p^{(2)^2}}}\sqrt{Y_p^{(1)} + \sqrt{Y_p^{(1)^2} + Y_p^{(2)^2}}} \qquad (3.4.16c)$$

$$\tilde{q}_3 = \frac{\sqrt{\frac{3}{2}\,\gamma_m}\,b\omega_p}{\sqrt{Y_p^{(1)^2} + Y_p^{(2)^2}}}\sqrt{-Y_p^{(1)} + \sqrt{Y_p^{(1)^2} + Y_p^{(2)^2}}} \qquad (3.4.16d)$$

$$\bar{q}_4 = \frac{\sqrt{\gamma_m}\,b\omega_p}{\sqrt{Y_{sp}^{(1)^2} + Y_{sp}^{(2)^2}}}\sqrt{Y_{sp}^{(1)} + \sqrt{Y_{sp}^{(1)^2} + Y_{sp}^{(2)^2}}} \qquad (3.4.16e)$$

$$\tilde{q}_4 = \frac{\sqrt{\gamma_m}\,b\omega_p}{\sqrt{Y_{sp}^{(1)^2} + Y_{sp}^{(2)^2}}}\sqrt{-Y_{sp}^{(1)} + \sqrt{Y_{sp}^{(1)^2} + Y_{sp}^{(2)^2}}} \qquad (3.4.16f)$$

For the viscoelastic counterparts of the Lamé constant λ_m and the shear modulus μ_m, we obtain

$$\lambda_m = \bar{\lambda} + i\tilde{\lambda} , \qquad (3.4.17a)$$

$$\mu_m = \bar{\mu} + i\tilde{\mu} , \qquad (3.4.17b)$$

28

where

$$\bar{\lambda} = \tfrac{1}{2}\left[Y_{vp}^{(1)} - Y_{sp}^{(1)} \right] ,$$

$$\tilde{\lambda} = \tfrac{1}{2}\left[Y_{vp}^{(2)} - Y_{sp}^{(2)} \right] ,$$

(3.4.17c)

$$\bar{\mu} = \tfrac{1}{2} Y_{sp}^{(1)} ,$$

$$\tilde{\mu} = \tfrac{1}{2} Y_{sp}^{(2)} .$$

(3.4.17d)

And for the viscoelastic counterpart of ϵ,

$$\epsilon = \bar{\epsilon} + i\tilde{\epsilon} ,$$

(3.4.18a)

where

$$\bar{\epsilon} = \frac{\bar{\lambda}(\bar{\lambda} + 2\bar{\mu}) + \tilde{\lambda}(\tilde{\lambda} + 2\tilde{\mu})}{(\bar{\lambda} + 2\bar{\mu})^2 + (\tilde{\lambda} + 2\tilde{\mu})^2} ,$$

(3.4.18b)

$$\tilde{\epsilon} = - \frac{\bar{\lambda}(\tilde{\lambda} + 2\tilde{\mu}) - \tilde{\lambda}(\bar{\lambda} + 2\bar{\mu})}{(\bar{\lambda} + 2\bar{\mu})^2 + (\tilde{\lambda} + 2\tilde{\mu})^2} .$$

(3.4.18c)

5. Viscoelastic Model

The standard linear solid viscoelastic model considered in Ref. 15 and shown in Fig. 4 was selected for the present analysis. It was chosen because it is the simplest model that exhibits the four most common features of viscoelastic behavior: instantaneous elasticity, creep, stress relaxation and creep strain recovery.

29

The operator representation of the model is

$$2\mu_m + \lambda_m = \frac{\gamma_m c_{dm}^2 \left[\tau_1 + \frac{\partial}{\partial t}\right]}{\left[\Omega_1 + \frac{\partial}{\partial t}\right]} , \qquad (3.5.1a)$$

$$\mu_m = \frac{\gamma_m c_{tm}^2 \left[\tau_2 + \frac{\partial}{\partial t}\right]}{\left[\Omega_2 + \frac{\partial}{\partial t}\right]} , \qquad (3.5.1b)$$

where the notation of Ref. 15 has been changed, and the symbols employed above have the following meaning:

c_{dm} velocity of propagation of high frequency dilatational waves

c_{tm} velocity of propagation of high frequency distortional waves

$\frac{1}{\tau_1}$ strain recovery time in uniaxial strain case

$\frac{1}{\tau_2}$ recovery time for shear strain

$\frac{1}{\Omega_1}$ relaxation time for normal stress in uniaxial strain case

$\frac{1}{\Omega_2}$ relaxation time for shear stress.

The choice of the specific model defined by (3.5.1) now enables us to evaluate the <u>operators</u> represented in general form in Eq. (3.4.5) and associated with the stress strain relations in (3.4.4).

30

From (3.4.12b) and (3.4.9a),

$$\mu_m = \tfrac{1}{2} Y_s = \tfrac{1}{2} \frac{Q(1\omega)}{P(1\omega)} \ .$$

Therefore,

$$Q \equiv 2\gamma_m c_{tm}^2 \left[\tau_2 + \frac{\partial}{\partial t} \right] \ ,$$

$$P \equiv \Omega_2 + \frac{\partial}{\partial t} \ .$$

$$(3.5.2)$$

From (3.4.12) and (3.4.9)

$$2\mu_m + \lambda_m = Y_s + \tfrac{1}{3}(Y_v - Y_s) = \tfrac{1}{3}\left[\frac{Q'}{P'} + 2\,\frac{Q}{P} \right] \ ,$$

or

$$\frac{Q'}{P'} = 3(2\mu_m + \lambda_m) - 4\mu_m \ ,$$

and from (3.5.1)

$$Q' \equiv \gamma_m \Big\{ 3c_{dm}^2 \tau_1 \Omega_2 - 4c_{tm}^2 \tau_2 \Omega_1 + \left[3c_{dm}^2(\tau_1 + \Omega_2) \right.$$

$$\left. - 4c_{tm}^2(\tau_2 + \Omega_1) \right] \frac{\partial}{\partial t} + \left(3c_{dm}^2 - 4c_{tm}^2 \right)\frac{\partial^2}{\partial t^2} \Big\}$$

$$P' \equiv \Omega_1 \Omega_2 + (\Omega_1 + \Omega_2)\,\frac{\partial}{\partial t} + \frac{\partial^2}{\partial t^2} \ .$$

$$(3.5.3)$$

31

The present analysis is concerned with steady-state solutions in which the factor $e^{i\omega_p t}$ is present. Therefore, when the operators Q, P, Q', and P', as defined by (3.5.2) and (3.5.3), are used in the creep laws (3.4.4), they generate the polynomials $Q(i\omega_p)$, $P(i\omega_p)$, $Q'(i\omega_p)$, $P'(i\omega_p)$ indicated in (3.4.8). These polynomials now take the form:

$$Q = 2\gamma_m c_{tm}^2 \left[\tau_2 + i\omega_p \right] ,$$

$$P = \Omega_2 + i\omega_p ,$$

$$Q' = Q'_0 + i\omega_p Q'_1 - Q'_2 \omega_p^2 , \qquad (3.5.4)$$

$$P' = P'_0 + i\omega_p P'_1 - \omega_p^2 ,$$

where

$$Q'_0 = \gamma_m \left(3c_{dm}^2 \tau_1 \Omega_2 - 4c_{tm}^2 \tau_2 \Omega_1 \right) ,$$

$$Q'_1 = \gamma_m \left[3c_{dm}^2 (\tau_1 + \Omega_2) - 4c_{tm}^2 (\tau_2 + \Omega_1) \right] ,$$

$$Q'_2 = \gamma_m \left[3c_{dm}^2 - 4c_{tm}^2 \right] ,$$

$$P'_0 = \Omega_1 \Omega_2 ,$$

$$P'_1 = \Omega_1 + \Omega_2 .$$

The deviatoric and dilatational complex modulii Y_s and Y_v, Eq. (3.4.9), may be written in terms of the basic properties of the viscoelastic model by utilizing the polynomials obtained above.

32

By using (3.5.4), the deviatoric modulus, $Y_s = \dfrac{Q(i\omega_p)}{P(i\omega_p)}$, may be written in terms of real and imaginary parts as

$$Y_s = Y_{sp}^{(1)} + iY_{sp}^{(2)} \ ,$$

where

$$Y_{sp}^{(1)} = \frac{2\gamma_m c_{tm}^2 \left[\dfrac{\tau_2}{\Omega_2} + (p\pi)^2 \left(\dfrac{c_{dm}/\Omega_2 b}{c_{dm}T/b} \right)^2 \right]}{1 + (p\pi)^2 \left(\dfrac{c_{dm}/\Omega_2 b}{c_{dm}T/b} \right)^2} \ ,$$

(3.5.5)

$$Y_{sp}^{(2)} = \frac{2\gamma_m c_{tm}^2 p\pi \left[1 - \dfrac{\tau_2}{\Omega_2} \right] \left(\dfrac{c_{dm}/\Omega_2 b}{c_{dm}T/b} \right)}{1 + (p\pi)^2 \left(\dfrac{c_{dm}/\Omega_2 b}{c_{dm}T/b} \right)^2} \ .$$

Similarly, the dilatational complex modulus, $Y_\nu = \dfrac{Q'(i\omega_p)}{P'(i\omega_p)}$, may be written in terms of its real and imaginary parts as

$$Y_\nu = Y_{\nu p}^{(1)} + iY_{\nu p}^{(2)} \ ,$$

where

$$Y_{\nu p}^{(1)} = \frac{\gamma_m c_{dm}^2 \left\{ \left[\bar{Q}_0 - \bar{Q}_2 (p\pi)^2 \right] \left[\bar{P}_0 - (p\pi)^2 \right] + \bar{Q}_1 \bar{P}_1 (p\pi)^2 \right\}}{\left[\bar{P}_0 - (p\pi)^2 \right]^2 + \bar{P}_1^2 (p\pi)^2} \ ,$$

(3.5.6)

$$Y_{\nu p}^{(2)} = \frac{\gamma_m c_{dm}^2 (p\pi) \left\{ \left[\bar{P}_0 - (p\pi)^2 \right] \bar{Q}_1 - \left[\bar{Q}_0 - \bar{Q}_2 (p\pi)^2 \right] \bar{P}_1 \right\}}{\left[\bar{P}_0 - (p\pi)^2 \right]^2 + \bar{P}_1^2 (p\pi)^2} \ ,$$

33

where, from Eq. (3.5.4),

$$\bar{Q}_0 = \frac{Q_0' T^2}{\gamma_m c_{dm}^2} = \left(\frac{c_{dm}T/b}{c_{dm}/\Omega_2 b}\right)^2 \left(\frac{\Omega_1}{\Omega_2}\right) \left[3\,\frac{\tau_1}{\Omega_1} - 4\left(\frac{c_{tm}}{c_{dm}}\right)^2 \frac{\tau_2}{\Omega_2}\right] ,$$

$$\bar{Q}_1 = \frac{Q_1' T}{\gamma_m c_{dm}^2} = \left(\frac{c_{dm}T/b}{c_{dm}/\Omega_2 b}\right) \left\{3\left[\left(\frac{\Omega_1}{\Omega_2}\right)\left(\frac{\tau_1}{\Omega_1}\right) + 1\right] - 4\left(\frac{c_{tm}}{c_{dm}}\right)^2 \left[\frac{\tau_2}{\Omega_2} + \frac{\Omega_1}{\Omega_2}\right]\right\} ,$$

$$\bar{Q}_2 = \frac{Q_2'}{\gamma_m c_{dm}^2} = 3 - 4\left(\frac{c_{tm}}{c_{dm}}\right)^2 , \qquad\qquad\qquad (3.5.7)$$

$$\bar{P}_0 = P_0' T^2 = \left(\frac{c_{dm}T/b}{c_{dm}/\Omega_2 b}\right)^2 \left(\frac{\Omega_1}{\Omega_2}\right) ,$$

$$\bar{P}_1 = P_1' T = \left(\frac{c_{dm}T/b}{c_{dm}/\Omega_2 b}\right) \left(1 + \frac{\Omega_1}{\Omega_2}\right) .$$

Note that, by the way Eqs. (3.5.5), (3.5.6), and (3.5.7) are
written, we have introduced in the formulation of the problem
the following nondimensional ratios to represent the visco-
elastic properties of the medium:

$\dfrac{\Omega_1}{\Omega_2}$ shear relaxation time to uniaxial strain
relaxation time

$\dfrac{\tau_1}{\Omega_1}$ stress relaxation time to strain recovery time
for uniaxial strain

$\dfrac{\tau_2}{\Omega_2}$ shear stress relaxation time to shear strain
relaxation time

$\dfrac{c_{dm}}{\Omega_2 b}$ shear relaxation time to half transit time.

34

The ratios τ_1/Ω_1 and τ_2/Ω_2 also represent the ratios of the relaxed to unrelaxed elastic properties of the medium, namely, in the notation introduced in Eq. (3.4.17),

$$\frac{\tau_1}{\Omega_1} = \frac{(2\mu_m + \lambda_m)\omega_p \to 0}{(2\mu_m + \lambda_m)\omega_p \to \infty} \quad ; \quad \frac{\tau_2}{\Omega_2} = \frac{(\mu_m)\omega_p \to 0}{(\mu_m)\omega_p \to \infty} \quad . \tag{3.5.8}$$

This can be verified by letting $p \to 0$ and ∞ in Eqs. (3.5.5) and (3.5.6) and referring back to Eq. (3.4.17). Note that for finite ω_p, the ratios in (3.5.8) can also be obtained by letting $c_{dm}/\Omega_2 b$, instead of ω_p, approach 0 and ∞.

6. Stresses and Displacements Applied to the Cylinder by an Incident Dilatational Plane Wave in a Viscoelastic Medium

In this section, we consider the elastic cylinder to be embedded in a viscoelastic medium, and obtain the stresses and displacements applied to the cylinder by an incident dilatational plane wave. In doing this we use the form of the equations developed in Section III.1 for the case of an elastic embedding medium, and invoke the correspondence principle discussed in Section III.4. That is, we take the results obtained for an elastic medium and replace the parameters involving elastic modulii, by their viscoelastic equivalents.

For convenience of reference, we rewrite the pertinent results obtained in Section III.1. From Eqs. (3.1.13) the normal and shearing stresses applied to the cylinder boundary by the incident plane dilatational wave are given in polar coordinates by

$$\sigma_{rr}^{B} = \sum_{p=1}^{\infty} \sigma_{r,p} \, e^{i\omega_p t} , \tag{3.6.1a}$$

$$\sigma_{r\theta}^{B} = -\sum_{p=1}^{\infty} \sigma_{r\theta,p} \, e^{i\omega_p t} , \tag{3.6.1b}$$

in which

$$\sigma_{i,p} = (-ia_p)(\cos^2\theta + \epsilon \sin^2\theta) e^{iq_3(\cos\theta-1)} \tag{3.6.1c}$$

$$\sigma_{r\theta,p} = (-ia_p)\left(\frac{1-\epsilon}{2}\right) \sin 2\theta \ e^{iq_3(\cos\theta-1)}, \tag{3.6.1d}$$

where the viscoelastic parameters q_3 and ϵ are given by Eqs. (3.4.16) and (3.4.18) in the form

$$q_3 = \bar{q}_3 - i\tilde{q}_3, \tag{3.6.2a}$$

$$\epsilon = \bar{\epsilon} + i\tilde{\epsilon}. \tag{3.6.2b}$$

As in previous cases, we expand the boundary tractions in the Fourier series

$$\sigma_{rr}^B = \sum_{p=1}^{\infty} \sum_{n=0}^{\infty} a_p A_{pn} \cos n\theta \ e^{i\omega_p t}, \tag{3.6.3a}$$

$$\sigma_{r\theta}^B = \sum_{p=1}^{\infty} \sum_{n=1}^{\infty} a_p B_{pn} \sin n\theta \ e^{i\omega_p t}, \tag{3.6.3b}$$

and, comparing (3.6.3) with (3.6.1), we obtain the coefficients A_{pn}, B_{pn} as

$$A_{pn} = -\frac{2i}{\pi} \int_0^{\pi} (\cos^2\theta + \epsilon \sin^2\theta) e^{iq_3(\cos\theta-1)} \cos n\theta \ d\theta \qquad n \geq 1 \tag{3.6.4a}$$

36

$$A_{p0} = - \frac{1}{\pi} \int_0^{\pi} (\cos^2\theta + \epsilon \sin^2\theta) \, e^{iq_3(\cos\theta - 1)} \, d\theta \, , \qquad (3.6.4b)$$

$$B_{pn} = \frac{i(1 - \epsilon)}{\pi} \int_0^{\pi} e^{iq_3(\cos\theta - 1)} \sin 2\theta \sin n\theta \, d\theta \, . \qquad (3.6.4c)$$

These expressions are evaluated in terms of Bessel functions of a complex argument in Appendix B. As given in (3.6.4), they are identical in form to their elastic counterparts, (3.1.15), but of course are different in value.

A minor variation is necessary in the development of the displacement representation. From Eq. (3.1.17),

$$u_r^B = \sum_{p=1}^{\infty} u_{r,p} \, e^{i\omega_p t} \, , \qquad (3.6.5a)$$

$$u_\theta^B = \sum_{p=1}^{\infty} u_{\theta,p} \, e^{i\omega_p t} \, , \qquad (3.6.5b)$$

in which we take (3.1.17e and f) as the form appropriate for the viscoelastic representation of $u_{r,p}$, $u_{\theta,p}$. Thus,

$$u_{r,p} = - \frac{a_p}{\gamma_m c_{dm} \omega_p} \left(\frac{c_{dm} q_3}{\omega_p b} \right) \cos\theta \, e^{iq_3(\cos\theta - 1)} \, , \qquad (3.6.5c)$$

$$u_{\theta,p} = \frac{a_p}{\gamma_m c_{dm} \omega_p} \left(\frac{c_{dm} q_3}{\omega_p b} \right) \sin\theta \, e^{iq_3(\cos\theta - 1)} \, , \qquad (3.6.5d)$$

where we note again that q_3 is a viscoelastic parameter, defined by (3.6.2a) and the symbol c_{dm} is the speed of propagation of dilatational waves in an elastic medium that has the unrelaxed elastic properties of the viscoelastic material.

37

Expanding the displacements u_r^B and u_θ^B in the Fourier series:

$$u_r^B = - \sum_{p=1}^{\infty} \left\{ \sum_{n=0}^{\infty} \frac{a_p}{\gamma_m c_{dm} \omega_p} C_{pn} \cos n\theta \right\} e^{i\omega_p t} , \qquad (3.6.6a)$$

$$u_\theta^B = \sum_{p=1}^{\infty} \left\{ \sum_{n=1}^{\infty} \frac{a_p}{\gamma_m c_{dm} \omega_p} D_{pn} \sin n\theta \right\} e^{i\omega_p t} , \qquad (3.6.6b)$$

and comparing (3.6.6) with (3.6.5), we obtain

$$C_{pn} = \frac{2}{\pi} \left(\frac{c_{dm} q_3}{\omega_p b} \right) \int_0^{\pi} e^{i q_3 (\cos \theta - 1)} \cos \theta \cos n\theta \, d\theta , \qquad (3.6.7a)$$
$$n \geq 1$$

$$C_{p0} = \frac{1}{\pi} \left(\frac{c_{dm} q_3}{\omega_p b} \right) \int_0^{\pi} e^{i q_3 (\cos \theta - 1)} \cos \theta \, d\theta , \qquad (3.6.7b)$$

$$D_{pn} = \frac{2}{\pi} \left(\frac{c_{dm} q_3}{\omega_p b} \right) \int_0^{\pi} e^{i q_3 (\cos \theta - 1)} \sin \theta \sin n\theta \, d\theta . \qquad (3.6.7c)$$

The form of the quantities in (3.6.7) differs from the counterparts in Eq. (3.1.19) only by the presence of the factor $(c_{dm} q_3 / \omega_p b)$. When the parameter q_3 applies to an elastic medium, this factor is unity. The explicit representation of (3.6.7) in terms of Bessel functions of a complex argument is given in Appendix B.

$$A_{p0} = -\frac{i}{?} \int_0^? (\cos^2 + \epsilon \sin^2) \, e^{iq_3(\cos - 1)} \, d \quad , \tag{3.6.4b}$$

$$B_{pn} = \frac{i(1 - \epsilon)}{\pi} \int_0^\pi e^{iq_3(\cos \theta - 1)} \sin 2\theta \sin n\theta \, d\theta \quad . \tag{3.6.4c}$$

These expressions are evaluated in terms of Bessel functions of a complex argument in Appendix B. As given in (3.6.4), they are identical in form to their elastic counterparts, (3.1.15), but of course are different in value.

A minor variation is necessary in the development of the displacement representation. From Eq. (3.1.17),

$$u_r^B = \sum_{p=1}^\infty u_{r,p} \, e^{i\omega_p t} \quad , \tag{3.6.5a}$$

$$u_\theta^B = \sum_{p=1}^\infty u_{\theta,p} \, e^{i\omega_p t} \quad , \tag{3.6.5b}$$

in which we take (3.1.17e and f) as the form appropriate for the viscoelastic representation of $u_{r,p}$, $u_{\theta,p}$. Thus,

$$u_{r,p} = \frac{a_p}{\gamma_m c_{dm} \omega_p} \left(\frac{c_{dm} q_3}{\omega_p b} \right) \cos \theta \, e^{iq_3(\cos \theta - 1)} \quad , \tag{3.6.5c}$$

$$u_{\theta,p} = \frac{a_p}{\gamma_m c_{dm} \omega_p} \left(\frac{c_{dm} q_3}{\omega_p b} \right) \sin \theta \, e^{iq_3(\cos \theta - 1)} \quad , \tag{3.6.5d}$$

where we note again that q_3 is a viscoelastic parameter, defined by (3.6.2a) and the symbol c_{dm} is the speed of propagation of dilatational waves in an elastic medium that has the unrelaxed elastic properties of the viscoelastic material.

37

7. Solution to the Wave Equation in a Viscoelastic Medium

    In Section III.3, the solution to the wave equation in a surrounding elastic medium was constructed from displacement potentials. The displacements and stresses associated with this solution are given by Eqs. (3.3.2) and (3.3.4). By utilizing the correspondence principle (Section III.4), we may obtain the solution in a viscoelastic medium from the solution in the elastic medium. The modulii appearing in the elastic solution are simply replaced by their viscoelastic equivalents. Thus, the desired solution in the viscoelastic medium, that is, stresses and displacements, are given by Eqs. (3.3.2) and (3.3.4), provided that the parameters appearing in these equations are defined as follows:

$$k_{p3} = \bar{k}_{p3} - i\tilde{k}_{p3} ,$$

$$\lambda_m = \bar{\lambda} + i\tilde{\lambda} , \tag{3.7.1}$$

$$\mu_m = \bar{\mu} + i\tilde{\mu} .$$

    For convenience of reference, the stresses and displacements given by Eqs. (3.3.2) and (3.3.4) are rewritten here, with Eq. (3.7.1) now applying.

$$u_r^{dm} = \frac{1}{b} \sum_{p=1}^{\infty} \sum_{n=0}^{\infty} \left\{ Z_{5,pn} \left[\frac{n}{\rho} J_n(q_3\rho) - q_3 J_{n+1}(q_3\rho) \right] \right.$$

$$\tag{3.7.2a}$$

$$\left. - i Z_{5,pn} \left[\frac{n}{\rho} Y_n(q_3\rho) - q_3 Y_{n+1}(q_3\rho) \right] \right\} \cos n\theta \; e^{i\omega_p t} + \sum_{p=1}^{\infty} C_{p1} \cos \theta ,$$

$$u_\theta^{dm} = - \frac{1}{b} \sum_{p=1}^{\infty} \sum_{n=1}^{\infty} \left\{ Z_{5,pn} \left[\frac{\bar{n}}{\rho} J_n(q_3\rho) \right] \right.$$

$$\tag{3.7.2b}$$

$$\left. - i Z_{5,pn} \left[\frac{\bar{n}}{\rho} Y_n(q_3\rho) \right] \right\} \sin n\theta \; e^{i\omega_p t} - \sum_{p=1}^{\infty} C_{p1} \sin \theta ,$$

39

$$\sigma_{rr}^{dm} = -\frac{1}{b^2} \sum_{p=1}^{} \sum_{n=0}^{} q_3^2 \left\{ Z_{5,pn} \left[\left\{ \lambda_m - 2\mu_m \left(\frac{n(n-1)}{(q_3\rho)^2} - 1 \right) \right\} J_n(q_3\rho) \right. \right.$$

$$\left. - \frac{2\mu_m}{(q_3\rho)} J_{n+1}(q_3\rho) \right]$$

$$\text{(3.7.2c)}$$

$$- i Z_{5,pn} \left[\left\{ \lambda_m - 2\mu_m \left(\frac{n(n-1)}{(q_3\rho)^2} - 1 \right) \right\} Y_n(q_3\rho) \right.$$

$$\left. \left. - \frac{2\mu_m}{(q_3\rho)} Y_{n+1}(q_3\rho) \right] \right\} \cos n\theta \, e^{i\omega_p t} \, ,$$

$$\sigma_{r\theta}^{dm} = \frac{2\mu_m}{b^2} \sum_{p=1}^{\infty} \sum_{n=1}^{\infty} \frac{\bar{n}}{\rho^2} \left\{ Z_{5,pn} \left[(q_3\rho) J_{n+1}(q_3\rho) - (n-1) J_n(q_3\rho) \right] \right.$$

$$\text{(3.7.2d)}$$

$$\left. - i Z_{5,pn} \left[(q_3\rho) Y_{n+1}(q_3\rho) - (n-1) Y_n(q_3\rho) \right] \right\} \sin n\theta \, e^{i\omega_p t} \, ,$$

$$u_r^{sm} = \frac{1}{b} \sum_{p=1}^{\infty} \sum_{n=1}^{\infty} \frac{\bar{n}}{\rho} \left\{ Z_{6,pn} \left[J_n(q_4\rho) \right] \right.$$

$$\text{(3.7.3a)}$$

$$\left. - i Z_{6,pn} \left[Y_n(q_4\rho) \right] \right\} \cos n\theta \, e^{i\omega_p t} + \sum_{p=1}^{\infty} D_{p1} \cos \theta \, .$$

$$u_\theta^{sm} = -\frac{1}{b} \sum_{p=1}^{\infty} \sum_{n=1}^{\infty} \left\{ Z_{6,pn} \left[\frac{n}{\rho} J_n(q_4\rho) - q_4 J_{n+1}(q_4\rho) \right] \right.$$

$$\left. - i Z_{6,pn} \left[\frac{n}{\rho} Y_n(q_4\rho) - q_4 Y_{n+1}(q_4\rho) \right] \right\} \sin n\theta \, e^{i\omega_p t} \quad \text{(3.7.3b)}$$

$$- \sum_{p=1}^{\infty} D_{p1} \sin \theta \, ,$$

$$\sigma_{rr}^{sm} = \frac{2\mu_m}{b^2} \sum_{p=1} \sum_{n=1} \frac{n}{\rho^2} \left\{ z_{6,pn} \left[(n-1) J_n(q_4\rho) - (q_4\rho) J_{n+1}(q_4\rho) \right] \right.$$

$$\left. - i z_{6,pn} \left[(n-1) Y_n(q_4\rho) - (q_4\rho) Y_{n+1}(q_4\rho) \right] \right\} \cos n\theta \; e^{i\omega_p t} , \qquad (3.7.3c)$$

$$\sigma_{r\theta}^{sm} = -\frac{\mu_m}{b^2} \sum_{p=1}^{\infty} \sum_{n=1}^{\infty} q_4^2 \left\{ z_{6,pn} \left[\left\{ \frac{2n(n-1)}{(q_4\rho)^2} - 1 \right\} J_n(q_4\rho) \right. \right.$$

$$\left. + \frac{2}{(q_4\rho)} J_{n+1}(q_4\rho) \right] - i z_{6,pn} \left[\left\{ \frac{2n(n-1)}{(q_4\rho)^2} - 1 \right\} Y_n(q_4\rho) \right. \qquad (3.7.3d)$$

$$\left. \left. + \frac{2}{(q_4\rho)} Y_{n+1}(q_4\rho) \right] \right\} \sin n\theta \; e^{i\omega_p t} .$$

It is observed that the viscoelastic parameters q_3 and q_4 necessitate the computation of Bessel functions of a complex argument.

8. Superposition of Solutions to Enforce the Boundary Conditions

In the preceding sections, we have presented contributions to the complete solution. These consisted of: 1) stresses and displacements associated with the incident wave; 2) the solution to the wave equation in the elastic cylinder; and 3) the solution to the wave equation in the surrounding medium. These contributions must be combined to enforce the required conditions at the cylinder boundaries, namely, that: 1) the inner boundary be traction free; and 2) at the outer boundary the cylinder displacements and appropriate stress components be continuous with those of the surrounding medium.

Recalling the introduction of the nondimensional radial coordinate $\rho = r/b$ [Eq. (3.2.9c)], and letting $\beta = a/b$, we obtain the boundary conditions at $\rho = \beta$ (inner boundary of the cylinder) in the form

41

$$\sigma^{d}_{rr}(\rho) + \sigma^{s}_{rr}(\rho) = 0 ,$$

$$\sigma^{d}_{r\theta}(\rho) + v^{s}_{r\theta}(\rho) = 0 .$$

(3.8.1a)

At $\rho = 1$ (outer boundary of the cylinder),

$$\sigma^{d}_{rr}(1) + \sigma^{s}_{rr}(1) - \sigma^{dm}_{rr}(1) - \sigma^{sm}_{rr}(1) = \sigma^{B}_{rr} ,$$

$$\sigma^{d}_{r\theta}(1) + \sigma^{s}_{r\theta}(1) - \sigma^{dm}_{r\theta}(1) - \sigma^{sm}_{r\theta}(1) = \sigma^{B}_{r\theta} ,$$

$$u^{d}_{r}(1) + u^{s}_{r}(1) - u^{dm}_{r}(1) - u^{sm}_{r}(1) = u^{B}_{r} ,$$

$$u^{d}_{\theta}(1) + u^{s}_{\theta}(1) - u^{dm}_{\theta}(1) - u^{sm}_{\theta}(1) = u^{B}_{\theta} ,$$

(3.8.1b)

where: 1) the superscripts d and s are affixed to quantities
stemming from the dilatational and shear solutions, respectively,
to the wave equation in the cylinder (see Section III.2); 2) the
superscripts dm and sm are appended to stresses and displace-
ments resulting from the dilatational and shear solutions, respec-
tively, to the wave equation in the medium (for an elastic medium,
these quantities are given in Section III.3; for a viscoelastic
medium, they are given in Section III.7); and 3) the superscripts
B identify the stresses and displacements associated with the
incident wave at the outer boundary of the cylinder (for a wave
traveling through an elastic medium, these quantities are given
in Section III.1; when the wave propagates through a viscoelastic
medium, they are given in Section III.6).

In the following development, advantage will be taken of the
fact that by an appropriate choice of the values of the visco-
elastic parameters, the viscoelastic solutions in the medium re-
duce to elastic solutions. Therefore, quantities labeled with
the superscripts B, dm, and sm will be written as they are
given in Sections III.6 and III.7. Thus, the solution presented
will apply to an elastic cylinder embedded in a viscoelastic
medium, and as a limiting case will contain the solution for an
elastic cylinder embedded in an elastic medium.

After the terms entering into Eq. (3.8.1) are computed from the appropriate expressions, and the common trigonometric and exponential factors are divided out, the resulting nonhomogeneous system of linear equations in the unknown coefficients of superposition $Z_{j,pn}$ may be written in matrix form as

$$[C_{ij,pn}] \{Z_{j,pn}\} = \{D_{i,pn}\} \qquad i,j = 1, 2, \ldots, 6$$

$$p = 1, 2, 3, \ldots \qquad n = 0, 1, 2, \ldots,$$

$$(3.8.2)$$

where $C_{ij,pn}$ stems from the coefficient of $Z_{j,pn}$ in the ith equation of Eqs. (3.8.1); $D_{i,pn}$ results from the term on the right-hand side of the ith equation of Eqs. (3.8.1); and $\{Z_{j,pn}\}$, the solution vector, is a 6 x 1 column matrix, whose complex elements are the unknown coefficients of superposition. It should be noted that there is a different matrix equation (3.8.2) for each pair of values of p and n.

The elements $C_{ij,pn}$ and $D_{i,pn}$ are shown in detail in Appendices A and B.

The system (3.8.2) may be solved by matrix inversion for the solution vector $\{Z_{j,pn}\}$. Having solved for $\{Z_{j,pn}\}$ for a sufficient number of values of p and n to ensure adequate convergence, we may calculate to the desired accuracy the stresses and displacements in the cylinder as:

$$\sigma_{rr} = \sigma_{rr}^d + \sigma_{rr}^s \quad , \quad \sigma_{r\theta} = \sigma_{r\theta}^d + \sigma_{r\theta}^s \quad , \quad \sigma_{\theta\theta} = \sigma_{\theta\theta}^d + \sigma_{\theta\theta}^\varepsilon \quad ,(3.8.3a)$$

$$u_r = u_r^d + u_r^s \quad , \quad u_\theta = u_\theta^d + u_\theta^s \quad , \qquad (3.8.3b)$$

where the terms appearing on the right-hand side of the above expressions are given in Eqs. (3.2.10) and (3.2.17).

43

SOLUTION FOR AN INCIDENT DISTORTIONAL PLANE WAVE

1. Discussion of Approach Used

This section is concerned with the cylinder response to an incident shear wave. As discussed in Section III.4, the visco-elastic analysis may be obtained from the corresponding elastic analysis by using the correspondence principle, that is, by re-placing the elastic modulii by appropriate viscoelastic modulii. Conversely, the elastic case can be obtained as a special case of the viscoelastic formulation by a proper choice of the value of certain parameters. Therefore, in treating the response to an incoming shear wave, we shall regard the cylinder as first em-bedded in an elastic medium. The viscoelastic analysis will then be obtained by employing the correspondence principle. The numeri-cal results will be computed from the viscoelastic formulation for both the elastic and viscoelastic case, treating the elastic prob-lem as a limiting case of the viscoelastic problem.

The first section in this chapter deals with the contribution of the free field quantities, that is, the stresses and displace-ments applied to the outer boundary of the cylinder by the inci-dent shear wave. This contribution will be derived independently of any of the results presented in Section III. The remaining contributions to the solution, namely, the solution to the wave equation in the cylinder and the scattered response in the sur-rounding medium, will be obtained by making minor changes in the corresponding solution for an incoming dilatational wave. As outlined in Section III.2, these alterations involve interchanging $\sin n\theta$ and $\cos n\theta$, and setting $\bar{n} = -n$. It will be recalled that the $\bar{n}$ are those integers stemming from differentiation with respect to θ.

2. Stresses and Displacements Applied to the Cylinder by an Incident Distortional Plane Wave

To avoid confusion with the response to an incoming dilata-tional wave, we shall identify corresponding quantities associated with the response to an incoming shear wave by using notation that differs slightly from that employed in Section III.

44

The Cartesian coordinate system in which the incident plane distortional wave is described, as well as some of the notation used, is shown in Fig. 3b. The disturbance is assumed to be traveling in the negative $\bar{x}$-direction. The propagation of the wave depends only on the space coordinate $\bar{x}$, and the time coordinate t.

We may obtain the governing equations of motion from a scalar potential, Ψ, Ref. 9, where $\Psi = \Psi(\bar{x},t)$ and is a solution of

$$\mu_m \frac{\partial^2 \Psi}{\partial \bar{x}^2} - \gamma_m \frac{\partial^2 \Psi}{\partial t^2} = 0 .$$ (4.2.1)

The nonvanishing Cartesian displacement and stress quantities $v_{\bar{y}}$ and $\tau_{\bar{x}\bar{y}}$ are given by

$$v_{\bar{y}} = - \frac{\partial \Psi}{\partial \bar{x}} ,$$ (4.2.2a)

$$\tau_{\bar{x}\bar{y}} = - \mu_m \frac{\partial^2 \Psi}{\partial \bar{x}^2} .$$ (4.2.2b)

As developed in Ref. 9, Eqs. (4.2.1) and (4.2.2) apply to an elastic medium, and μ_m is the elastic shear modulus. However, on the basis of the correspondence principle, these equations may also be applied to a viscoelastic medium if μ_m is regarded as the viscoelastic parameter defined in Section II.4 by Eqs. (3.4.17b) and (3.4.17d) and given in terms of the viscoelastic model representation used in the present analysis by Eq. (3.5.5).

Steady state solutions of (4.2.1) may be taken in the form

$$\Psi = \Psi_p(\bar{x}) e^{i\omega_p t} ,$$ (4.2.3a)

where the frequency ω_p is given by

$$\omega_p = \frac{p\pi}{T} ,$$ (4.2.3b)

45

with p a positive integer, and T an arbitrary time interval. Thus, the wave equation (4.2.1) becomes the Helmholz equation

$$\frac{\partial^2 \Psi_p}{\partial \bar{x}^2} + k^2_{p4} \Psi_p = 0 , \qquad (4.2.4a)$$

where

$$k^2_{p4} = \frac{\omega^2_p}{\left(\dfrac{\mu_m}{\gamma_m}\right)} . \qquad (4.2.4b)$$

In the case of a viscoelastic medium, k_{p4} is the complex parameter defined in Eq. (3.4.16). For an elastic medium, k_{p4} reduces to

$$k^2_{p4} = \frac{\omega^2_p}{c^2_{tm}} , \qquad (4.2.4c)$$

where c_{tm} is the velocity of propagation of distortional waves in that medium, with

$$c_{tm} = \sqrt{\frac{\mu_m}{\gamma_m}} . \qquad (4.2.4d)$$

Steady-state solutions of (4.2.1) may be constructed from the solutions to (4.2.4a), by using (4.2.3a). Thus $\Psi(\bar{x}, t)$ may be taken as

$$\Psi(\bar{x}, t) = \sum_{p=1}^{\infty} A_p e^{i[k_{p4}(\bar{x}-b) + \omega_p t]} . \qquad (4.2.5)$$

We now represent the incoming shear wave in the form

$$\tau_{xy} = \sum_{p=1}^{\infty} a_p \sin \omega_p \left[\frac{k_{p4}(\bar{x} - b)}{\omega_p} + t \right] , \qquad (4.2.6)$$

46

and proceed to relate the coefficients, a_p, in this equation to the coefficients. A_r. in Eq. (4.2.5). In the elastic case $\omega_p/k_{p4} = c_{tm}$, the uniform speed of propagation of distortional waves. In the viscoelastic case the parameter ω_p/k_{p4} represents the limiting value of the velocity of propagation when the frequency tends to infinity. At $\bar{x} = b$,

$$\tau_{\bar{x}\bar{y}} = \sum_{p=1}^{\infty} a_p \sin \omega_p t . \tag{4.2.7}$$

The Fourier coefficients a_p define the wave form over the arbitrary half period, T. In the viscoelastic case, since attenuation occurs, the wave form is altered as it progresses through the medium.

An expression for $\tau_{\bar{x}\bar{y}}$ identical with (4.2.6) is given by the real part of

$$\tau_{\bar{x}\bar{y}} = \sum_{p=1}^{\infty} (-ia_p) e^{i[k_{p4}(\bar{x}-b) + \omega_p t]} , \tag{4.2 }$$

From (4.2.2b) and (4.2.5),

$$\tau_{\bar{x}\bar{y}} = \sum_{p=1}^{\infty} \mu_m k_{p4}^2 A_p e^{i[k_{p4}(\bar{x}-b) + \omega_p t]} . \tag{4.2.9}$$

Comparing (4.2.8) and (4.2.9), we obtain

$$A_p = - \frac{ia_p}{\mu_m k_{p4}^2} . \tag{4.2.10}$$

From (4.2.2a) and (4.2.5), and by noting (4.2.10), we get

$$v_{\bar{y}} = - \sum_{p=1}^{\infty} \frac{a_p}{\mu_m k_{p4}} e^{i[k_{p4}(\bar{x}-b) + \omega_p t]} .$$

It will be convenient for the computational effort to rewrite the above expression. By (4.2.4b), $\mu_m k_{p4} = (\gamma_m \omega_p^2 / k_{p4})$ and from the definitions of ω_p [Eq. (4.2.3b)] and q_4 [Eq. (3.4.16)], we may rewrite $\mu_m k_{p4}$ as

$$\frac{1}{\mu_m k_{p4}} = \frac{1}{\gamma_m c_{tm} \omega_p} \left(\frac{c_{tm} q_4}{\omega_p b} \right) .$$

Thus,

$$v_{\bar{y}} = - \sum_{p=1}^{\infty} \frac{a_p}{\gamma_m c_{tm} \omega_p} \left(\frac{c_{tm} q_4}{\omega_p b} \right) e^{i[k_{p4}(\bar{x}-b) + \omega_p t]} \qquad (4.2.11)$$

In polar coordinates the stresses and displacements associated with the incoming wave are given by

$$\tau_{rr}^B = \tau_{\bar{x}\bar{y}} \sin 2\bar{\theta} \quad , \quad \tau_{r\bar{\theta}}^B = \tau_{\bar{x}\bar{y}} \cos 2\bar{\theta} , \qquad (4.2.12)$$

$$v_r^B = v_{\bar{y}} \sin \bar{\theta} \quad , \quad v_{\bar{\theta}}^B = v_{\bar{y}} \cos \bar{\theta} . \qquad (4.2.13)$$

Substituting (4.2.8) into (4.2.12), and setting $\bar{x} = b \cos \bar{\theta}$, we obtain the following expressions for the stresses applied to the boundary by the incident wave:

$$\tau_{rr}^B = \sum_{p=1}^{\infty} \tau_{r,p} e^{i\omega_p t} , \qquad (4.2.14a)$$

$$\tau_{r\bar{\theta}}^B = \sum_{p=1}^{\infty} \tau_{r\bar{\theta},p} e^{i\omega_p t} , \qquad (4.2.14b)$$

48

where

$$\tau_{r,p} = (-ia_p) \sin 2\bar{\theta} \; e^{iq_4(\cos\bar{\theta}-1)} \;, \tag{4.2.14c}$$

$$\tau_{r\bar{\theta},p} = (-ia_p)(\cos 2\bar{\theta}) \; e^{iq_4(\cos\bar{\theta}-1)} \;, \tag{4.2.14d}$$

with

$$q_4 = bk_{p4} \;, \tag{4.2.14e}$$

q_4 is defined in Eq. (3.4.16) for the viscoelastic case. In the elastic case it simplifies to

$$q_4 = \frac{b\omega_p}{c_{tm}} \;.$$

The Fourier expansions of Eq. (4.2.14) in the circumferential coordinate $\bar{\theta}$ are

$$\tau_{rr}^B = \sum_{p=1}^{\infty} \sum_{n=1}^{\infty} a_p A_{pn} \sin n\bar{\theta} \; e^{i\omega_p t} \;, \tag{4.2.15a}$$

$$\tau_{r\bar{\theta}}^B = \sum_{p=1}^{\infty} \sum_{n=0}^{\infty} a_p B_{pn} \cos n\bar{\theta} \; e^{i\omega_p t} \;. \tag{4.2.15b}$$

The complex Fourier coefficients A_{pn} and B_{pn} are obtained by comparing (4.2.15) with (4.2.14), and are

$$A_{pn} = -\frac{2i}{\pi} \int_0^{\pi} e^{iq_4(\cos\bar{\theta}-1)} \sin 2\bar{\theta} \sin n\bar{\theta} \; d\bar{\theta} \;, \tag{4.2.16a}$$

49

$$B_{pn} = -\frac{2i}{\pi}\int_0^\pi e^{iq_4(\cos\bar\theta-1)}\cos 2\bar\theta\,\cos n\bar\theta\,d\bar\theta\;, \qquad n \geq 1 \qquad (4.2.16b)$$

$$B_{p0} = -\frac{1}{\pi}\int_0^\pi e^{iq_4(\cos\bar\theta-1)}\cos 2\bar\theta\,d\bar\theta\;. \qquad (4.2.16c)$$

The representation of these coefficients in terms of Bessel functions of a complex argument is given in Appendix B.

If we introduce (4.2.11) into (4.2.13) and set $\bar x = b\cos\bar\theta$, we obtain the following representation for the displacements v_r^B and $v_{\bar\theta}^B$:

$$v_r^B = -\sum_{p=1}^\infty v_{r,p}\,e^{i\omega_p t}\;, \qquad (4.2.17a)$$

$$v_{\bar\theta}^B = -\sum_{p=1}^\infty v_{\bar\theta,p}\,e^{i\omega_p t}\;, \qquad (4.2.17b)$$

where

$$v_{r,p} = \frac{a_p}{\gamma_m c_{tm}\omega_p}\left(\frac{c_{tm}}{\omega_p b}\right)q_4\,e^{iq_4(\cos\bar\theta-1)}\sin\bar\theta\;, \qquad (4.2.17c)$$

$$v_{\bar\theta,p} = \frac{a_p}{\gamma_m c_{tm}\omega_p}\left(\frac{c_{tm}}{\omega_p b}\right)q_4\cos\bar\theta\,e^{iq_4(\cos\bar\theta-1)}\;. \qquad (4.2.17d)$$

To facilitate the application of conditions of continuity of displacement at the outer boundary of the cylinder, we expand v_r^B and $v_{\bar\theta}^B$ in Fourier series in $\bar\theta$. Thus,

$$v_r^B = - \sum_{p=1}^{\infty} \sum_{n=1}^{\infty} \frac{a_p}{\gamma_m c_{tm} \omega_p} C_{pn} \sin n\bar{\theta} \; e^{i\omega_p t} \; .\tag{4.2.18a}$$

$$v_{\bar{\theta}}^B = - \sum_{p=1}^{\infty} \sum_{n=0}^{\infty} \frac{a_p}{\gamma_m c_{tm} \omega_p} D_{pn} \cos n\bar{\theta} \; e^{i\omega_p t} \; .\tag{4.2.18b}$$

Comparing (4.2.18) with (4.2.17), we obtain for the coefficients C_{pn} and D_{pn},

$$C_{pn} = \frac{2}{\pi} \left(\frac{c_{tm}}{\omega_p b} \right) q_4 \int_0^{\pi} e^{iq_4(\cos \bar{\theta} - 1)} \sin \bar{\theta} \sin n\bar{\theta} \; d\bar{\theta} \; ,\tag{4.2.19a}$$

$$D_{pn} = \frac{2}{\pi} \left(\frac{c_{tm}}{\omega_p b} \right) q_4 \int_0^{\pi} e^{iq_4(\cos \bar{\theta} - 1)} \cos \bar{\theta} \cos n\bar{\theta} \; d\bar{\theta} \; ,\tag{4.2.19b}$$
$$n \geq 1$$

$$D_{p0} = \frac{1}{\pi} \left(\frac{c_{tm}}{\omega_p b} \right) q_4 \int_0^{\pi} e^{iq_4(\cos \bar{\theta} - 1)} \cos \bar{\theta} \; d\bar{\theta} \; .\tag{4.2.19c}$$

These coefficients are represented in terms of Bessel functions of a complex argument in Appendix B.

3. Solution to the Wave Equation in the Elastic Cylinder

We have already discussed the manner in which it is possible to apply the analysis derived for the response to an incident dilatational wave to the corresponding analysis for the response to an incident shear wave (see Section IV.1 and the comments preceding Eq. (3.2.8) in Section III.2). Thus, if in the results obtained in Section III.2, we interchange $\sin n\theta$ and $\cos n\theta$ and regard $\bar{n}$ as equal to $-n$, we may write the contribution, associated with waves of dilatation in the cylinder, in response to an incident shear wave, as follows:

51

$$v_r^d = \frac{1}{b} \sum_{p=1}^{\infty} \sum_{n=1}^{\infty} q_1 \left\{ Z_{1,pn} \left[\frac{n}{q_1\rho} J_n(q_1\rho) - J_{n+1}(q_1\rho) \right] \right.$$

$$\left. + Z_{2,pl} \left[\frac{n}{q_1\rho} Y_n(q_1\rho) - Y_{n+1}(q_1\rho) \right] \right\} \sin n\bar{\theta} \; e^{i\bar{\omega}_p t} \qquad (4.3.1a)$$

$$+ \sum_{p=1}^{\infty} A_{pl} \sin \bar{\theta} \; ,$$

$$v_{\bar{\theta}}^d = \frac{1}{b} \sum_{p=1}^{\infty} \sum_{n=0}^{\infty} \frac{n}{\rho} \left\{ Z_{1,pn} J_n(q_1\rho) + Z_{2,pn} Y_n(q_1\rho) \right\} \cos n\bar{\theta} \; e^{i\bar{\omega}_p t}$$

$$(4.3.1b)$$

$$+ \sum_{p=1}^{\infty} A_{pl} \cos \bar{\theta} \; ,$$

$$\tau_{rr}^d = -\frac{1}{b^2} \sum_{p=1}^{\infty} \sum_{n=1}^{\infty} q_1^2 \left\{ Z_{1,pn} \left[\left\{ \lambda - 2\mu \left(\frac{n(n-1)}{(q_1\rho)^2} - 1 \right) \right\} J_n(q_1\rho) \right. \right.$$

$$\left. - \frac{2\mu}{q_1\rho} J_{n+1}(q_1\rho) \right]$$

$$(4.3.1c)$$

$$+ Z_{2,pn} \left[\left\{ \lambda - 2\mu \left(\frac{n(n-1)}{(q_1\rho)^2} - 1 \right) \right\} Y_n(q_1\rho) \right.$$

$$\left. \left. - \frac{2\mu}{q_1\rho} Y_{n+1}(q_1\rho) \right] \right\} \sin n\bar{\theta} \; e^{i\bar{\omega}_p t} \; ,$$

52

$$\tau_{\theta\theta}^d = -\frac{1}{b^2} \sum_{p=1}^{\infty} \sum_{n=1}^{\infty} q_1^2 \Bigg\{ Z_{1,pn} \Bigg[\left\{ \lambda + \frac{2\mu n(n-1)}{(q_1\rho)^2} \right\} J_n(q_1\rho)$$

$$+ 2\mu \frac{1}{q_1\rho} J_{n+1}(q_1\rho) \Bigg] + Z_{2,pn} \Bigg[\left\{ \lambda + \frac{2\mu n(n-1)}{(q_1\rho)^2} \right\} Y_n(q_1\rho) \quad (4.3.1d)$$

$$+ \frac{2\mu}{q_1\rho} Y_{n+1}(q_1\rho) \Bigg] \Bigg\} \sin n\bar{\theta} \; e^{i\omega_p t} \; ,$$

$$\tau_{r\theta}^d = -\frac{2\mu}{b^2} \sum_{p=1}^{\infty} \sum_{n=0}^{\infty} \frac{n}{\rho^2} \Big\{ Z_{1,pn} \Big[q_1\rho J_{n+1}(q_1\rho) - (n-1) J_n(q_1\rho) \Big]$$

$$(4.3.1e)$$

$$+ Z_{2,pn} \Big[(q_1\rho) Y_{n+1}(q_1\rho) - (n-1) Y_n(q_1\rho) \Big] \Big\} \cos n\bar{\theta} \; e^{i\omega_p t}$$

where the superscript d has been used to designate the contribution from the dilatational wave solution in the cylinder.

The contribution from the shear wave solution in the cylinder is obtained from Section III.2, in a similar manner, and is given as follows:

$$v_r^s = -\frac{1}{b} \sum_{p=1}^{\infty} \sum_{n=1}^{\infty} \frac{n}{\rho} \Big\{ Z_{3,pn} J_n(q_2\rho)$$

$$(4.3.2a)$$

$$+ Z_{4,pn}(q_2\rho) Y_n(q_2\rho) \Big\} \sin n\bar{\theta} \; e^{i\omega_p t} - \sum_{p=1}^{\infty} B_{p1} \sin \bar{\theta} \; ,$$

53

$$v_{\bar{\theta}}^s = -\frac{1}{b} \sum_{p=1}^{\infty} \sum_{n=0}^{\infty} q_2 \left\{ Z_{3,pn} \left[\frac{n}{q_2\rho} J_n(q_2\rho) - J_{n+1}(q_2\rho) \right] \right.$$

$$\left. + Z_{4,pn} \left[\frac{n}{q_2\rho} Y_n(q_2\rho) - Y_{n+1}(q_2\rho) \right] \right\} \cos n\bar{\theta} \, e^{i\omega_p t} \qquad (4.3.2b)$$

$$- \sum_{p=1}^{\infty} B_{p1} \cos \bar{\theta} \, ,$$

$$\tau_{rr}^s = -\frac{2\mu}{b^2} \sum_{p=1}^{\infty} \sum_{n=1}^{\infty} \frac{n}{\rho^2} \left\{ Z_{3,pn} \left[(n-1) J_n(q_2\rho) - (q_2\rho) J_{n+1}(q_2\rho) \right] \right.$$

$$(4.3.2c)$$

$$\left. + Z_{4,pn} \left[(n-1) Y_n(q_2\rho) - (q_2\rho) Y_{n+1}(q_2\rho) \right] \right\} \sin n\bar{\theta} \, e^{i\omega_p t} \, ,$$

$$\tau_{\bar{\theta}\bar{\theta}}^s = -\tau_{rr}^s \, , \qquad (4.3.2d)$$

$$\tau_{r\bar{\theta}}^s = -\frac{\mu}{b^2} \sum_{p=1}^{\infty} \sum_{n=0}^{\infty} q_2^2 \left\{ Z_{3,pn} \left[\left(\frac{2n(n-1)}{(q_2\rho)^2} - 1 \right) J_n(q_2\rho) \right. \right.$$

$$\left. + \frac{2}{q_2\rho} J_{n+1}(q_2\rho) \right] + Z_{4,pn} \left[\left(\frac{2n(n-1)}{(q_2\rho)^2} - 1 \right) Y_n(q_2\rho) \right. \qquad (4.3.2e)$$

$$\left. \left. + \frac{2}{q_2\rho} Y_{n+1}(q_2\rho) \right] \right\} \cos n\bar{\theta} \, e^{i\omega_p t} \, .$$

4. Scattered Wave Solution in the Surrounding Medium

In this section, we write the stresses and displacements associated with the scattered wave solution in the surrounding medium and which contribute to the response of the cylinder to an incoming shear wave. In doing this we use the results of Section III.3, with $\sin n\theta$ and $\cos n\theta$ interchanged and $\bar{n} = -n$. Thus,

$$
v_r^{dm} = \frac{1}{b} \sum_{p=1}^{\infty} \sum_{n=1}^{\infty} \left\{ Z_{5,pn}\left[\frac{n}{\rho} J_n(q_3\rho) - q_3 J_{n+1}(q_3\rho)\right] \right.
$$

$$
\left. - iZ_{5,pn}\left[\frac{n}{\rho} Y_n(q_3\rho) - q_3 Y_{r+1}(q_3\rho)\right] \right\} \sin n\bar{\theta}\ e^{i\omega_p t} \qquad (4.4.1a)
$$

$$
+ \sum_{p=1}^{\infty} C_{p1} \sin \bar{\theta} ,
$$

$$
v_{\bar{\theta}}^{dm} = \frac{1}{b} \sum_{p=1}^{\infty} \sum_{n=0}^{\infty} \left\{ Z_{5,pn}\left[\frac{n}{\rho} J_n(q_3\rho)\right] \right.
$$

$$
\qquad (4.4.1b)
$$

$$
\left. - iZ_{5,pn}\left[\frac{n}{\rho} Y_n(q_3\rho)\right] \right\} \cos n\bar{\theta}\ e^{i\omega_p t} + \sum_{p=1}^{\infty} C_{p1} \cos \bar{\theta} ,
$$

$$
\tau_{rr}^{dm} = -\frac{1}{b^2} \sum_{p=1}^{\infty} \sum_{n=1}^{\infty} q_3^2 \left\{ Z_{5,pn}\left[\left\{\lambda_m - 2\mu_m\left(\frac{n(n-1)}{(q_3\rho)^2} - 1\right)\right\} J_n(q_3\rho) \right.\right.
$$

$$
\left. - \frac{2\mu_m}{(q_3\rho)} J_{n+1}(q_3\rho)\right]
$$

$$
\qquad (4.4.1c)
$$

$$
- iZ_{5,pn}\left[\left\{\lambda_m - 2\mu_m\left(\frac{n(n-1)}{(q_3\rho)^2} - 1\right)\right\} Y_n(q_3\rho) \right.
$$

$$
\left.\left. - \frac{2\mu_m}{(q_3\rho)} Y_{n+1}(q_3\rho)\right]\right\} \sin n\bar{\theta}\ e^{i\omega_p t} ,
$$

$$\tau_{r\bar{\theta}}^{dm} = -\frac{2\mu_m}{b^2} \sum_{p=1}^{\infty} \sum_{n=0}^{\infty} \frac{n}{\rho^2} \left\{ Z_{5,pn}\left[(q_3\rho)J_{n+1}(q_3\rho) \right.\right.$$

$$\left. - (n-1)J_n(q_3\rho) \right] - iZ_{5,pn}\left[(q_3\rho)Y_{n+1}(q_3\rho) \right. \qquad (4.4.1d)$$

$$\left.\left. - (n-1)Y_n(q_3\rho) \right] \right\} \cos n\bar{\theta}\ e^{i\omega_p t}\ ,$$

$$v_r^{sm} = -\frac{1}{b} \sum_{p=1}^{\infty} \sum_{n=1}^{\infty} \frac{n}{\rho} \left\{ Z_{6,pn}\left[J_n(q_4\rho) \right]\right.$$

$$\qquad (4.4.2a)$$

$$\left. - iZ_{6,pn}\left[Y_n(q_4\rho) \right] \right\} \sin n\bar{\theta}\ e^{i\omega_p t} - \sum_{p=1}^{\infty} D_{p1} \sin \bar{\theta}\ ,$$

$$v_{\bar{\theta}}^{sm} = -\frac{1}{b} \sum_{p=1}^{\infty} \sum_{n=0}^{\infty} \left\{ Z_{6,pn}\left[\frac{n}{\rho} J_n(q_4\rho) - q_4 J_{n+1}(q_4\rho) \right]\right.$$

$$\left. - iZ_{6,pn}\left[\frac{n}{\rho} Y_n(q_4\rho) - q_4 Y_{n+1}(q_4\rho) \right] \right\} \cos n\bar{\theta}\ e^{i\omega_p t} \qquad (4.4.2b)$$

$$- \sum_{p=1}^{\infty} D_{p1} \cos \bar{\theta}\ ,$$

$$\tau_{rr}^{sm} = -\frac{2\mu_m}{b^2} \sum_{p=1}^{\infty} \sum_{n=1}^{\infty} \frac{n}{\rho^2} \left\{ Z_{6,pn}\left[(n-1)J_n(q_4\rho) \right.\right.$$

$$\left. - (q_4\rho)J_{n+1}(q_4\rho) \right] - iZ_{6,pn}\left[(n-1)Y_n(q_4\rho) \right. \qquad (4.4.2c)$$

$$\left.\left. - (q_4\rho)Y_{n+1}(q_4\rho) \right] \right\} \sin n\bar{\theta}\ e^{i\omega_p t}\ ,$$

$$\tau_{r\bar{\theta}}^{sm} = -\frac{\mu_m}{\nu^2} \sum_{p=1}^{\infty} \sum_{n=0}^{\infty} q_4^2 \left\{ Z_{6,pn} \left[\left\{ \frac{2n(n-1)}{(q_4\rho)^2} - 1 \right\} J_n(q_4\rho) \right. \right.$$

$$\left. + \frac{2}{(q_4\rho)} J_{n+1}(q_4\rho) \right] - i Z_{6,pn} \left[\left\{ \frac{2n(n-1)}{(q_4\rho)^2} - 1 \right\} Y_n(q_4\rho) \right. \qquad (4.4.2d)$$

$$\left. \left. + \frac{2}{(q_4\rho)} Y_{n+1}(q_4\rho) \right] \right\} \cos n\bar{\theta} \; e^{i\omega_p t} \; .$$

In the preceding expressions, the superscripts dm and sm denote quantities associated with waves of dilatation and waves of distortion, respectively. The definitions of q_3 and q_4 are those appropriate to a viscoelastic medium as given in Eq. (3.4.16). In the case of an elastic medium, these expressions reduce to $q_3 = bk_{p3}$ and $q_4 = bk_{p4}$, where k_{p3} and k_{p4} are defined in the text immediately following Eqs. (3.3.1) and (3.3.3), respectively.

5. Superposition of Solutions to Enforce the Boundary Conditions

The procedure in this section parallels that followed in Section III.8. We combine the contributions presented in the preceding sections so as to satisfy the boundary conditions, namely, that the inner boundary of the cylinder be traction free, and that, at the outer boundary, the cylinder displacements and appropriate stress components are continuous with those of the surrounding medium. Thus,

at $\rho = \beta$ (inner boundary of the cylinder),

$$\tau_{rr}^d + \tau_{rr}^s = 0 \; , \qquad (4.5.1a)$$

$$\tau_{r\bar{\theta}}^d + \tau_{r\bar{\theta}}^s = 0 \; , \qquad (4.5.1b)$$

57

and at $\rho = 1$ (outer boundary of the cylinder),

$$\tau_{rr}^{d} + \tau_{rr}^{s} - \tau_{rr}^{dm} - \tau_{rr}^{sm} = \tau_{rr}^{B} , \qquad (4.5.1c)$$

$$\tau_{r\theta}^{d} + \tau_{r\theta}^{s} - \tau_{r\theta}^{dm} - \tau_{r\theta}^{sm} = \tau_{r\theta}^{B} , \qquad (4.5.1d)$$

$$v_{r}^{d} + v_{r}^{s} - v_{r}^{dm} - v_{r}^{sm} = v_{r}^{B} , \qquad (4.5.1e)$$

$$v_{\theta}^{d} + v_{\theta}^{s} - v_{\theta}^{dm} - v_{\theta}^{sm} = v_{\theta}^{B} , \qquad (4.5.1f)$$

where, again: 1) the superscripts d and s are affixed to quantities stemming from the dilatational and shear solutions to the wave equation in the cylinder; 2) the superscripts dm and sm are appended to stresses and displacements resulting from the dilatational and shear solutions to the wave equation in the medium; and 3) the superscript B identifies the boundary tractions and displacements associated with the incident wave.

After the terms entering into (4.5.1) are computed from the appropriate expressions, and the common trigonometric and exponential factors are divided out, the resulting nonhomogeneous system of linear equations in the unknown coefficients of superposition, $Z_{j,pn}$, may be written in matrix form as

$$\left[c_{ij,pn} \right] \left\{ \zeta_{j,pn} \right\} = \left\{ \mathcal{B}_{i,pn} \right\}$$

$$(4.5.2)$$

$$(p = 1, 2, 3, \ldots), \quad (n = 0, 1, 2, \ldots) ,$$

where $c_{ij,pn}$ stems from the coefficient of $\zeta_{j,pn}$ in the ith equation of Eq. (4.5.1); $\mathcal{B}_{i,pn}$ stems from the term on the right-hand side of the ith equation of Eq. (4.5.1); $\{\zeta_{j,pn}\}$, the solution vector, is a 6 x 1 column matrix, whose complex elements are the unknown coefficients of superposition. It should be noted again that there is a different matrix equation (4.5.2) for each pair of values of p and n.

58

The elements of $c_{ij,pn}$ and $\mathcal{B}_{i,pn}$ are shown in detail in Appendices A and B.

After solving for $\{\zeta_{j,pn}\}$ for a sufficient number of values of p and n to ensure adequate convergence, we may calculate, to the desired accuracy, the stresses and displacements in the cylinder as

$$\tau_{rr} = \tau_{rr}^d + \tau_{rr}^s \quad , \quad \tau_{r\theta} = \tau_{r\theta}^d + \tau_{r\theta}^s \quad , \quad \tau_{\theta\theta} = \tau_{\theta\theta}^d + \tau_{\theta\theta}^s \quad , \quad (4.5.3a)$$

$$v_r = v_r^d + v_r^s \quad , \quad v_\theta = v_\theta^d + v_\theta^s \quad , \quad (4.5.3b)$$

where the terms appearing on the right-hand side of the above expressions are given in Eqs. (4.3.1) and (4.3.2).

SPECIAL FEATURES OF THE PRESENT ANALYSIS

1. Initial Conditions

We recall that the solution constructed in the preceding sections is the response of an elastic cylinder to a periodic train of pulses. However, by measuring time from the moment of pulse arrival, we may obtain the response to a single pulse acting on a cylinder initially unstrained and at rest, provided that we adjust the time between pulses so that, to a sufficient degree of accuracy, we achieve conditions of vanishing stresses and displacements in the cylinder and its vicinity — prior to the arrival of each pulse. Indeed, the success of the present technique depends chiefly on the possibility of obtaining stresses and displacements, before the pulse arrives, which are negligibly small compared to significant stress and displacement levels at later times. Essentially, this end is attained by providing sufficient "rest time," that is, making the time interval between pulses long enough to permit the cylinder wall to radiate sufficient energy out into the medium and return to an undeformed state of rest. Because the half period, T, is arbitrary, the parameters that control the rest time are to some extent arbitrary, enabling us to make an optimum choice of the rest time. Some discussion of this procedure is in order here. The rest time parameter, t_0, can be nondimensionalized as $(t_0 c_{dm}/b)$, that is, as the ratio of the rest time to the time required by the incident wave to perform a transit of the cylinder. By referring to Fig. 2, it can be seen that the rest time parameter can be expressed in terms of two additional nondimensional parameters that appear in the analysis, $(c_{dm}T/2b)$ and $(c_{dm}\Delta/2b)$, as

$$\frac{c_{dm}t_0}{b} = \frac{c_{dm}T}{2b} - \frac{c_{dm}\Delta}{2b} .$$

(5.1.1)

The pulse duration parameter, $(c_{dm}\Delta/2b)$, while not shown explicitly in the development preceding Eq. (5.1.1), enters into the Fourier coefficient a_p that determines the wave form. As Eq. (5.1.1) indicates, when the pulse duration is prescribed, the rest time parameter, and hence the rest time between pulses, may be varied by varying the parameter $(c_{dm}T/2b)$. This stems from the fact that the half time, T, enters the analysis as an arbitrary parameter. Thus, in any computations, the stresses and

displacements are obtained accurately only when by means of trial computations, the value of $(c_{dm}T/2b)$, and hence the rest time, has been so selected as to reduce the initial stresses and displacements of the response to a sufficiently low level. Fortunately, it has been found in the many cases presented that satisfactory results may be obtained if $(c_{dm}T/2b)$ is kept in the reasonably narrow range $10 \leq (c_{dm}T/2b) \leq 100$. The cases considered covered a wide range of cylinder-medium impedance mismatch and cylinder thicknesses, as well as a variety of pulse shapes.

Improved accuracy may be obtained by treating separately the response for small and for large values of the nondimensional time variable, $(c_{dm}\bar{t}/2b)$, where $\bar{t} = (t - t_0)$ and measures time with respect to the arrival of the incident wave. From Eq. (5.1.1), it can be anticipated that a decrease in the parameter $(c_{dm}\Delta/2b)$ would lead to further improvement in the initial conditions. Thus, for times less than the pulse duration, it may be advantageous to assign a value to $(c_{dm}\Delta/2b)$ that is less than the specified pulse duration. The corresponding computations are valid for times less than this altered pulse duration (for later times the actual pulse duration parameter must be used). This technique is particularly suitable for the case of a rectangular pulse, since in that case no change in the value of a_p is required. The foregoing considerations provide the basis for the device by which an incoming step pulse may be treated, namely, by making the pulse duration long enough so that the response reaches a steady state while $c_{dm}\bar{t}/2b$ remains less than $(c_{dm}\Delta/2b)$.

One further consideration is necessary to satisfactorily treat the initial conditions requirement. Since we have not fixed the cylinder with respect to any frame of reference, it will translate in response to each of the periodic pulses. In order that the solution be applicable to the case of a single transient pulse, we must remove from the displacements the rigid body contribution resulting from the preceding pulse. That is, we require that before the pulse arrives,

$$u_r \cos \theta - u_\theta \sin \theta \approx 0 . \qquad (5.1.2)$$

61

Referring to Fig. 2 we note that we may apply this condition at any time t^* where $-t_0 < t^* \leq t_0$, provided that the interval $(-t_0, t^*)$ represents a sufficient rest time. The manner in which the requirement, (5.1.2), is enforced is now described.

Using the dilatational and distortional potentials given by (3.2.7) and (3.2.14), we may write the displacements in the cylinder by using (3.2.4) and (3.2.11). The resulting expressions may be put in the form

$$
u_r = \sum_{p=1}^{\infty} \sum_{n=0}^{\infty} u_r^{pn} \cos n\theta \; e^{i\omega_p t} + \sum_{p=1}^{\infty} (\bar{A}_{p1} + \bar{B}_{p1}) \cos \theta \, , \qquad (5.1.3a)
$$

$$
u_\theta = \sum_{p=1}^{\infty} \sum_{n=1}^{\infty} u_\theta^{pn} \sin n\theta \; e^{i\omega_p t} - \sum_{p=1}^{\infty} (\bar{A}_{p1} + \bar{B}_{p1}) \sin \theta \, , \qquad (5.1.3b)
$$

where the u_r^{pn} and u_θ^{pn} are functions of the radial coordinate r. Enforcing (5.1.2) with the displacements (5.1.3) evaluated at $t = t^*$ requires that

$$
\sum_{p=1}^{\infty} (\bar{A}_{p1} + \bar{B}_{p1}) \approx - \sum_{p=1}^{\infty} u_r^{p1} e^{i\omega_p t^*} \approx \sum_{p=1}^{\infty} u_\theta^{p1} e^{i\omega_p t^*} \, , \qquad (5.1.4)
$$

as well as

$$
\sum_{p=1}^{\infty} \left[u_r^{po} + \sum_{n=2}^{\infty} u_r^{pn} \cos n\theta \right] e^{i\omega_p t^*} \approx \sum_{p=1}^{\infty} \sum_{n=2}^{\infty} u_\theta^{pn} \sin n\theta \; e^{i\omega_p t^*} \approx 0. \qquad (5.1.5)
$$

For convenience, the quantities u_r^{p1} and u_θ^{p1}, appearing in Eq. (5.1.4), are evaluated at $r = a$. Thus, after substituting (5.1.4) into (5.1.3), we may calculate the displacements in the cylinder as

$$u_r = \sum_{p=1}^{\infty} \left\{ u_r^{po}(r) + \left[u_r^{p1}(r) - u_r^{p1}(a) \, e^{-i\omega_p(t-t^*)} \right] \cos\theta \right.$$

$$\left. + \sum_{n=2}^{\infty} u_r^{pn}(r) \cos n\theta \right\} e^{i\omega_p t} ,$$

(5.1.6a)

$$u_\theta = \sum_{p=1}^{\infty} \left\{ \left[u_\theta^{p1}(r) - u_\theta^{p1}(a) \, e^{-i\omega_p(t-t^*)} \right] \sin\theta \right.$$

$$\left. + \sum_{n=2}^{\infty} u_\theta^{pn}(r) \sin n\theta \right\} e^{i\omega_p t} .$$

(5.1.6b)

For the case of an incident shear wave we may cast the displacement expressions, in a form similar to those given by (5.1.3), as

$$v_r = \sum_{p=1}^{\infty} \sum_{n=1}^{\infty} v_r^{pn} \sin n\bar{\theta} \, e^{i\omega_p t} + \sum_{p=1}^{\infty} (\bar{A}_{p1} - \bar{B}_{p1}) \sin\bar{\theta} ,$$

(5.1.7a)

$$v_{\bar{\theta}} = \sum_{p=1}^{\infty} \sum_{n=0}^{\infty} v_\theta^{pn} \cos n\bar{\theta} \, e^{i\omega_p t} + \sum_{p=1}^{\infty} (\bar{A}_{p1} - \bar{B}_{p1}) \cos\bar{\theta}$$

$$+ \sum_{p=1}^{\infty} \bar{C}_{p1} ,$$

(5.1.7b)

where v_r^{pn} and v_θ^{pn} are functions of the radial coordinate r. The term $\sum \bar{C}_{p1}$ has been included in the expression for $v_{\bar{\theta}}$ to account for the possibility of a rigid body rotation.

63

In this case, since the particle motion is perpendicular to the direction of wave propagation, the consequence of not fixing the cylinder with respect to any frame of reference, is a translation of the cylinder in response to each of the periodic pulses — in a direction normal to that of the progression of the wave. In addition, a rotation of the cylinder may occur. To remove the translation and rotation, we require that the following two conditions be satisfied separately:

$$v_r \sin \bar{\theta} + v_{\bar{\theta}} \cos \bar{\theta} = 0 , \tag{5.1.8a}$$

$$v_{\bar{\theta}} = 0 . \tag{5.1.8b}$$

Again, referring to Fig. 2, we see that we may apply these conditions at any time $\tilde{t}^*$ where $-t_0 \le \tilde{t}^* \le t_0$, provided that the interval $(-t_0, \tilde{t}^*)$ represents a sufficient rest time. Thus, enforcing (5.1.8), with the displacements evaluated at $t = \tilde{t}^*$ and $r = a$, leads to

$$v_r = \sum_{p=1}^{\infty} \left\{ \left[v_r^{p1}(r) - v_r^{p1}(a) \, e^{-i\omega_p(t-\tilde{t}^*)} \right] \sin \theta \right.$$

$$\left. + \sum_{n=2}^{\infty} v_r^{pn}(r) \sin n\bar{\theta} \right\} e^{i\omega_p t} , \tag{5.1.9a}$$

$$v_{\bar{\theta}} = \sum_{p=1}^{\infty} \left\{ \left[v_{\bar{\theta}}^{po}(r) - v_{\bar{\theta}}^{po}(a) \, e^{-i\omega_p(t-\tilde{t}^*)} \right] \right.$$

$$+ \left[v_{\bar{\theta}}^{p1}(r) - v_{\bar{\theta}}^{p1}(a) \, e^{-i\omega_p(t-\tilde{t}^*)} \right] \cos \bar{\theta} \tag{5.1.9b}$$

$$\left. + \sum_{n=2}^{\infty} v_{\bar{\theta}}^{pn}(r) \cos n\bar{\theta} \right\} e^{i\omega_p t} .$$

2. Convergence Criteria

Criteria to control the degree of convergence of the various summations involved in calculating the stress and displacement quantities were introduced into the computer program used in the present study. These criteria are now described.

The stresses and displacements may be represented in the form

$$\sigma_{ij} = \sum_{p=1}^{\infty} \sum_{n=0}^{\infty} \sigma_{ij}^{pn}(\rho, \theta, t) \quad , \quad i,j = r,\theta ,$$

$$u_i = \sum_{p=1}^{\infty} \sum_{n=0}^{\infty} u_i^{pn}(\rho, \theta, t) \quad , \quad i = r,\theta .$$

Integers N_a, N^*, M^*, relating to the degree of accuracy desired, were selected and the summations were carried out so that:

1) For each integer p, and for N^* consecutive terms in the n summation,

$$\frac{|\sigma_{ij}^{pk}(\rho,\theta,t)|}{|\sum_{n}^{k-1} \sigma_{ij}^{pn}(\rho,\theta,t)|} \leq 10^{-N_a} \quad , \quad \frac{|u_i^{pk}(\rho,\theta,t)|}{|\sum_{n}^{k-1} u_i^{pn}(\rho,\theta,t)|} \leq 10^{-N_a} .$$

The value N of the integer n, at which the condition required by step 1) is met, of course varied, with the integer p, the point (ρ, θ, t), and the subscript ij, or i.

2) Using the appropriate value of the summation over n up to n = N, the summation over p was carried out so that for M* consecutive terms.

$$\frac{\left|\sum_{n=1}^{N} \sigma_{ij}^{pn}(\rho,\theta,t)\right|}{\left|\sum_{k=1}^{p-1}\sum_{n=1}^{N} \sigma_{ij}^{kn}(\rho,\theta,t)\right|} \leq 10^{-N_a} \quad, \quad \frac{\left|\sum_{n=1}^{N} u_{i}^{pn}(\rho,\theta,t)\right|}{\left|\sum_{k=1}^{p-1}\sum_{n=1}^{N} u_{i}^{kn}(\rho,\theta,t)\right|} \leq 10^{-N_a} .$$

Control of the computations was maintained to evaluate the influence of the summations over n, on the current summation over p, so that the n-summation (number of circumferential modes) could be either terminated or increased if required. Codes present in the computer output indicated whether the convergence criteria were met. All the results presented were obtained with at least graph plotting accuracy. In the neighborhood of maximum values, accuracy to four figures was obtained in most cases.

66

SECTION VI

DISCUSSION OF NUMERICAL RESULTS

1. General Considerations

An IBM digital computer was employed to obtain the solution of the system of matrix equations (3.8.2) and (4.5.2) and to carry out the associated stress and displacement computations defined by Eqs. (3.8.3) and (4.5.3). The computer program is described in Volume II of the present report (Ref. 16). In the discussion that follows, even though results are presented for specific dimensional values of geometric and physical parameters, these results are applicable for the wider class of cases covered by the nondimensional values of these parameters, namely, the

ratios $\frac{h}{R}$, $\frac{\lambda}{\mu}$, $\frac{\lambda_m}{\mu}$, $\frac{\mu_m}{\mu}$, and $\frac{\gamma_m}{\gamma}$. This applies for the case of a viscoelastic medium as well as for an elastic medium.

It should be pointed out that the results presented throughout this report are given in nondimensional form. For example, in Fig. 5 we have given the hoop stress and displacement time

histories in terms of the quantities $\frac{\sigma_{\theta\theta}}{\sigma_0}$ and $\frac{2\mu}{\sigma_0}\frac{u_x}{b}$, respectively. The sign of the actual stress, or displacement, is thus determined by the sign of σ_0, the stress associated with the incident wave. In the case of the response to an incident shear wave, it is the sign of τ_0 that determines the sign of the actual stress or displacement.

2. Computations Performed to Illustrate the Validity of the Present Method

In this section, we illustrate the capability of the present technique to satisfy the requirements of an initial undeformed state of rest in the cylinder. For this purpose, the stress and displacement response to a rectangular pulse lasting five transits of the cylinder has been computed. The Fourier coefficients a_p, which define the incident wave form, are

67

$$a_p = \begin{cases} 0 & , \quad p \quad \text{even} \\ \dfrac{4\sigma_p}{p\pi} \sin \dfrac{p\pi}{2} \sin \dfrac{p\pi}{2} \left[\dfrac{c_{dm}\Delta}{2b} \Big/ \dfrac{c_{dm}T}{2b} \right] & , \quad p \quad \text{odd} \end{cases} \qquad (6.1.1)$$

where σ_p is the Lanczos factor (Ref. 17) that can be included
as a factor in the Fourier coefficients to improve convergence
of the series representing the incident wave in the neighborhood
of discontinuities. When σ_p is set equal to unity, Eq. (6.1.1)
leads to the usual Fourier series representation.

The results of the computations, and pertinent parameters
employed, are shown in Fig. 5. After the pulse has passed, and
as the disturbed cylinder radiates energy outward into the medium,
the maximum hoop stress, $\sigma_{\theta\theta}$ at $\theta = 90°$, is seen to vanish.
This shows that, although steady-state solutions are employed by
the present technique, an unstrained state of rest can be attained
in the cylinder and adjacent medium before the arrival of the next
pulse. Note, for exampl., the circled points in Fig. 5a. These
represent the computed values of $\sigma_{\theta\theta}$ in the intervals

$-1 \leq (c_{dm}t/2b) \leq 0$ and $11.5 \leq (c_{dm}t/2b)$. Referring to Fig. 5b,
we note that during early transit times the character of the dis-
placement response is nonlinear and suggests considerable rapid
deformation of the cylinder. Later, the displacement time his-
tories of the representative points selected become linear and
parallel — suggesting motion essentially of rigid body charac-
ter — and in response to an infinite step pulse would continue
to exhibit this behavior. After the rectangular pulse has passed,
the cylinder regains its original shape, but remains displaced in
the amount of the rigid body motion. It was precisely this rigid
body displacement that was removed from the periodic solution in
Section V.1, entitled "Initial Conditions." Thus, Figs. 5a and
5b illustrate the feasibility of the present technique.

3. Comparisons with Published Data for the Response to an
    Incident Dilatational Step Pulse

Comparisons of results obtained for limiting cases of the
present problem with corresponding published data are exhibited
in Figs. 6 through 9. In all comparison cases, the incident
wave is a step pulse. As stated earlier, an incident rectangular

pulse, of duration sufficient for the response to reach static conditions, can be substituted for an incident step pulse. Therefore, the Fourier coefficient a_p has the form given in (6.1.1).

Figures 6 and 7 are concerned with the response of an infinite cylindrical cavity in an elastic medium. In Fig. 6, the cavity displacements obtained by the present technique at $\theta = 0°$, $90°$, and $180°$, are compared with those given in Ref. 3. Agreement is excellent except for early times.

The maximum cavity stress response to a step pulse is the hoop stress at $\theta = 90°$. In Fig. 7a, values of this stress calculated by the present analysis are compared with those obtained in Refs. 2, 4, and 5. For times greater than the first half transit, essential agreement prevails between the present method and Refs. 4 and 5. The stresses predicted in Ref. 2 are somewhat lower than those given by the other analyses up to the time when maximum values are reached. Then all results approach the static value given by the Kirsch formulas (Ref. 18). The results of Refs. 4 and 5, shown on Fig. 7a, are for various truncations of the representation of the deformation in circumferential modes. As pointed out previously, the present analysis differs from those of the other references in that it does not constrain a priori the number of circumferential modes taken to represent the solution. Instead, it permits this choice to be governed, at each space and time point, by the condition that the solution converge to a specified degree of accuracy. For times less than the first half transit, there are significant differences between the results obtained in this fashion and those of the other references. By contrast, results from the present analysis for a three-mode truncation (and which, therefore, represent less accurate predictions of the response) are identical with the corresponding values obtained for the same truncation in Ref. 4 over the entire range. Thus, it may be inferred from Fig. 7a that, for the case of an incident step pulse, a three-mode representation gives reasonably satisfactory values during times in the neighborhood of the maximum response, but constitutes a highly inaccurate approximation to the deformation during early transit time. This is shown even more forcibly in Fig. 7b. Nevertheless, the close agreement that, for a three-mode truncation, exists between the results of the present analysis and those of Ref. 4, indicates that the time dependence is treated properly by the present technique.

69

In Fig. 7b the hoop stress computed by the present method at $\theta = 0°$, for the case of a step pulse impinging on a cylindrical cavity, is compared with corresponding data given in Refs. 2, 4, and 5. Again, these references present results obtained by various truncations of the representation in circumferential modes, and again, some degree of agreement prevails among these computations during later transit times. However, wide disagreement exists for earlier times, particularly during the first transit, when even the sign of the stress response is in contention.

As in the comparison at $\theta = 90°$, the results obtained at $\theta = 0°$ by the present method, for a three-mode truncation, agree very closely with those of Ref. 4 over the entire range. Over most of the range considered, and especially for the early transit times, these results are at variance with those obtained when the number of modes is adjusted to comply with the requirements of convergence at each space point and time being considered. This shows that the discrepancy stems from the circumferential mode representation and not from the treatment of the time dependence. It is unlikely that a deformation, and hence a stress response, which, during the early stages of transit of the incident wave, involves only part of the cavity (namely, its front), could be properly represented by three modes. In view of this, and since the initial value predicted by the present method for the hoop stress at $\theta = 0°$ is zero (pointed out in Ref. 4 to be the correct value), it is felt that the early response is more realistically described by the present technique, even as compared to Ref. 5, in which six modes were employed. After one quarter transit, the close agreement with Ref. 5 is to be noted.

In Fig. 8 the results of the present method, which stem from the theory of elasticity, are compared with the corresponding data given by Ref. 7 for the hoop stress response in a thin cylindrical shell of various thicknesses (h/R = .0048, .019, .0381) at $\theta = 90°$, to an incoming step pulse. Two media with significantly different shear modulii are considered. The results of Ref. 7 stem from an analysis of the cylinder by a thin shell theory in which the cylinder acts as a membrane. For each shell curve, two sets of points obtained by the present technique have been plotted, one for the hoop stress at the middle surface, and a second at the inner surface representing the additional effect of bending. As can be seen, the difference between the middle surface and inner boundary stresses appears to be negligible for the thinnest of the three shells. For the thickest, the difference reaches a value of about 10 per cent. Moreover, some

70

differences exist between the response as determined by the present analysis and that of Ref. 7. Of course, it is only to be expected that elasticity theory and thin shell theories will yield differing results. However, it is observed in Fig. 8 that as the shell becomes thinner, the shell theory predictions do not come into closer agreement with those of elasticity theory. Therefore, on the basis of the available information, it is not possible to determine at what value of the thickness to radius ratio the thin shell theory ceases to be valid. In an effort to determine the source of the divergence of the results, as the shells become thinner, between the shell theory predictions and those of the theory of elasticity, we note that in Ref. 7 the deformation of the shell is constrained to three modes. In addition to the total response, Fig. 9 shows the time history of the contribution of each mode as given in Ref. 7 for the case of the shell with thickness to radius ratio of .019. Points computed by the present method, but with the same truncation as in Ref. 7, for the total response and its component modes are also shown in Fig. 9, along with the total response (present analysis) that satisfies the convergence requirements. The agreement that, except for early transit times, prevails between the two responses demonstrates that the discrepancy between the present results and the case of Ref. 7 is not due to an insufficient number of circumferential modes in the analysis of Ref. 7. Figure 9 shows that the major discrepancy resides in the third mode (the n = 2, or inextensional, mode). It is further noted that the results for the cavity case and all the other shell cases considered in this report (including some of those of Ref. 7 shown in Fig. 8b) indicate that the number of transit times required to approach the static condition does not seem to be significantly dependent on the material as well as geometric properties of the shell and the surrounding medium. This value seems to remain at about six to eight transit times. By contrast, the response reproduced from Ref. 7 in Fig. 9 departs from this general behavior as the shells become thinner.

4 Results Obtained by the Present Analysis for the Response
   to an Incident Dilatational Wave (Elastic Medium)

Figure 10 illustrates the influence of liner thickness on the response to an incoming dilatational step pulse. The maximum stress response, the hoop stress at $\theta = 90°$, is shown. When the incident wave passes from the medium into a relatively stiffer cylinder (slow granite into concrete), the effect of increasing liner thickness is to reduce the peak liner stress. When passage of the incident wave is into a relatively softer cylinder (fast granite into concrete), increasing the liner thickness increases the peak stress. The appearance of a more oscillatory response, with increasing thickness, should be noted for the softer liner.

71

The influence of liner thickness on the displacement response, when the liner material is stiffer than that of the medium, is illustrated in Figs 11a and 11b (where, for ease of comparison, the curves of Fig. 5b are presented again in Fig. 11b). An incoming dilatational rectangular wave, five transit times in duration, is the input for both of these cases. The liners in Figs. 11a and 11b have a thickness to radius ratio, h/R, equal to .01 and .2, respectively. As expected, the thicker, and hence stiffer, shell experiences much less deformation of the cross section (measured by the vertical distance between the two $\tilde{u}_r$ curves).

Also, as can be determined from Figs. 11a and 11b by the onset of pure rigid body motion (parallel portions of the curves), the full deformation is realized earlier in the thicker shell. It may be noticed that, as the back of the wave passes over the cylinder, the front of the cylinder ($\theta = 0°$) experiences the sharper variation in displacement. This effect is accentuated by an increase in the liner thickness. After passage of the wave, the thicker shell regains its original shape first. As expected, the total translation of the shell is independent of the thickness. Additional results, Fig. 11c, suggest that when the liner material is sufficiently softer than that of the medium, a change in liner thickness does not appreciably influence the over-all deformation.

Figure 12 contains results obtained by the present analysis that apply to a dilatational step pulse traveling through an infinite elastic medium, and impinging upon an elastic cylinder, for four separate sets of cylinder and medium elastic properties. These were selected so as to study the influence of impedance mismatch. Curves G-C and G-S apply to an elastic environment having the properties of granite and lined by concrete and steel cylinders, respectively. In case G-C, the incident wave transmits energy from a relatively "stiffer" to a softer elastic environment (value of Young's Modulus). In case G-S, the disturbance is transmitted from a relatively softer to a stiffer elastic environment, with attendant magnification of peak stress in the cylinder. Curves Sa-C and Sa-S apply to an elastic environment having the properties of sandstone and lined also by concrete and steel cylinders, respectively. Again, the magnification of the peak stress is greater as the disturbance passes from a relatively softer to a stiffer medium. In this case, the difference in magnification of peak response is even more striking but not surprising, since sandstone is much softer than granite and has practically the same properties as concrete. The dependence of the magnification of the incident stress amplitude upon impedance mismatch has been demonstrated previously in Ref. 7 for thin shells. In this connection, the impedance ratio parameter, $(\gamma_m c_{dm}/\gamma c_d)$, has been indicated, for the case corresponding to each curve, on Fig. 12. It will be observed that decreasing values of this parameter are associated with increasing values of peak response.

72

The effect of the stress wave form upon the maximum stress for a liner embedded in an elastic medium is illustrated in Fig. 13. The results for three cases of incoming dilatational plane waves are presented. The wave forms (see Fig. 2b) are: 1) a step pulse; 2) a triangular wave; and 3) a linear rise-exponential decay wave form, having the same rise time as the triangular wave. The expressions for a_p, which describe wave forms 2) and 3), are given in Appendix B. All three waves have the peak value σ_0. As can be seen, the step pulse produces the most critical response, eventually reaching a static value of 2.37. The response in cases 2) and 3) are identical during the rise time. The value of the hoop stress in these cases continues to increase during the passage of the peak of the incident wave across the liner, and decreases after the peak has passed the back of the liner. The response to the triangular wave does not reach nearly as high a peak value and decreases more rapidly. This effect stems from the rate of decay parameter that defines the exponential decay and for this case gives a higher value of incident stress to that wave form than that of the triangular wave at corresponding transit times. All responses should give a value of $\sigma_{\theta\theta}$ equal to zero at less than 1/2 transit. The slight discrepancy from this, shown by the response to the step pulse in Fig. 13, reflects the fact that it is more difficult to represent a step function by a Fourier series than a linear rise.

5. Results Obtained by the Present Analysis for the Cylinder Response to an Incident Dilatational Plane Wave in a Viscoelastic Medium

Results of a computational effort concerned with the response of an elastic cylinder, embedded in a viscoelastic medium, to an incident dilatational plane wave, are presented in Figs. 14 through 19. The values of parameters defining th   are identical with those of the concrete cylinder er'   .t elastic medium discussed in the preceding subs(nnec-tion with Fig. 12. The viscoelastic propertie: ium are described by the standard linear solid discusse,   .on III.5 (see Fig. 4). The values of the instantaneous e.   .arameters and the mass of the medium were held constant. T   properties are identical with those of sandstone considered   viously as an elastic medium in the cases treated in Figs.   and 13. They are given by the values of E_m, ν_m, and γ_m shown in the figures along with the corresponding values for the elastic liner. Also

73

kept constant was the value of the viscoelastic parameter, Ω_1/Ω_2, which was set equal to unity. The three remaining nondimensional ratios that describe the viscoelastic properties of the medium were permitted to range through a set of values. The parameters τ_1/Ω_1 and τ_2/Ω_2, set equal to each other in each case, took on the magnitudes .25 and .1. The relaxation-time parameter, $c_{dm}/\Omega_2 b$, was assigned the spectrum of values 0, .1, 1, 10, and ∞. Note that the lower end of this spectrum, $c_{dm}/\Omega_2 b = 0$, corresponds to the limiting case of an elastic-relaxed material, while the upper end $c_{dm}/\Omega_2 b = \infty$, applies to another limiting case, that of an elastic-unrelaxed material.

It is well known that the model used in the present analysis describes only the general features of the actual viscoelastic behavior of soils under dynamic loading. Accordingly, the values assigned to the viscoelastic parameters should not be construed as being fully representative of specific materials. However, these values are significant in that they fall within practical ranges and lead to a spectrum of results from which meaningful qualitative conclusions can be drawn.

The influence on the response of the cylinder of variation in the viscoelastic parameters of the medium, when the time history of the incident stress wave at the front of the cylinder is a step function, is illustrated in Figs. 14 and 15. The maximum stress response, $\sigma_{\theta\theta}$ at the inner surface and $\theta = 90°$, is plotted in Fig. 14. In these figures, the upper and lower curves correspond to elastic media whose properties are described by the unrelaxed $(c_{dm}/\Omega_2 b = \infty)$ and relaxed $(c_{dm}/\Omega_2 b = 0)$ elastic modulii, respectively.

In general, the effect of viscoelasticity in the surrounding medium is to increase, in some cases drastically, the stress response in the liner over that associated with the elastic-unrelaxed medium. This increase is characterized by two major trends. One trend is associated with a decrease in the relaxation time (indicated by a decrease in the value of $c_{dm}/\Omega_2 b$), the other with a decrease in the ratios τ_1/Ω_1 and τ_2/Ω_2. At early times, before the maximum response associated with an elastic-unrelaxed medium is reached, the increase in stress corresponding to a decrease in the relaxation time is relatively slight for larger values (of order 100) of the parameter $c_{dm}/\Omega_2 b$, but

becomes far more significant as the magnitude of the relaxation time decreases to the order of one transit time of the elastic-unrelaxed wave front ($c_{dm}/\Omega_2 b = 10$, 1). This can be seen, for example, in Fig. 14a, which corresponds to the case $\tau_1/\Omega_1 = \tau_2/\Omega_2 = .25$. Up to the time when the peak stress is reached ($c_{dm}\bar{t}/2b \leq 2.5$), the stress response in the case $c_{dm}/\Omega_2 b = 100$ is identical with that corresponding to a purely elastic (unrelaxed) medium. During the same time interval, the stress for $c_{dm}/\Omega_2 b = 10$ grows to a value about 20 per cent larger than the peak stress in the case of the purely elastic medium while, for $c_{dm}/\Omega_2 b = 1.0$, it reaches a value 100 per cent larger. As $c_{dm}/\Omega_2 b \rightarrow 0$, the stress approaches the value associated with the purely elastic-relaxed medium, which is more than double that of the peak stress in the liner embedded in the purely elastic-unrelaxed medium. It should be noted that the peak stress in the case of the elastic-relaxed medium is almost three times that in the case of the elastic-unrelaxed medium. This pattern of increased stress response for decreased relaxation time, observed at $c_{dm}\bar{t}/2b = 2.5$, is magnified with time as the material in the viscoelastic environment continues to relax and the liner must resist larger deformations in the medium. Ultimately, the stress can be expected, in all the cases where the medium has a finite relaxation time, to reach the steady-state conditions associated with an elastic-relaxed medium. This process, clearly indicated in Fig.14, is shown to be extremely slow for large values of $c_{dm}/\Omega_2 b$, $100 \leq c_{dm}/\Omega_2 b \leq \infty$. However, the approach to the steady-state condition occurs far more rapidly as the value of $c_{dm}/\Omega_2 b$ decreases below 10. When this condition is reached, the stress has about 2-1/2 times the value of the peak stress associated with the elastic-unrelaxed medium. Setting $\tau_1/\Omega_1 = \tau_2/\Omega_2 = 1$ in the creep laws developed in Section III.5 is another way to reduce these laws to the stress-strain relations pertaining to the medium whose properties are purely elastic (unrelaxed). Thus, when τ_1/Ω_1 and τ_2/Ω_2 approach unity, the viscoelastic curves for the entire spectrum of relaxation times must merge into a common curve — the curve associated with the elastic-unrelaxed medium. Taking that curve as a basis for comparison, the sizable spread of the viscoelastic curves in Fig. 14a gives a clear indication of the magnitude of the magnification experienced by the major stress in the liner due to a

75

decrease in the value of τ_1/Ω_1 and τ_2/Ω_2. Figure 14b, in which $\tau_1/\Omega_1 = \tau_2/\Omega_2 = .1$, gives further evidence of this trend. It can be noticed in this figure that the peak stress in the case of the elastic-relaxed medium is now five times greater than the peak stress in the case of an elastic-unrelaxed medium, as compared to three times greater when $\tau_1/\Omega_1 = \tau_2/\Omega_2 = .25$ (Fig. 14a). Figures 14a and 14b both show that the curves corresponding to the two elastic media diverge quickly from each other. Since the curves corresponding to finite relaxation times range in between these two curves, it may be concluded that, if the ratios of τ_1/Ω_1 and τ_2/Ω_2 are appreciably less than unity, the representation of a viscoelastic medium purely by its elastic-unrelaxed or its elastic-relaxed properties may lead to results that are either unconservative or too conservative.

In the present discussion, valid conclusions can also be drawn for step pulses of finite duration. Depending on the pulse duration and the degree of viscoelasticity in the medium, stresses may be induced in the buried cylinder that are drastically larger than the peak stress predicted by considering the medium to be purely elastic (unrelaxed). The longer the duration of the pulse or the smaller the relaxation time, the higher the stress will be, with the elastic-relaxed condition constituting an upper bound. Conversely, short pulses in a medium with a sufficiently long relaxation time may not induce a response appreciably different from the response associated with the purely-unrelaxed medium. As a final note concerning Fig. 14 it should be mentioned that the discrepancies between the curves at the time of arrival of the pulse can be attributed to difficulties sometimes encountered in approximating, by means of Fourier series, the discontinuity of the incident step pulse for the values of the parameter $b/c_{dm}T$ necessary to obtain a sufficient rest time (see Section V).

Figure 15 is concerned with the deformation of the inner surface of the cylinder (described by $\tilde{u}_x$ at 0°, 90°, and 180°) due to the incident step pulse. As expected, the trends shown by the curves in this figure parallel those for the stress response. It is seen that the principal effect of viscoelasticity of the medium is to increase the deformations over those predicted for a purely elastic (unrelaxed) medium, without changing their character appreciably. The deformation increases with decreasing relaxation times or decreasing ratios of elastic-relaxed to elastic-unrelaxed properties $(\tau_1/\Omega_1, \tau_2/\Omega_2)$. The full liner deformation, indicated by the onset of rigid body motion, is

reached later when the medium is viscoelastic than when the medium is purely elastic (relaxed or unrelaxed). The rigid body motion itself increases when the relaxation time or the ratios of relaxed to unrelaxed elastic properties are reduced.

The influence of viscoelasticity of the surrounding medium on the response of the cylinder to an incident stress wave with a triangular time history at the front of the cylinder (see Fig. 13) is shown in Figs. 16 and 17. During the period of increasing stress response, the family of curves in Fig. 16 shows a magnification of the stress with decreasing relaxation time that is very similar to that observed in the case of the incident step pulse. The peak stress associated with the elastic-relaxed medium is nearly 2-1/2 times the peak stress associated with the elastic-unrelaxed medium. Again, the peak stresses corresponding to finite relaxation times in the medium are bracketed between these two stresses. Consequently, results obtained by treating a viscoelastic medium simply as an elastic-unrelaxed or elastic-relaxed medium may, for this incident wave form, again be either unconservative or too conservative.

It is interesting to note the combined effect that the rise time of the incident wave (1/2 transit) and the value of the relaxation time in the medium seem to have in the response of the cylinder. It is seen in Fig. 16 that early in the response, during a time interval comparable to the rise time of the incident wave, and for a medium with relaxation time at least as long as the rise time, the stress is identical with that associated with the elastic-unrelaxed medium. It should also be noted that, after the passage of the wave over the cylinder $(c_{dm}\tau/2b > 4)$, the liner stress decays more slowly in cases involving surrounding viscoelastic media than in cases involving elastic media. An explanation for the behavior of the stress response in the case of a viscoelastic medium is that it must involve primarily the slow process of creep strain recovery in the medium.

The deformation of the liner inner surface due to the incident triangular pulse is shown in Fig. 17, and is again described by $\tilde{u}_x$ at $0°$, $90°$, and $180°$. For the sake of simplicity we have presented only the curves corresponding to the elastic-relaxed and unrelaxed media and to the viscoelastic medium for which $c_{dm}/\Omega_2 b = 10$. The deformation for the case $c_{dm}/\Omega_2 b = 1.0$, is given in a subsequent figure (Fig. 19c). It is seen in Fig. 17 that, as in the case of an incident step pulse, the effect of viscoelasticity in the medium is to magnify the deformations without changing their essential character. The lower the relaxation time the larger the deformation, with the elastic-relaxed

77

curves constituting an upper bound. In the viscoelastic case, after the wave has passed, it is interesting to note how very long it takes for the cylinder to regain its original undeformed shape. This is indicated by the slow converging of the curves after the maximum deformation has been reached.

We now discuss another point of interest. Referring ahead to Fig. 19c, and in conjunction with Fig. 17, we note the attenuation of the maximum acceleration with decreasing values of the relaxation time down to at least $c_{dm}/\Omega_2 b = 1.0$, which the inner surface at $\theta = 0°$ experiences just after the passage of the pulse $(c_{dm}\bar{\tau}/2b \gtrless 5)$. However, the sharpness of the peaking of the displacement response at $\theta = 0°$ for the case of the elastic-relaxed medium indicates that, at some value of the relaxation time in the range $0 \leq c_{dm}/\Omega_2 b \leq 1.0$, the maximum acceleration would start to increase again and, for lower values of the relaxation time down to $c_{dm}/\Omega_2 b = 0$, would exceed that corresponding to the elastic-unrelaxed medium.

The influence of incident wave history on the response of a liner embedded in a viscoelastic medium is illustrated in Figs. 18 and 19. Figure 18, which is concerned with the maximum stress response, combines the results plotted in Fig. 14a for the case of an incident step pulse with those plotted in Fig. 16 for the case of a pulse of triangular form. It also includes results for the pulse with the linear rise-exponential decay history described in Fig. 13 and Section VI.4. For the sake of comparison, the curves presented in Fig. 13 are reproduced in Fig. 18a for the case where the medium is purely elastic (unrelaxed). The only other figure in this set containing results for a linear rise-exponential decay pulse is Fig. 18c, for the case $c_{dm}/\Omega_2 b = 1.0$.

It is seen from these figures that the effect of the viscoelasticity in the medium is to accentuate the differences between the stress responses to the three pulses. These differences increase with decreasing relaxation time. It can also be seen from the curves in Figs. 18a through 18d that the difficulties encountered in computing the onset of the stress response to a step pulse were not encountered in the case of the other two pulses.

A comparison of the deformations of the inner boundary of the cylinder due to the three incident stress waves is made in Fig. 19. This figure combines the curves presented in Figs. 15

and 17. It also presents the results obtained for the linear rise-exponential decay incident pulse in the case of the elastic-unrelaxed medium and the medium for which $c_{am}/\Omega_z b = 1.0$. For all the degrees of viscoelasticity considered, the step pulse induces the largest cylinder deformation (as measured by comparing the vertical distances between the $\tilde{u}_r$ curves) and the most rapid translation (indicated by $\tilde{u}_x$ at $90°$). The triangular pulse induces the smallest deformations. Of the two pulses of finite duration (triangular and linear rise-exponential decay), the triangular pulse causes the smaller final rigid body displacement of the cylinder and that displacement is attained earlier. Conversely, the peak acceleration during the decay of these two pulses shown to occur at $\theta = 0°$ by the sharper peaking of the corresponding $\tilde{u}_r$ curve, is the greatest in the case of the triangular pulse. Figure 19 demonstrates that the viscoelasticity of the medium has the effect of magnifying the differences in the response to the various pulses. This magnification is accentuated by reduction of the relaxation time.

6. Comparisons with Published Data of the Results Obtained by the Present Analysis for the Response to an Incident Shear Wave

In Fig. 20, the hoop stress response to an incident shear wave at $\bar{\theta} = 45°$ and $135°$ is compared with the results presented in Refs. 4 and 19. The remarks made in the discussion of Fig. 7 apply here as well. At times corresponding to the maximum stresses, the various results do not differ too widely, and all approach the static value given by the Kirsch formulas. However, for early times, when the incoming shear wave is still in transit across the cavity, three circumferential modes do not accurately describe the deformation. This again can be seen by comparing with the other references the results obtained by the present analysis, where we used that number of modes sufficient to obtain convergence of the solution and also a three-mode truncation. When the present computations were restricted to three modes, it can be seen that the results duplicated those of Ref. 4. However, the more accurate solution differs from that of Ref. 4 in that the maximum is reached at $\bar{\theta} = 135°$ at an earlier time than at $\bar{\theta} = 45°$.

79

7. Results Obtained by the Present Method for the Response to an Incident Shear Wave (Elastic Medium)

The cases presented in Figs. 21 and 22 were selected so as to study the influence of liner thickness on the response to an incident shear wave. The liner and medium parameters are the same as those selected to obtain the results shown in Fig. 10 for the case of an incident dilatational wave. The major stresses are the circumferential stresses, $\tau_{\theta\theta}$ at $\bar{\theta} = 45°$ and $135°$. As was noticed in the cavity comparison case (Fig. 20), the circumferential stress at $\bar{\theta} = 135°$ reaches its peak more rapidly than the corresponding response at $\theta = 45°$. The stresses at both angular positions, for these shells, apparently reach the same maximum. For these cases, the response per unit amplitude of the incident wave, as well as the overshoot, is greater than the corresponding response to an incident dilatational wave. These effects were also observed in the cavity response (Refs. 4 and 17). As in the case of an incident dilatational wave, an increase of liner thickness decreases (or increases) the response when the liner is stiffer (or softer) than the medium.

In Fig. 22, the influence of liner thickness on the displacement response is shown. Effects similar to those noticed in the response to an incident dilatational wave are indicated. As expected, the path of the rigid body motion is perpendicular to the direction of motion of the incident wave front. Also, as in the case of the incident dilatational wave, when the back of the wave passes over the cylinder, the front of the cylinder ($\theta = 0°$) experiences the sharper variation in displacement.

In Fig. 23, the influence of impedance mismatch on the response to an incident shear wave is illustrated. The parameters of the liner and surrounding medium are identical with those utilized to obtain the results presented on Fig. 12. The major stress response, $\tau_{\theta\theta}$, occurs at $\theta = 45°$ and $135°$, the maximum at $\bar{\theta} = 135°$ being reached earlier in time. It was noted in discussing Fig. 10, and is again observed here, that the magnification of peak stress is greater when the wave travels from a softer into a relatively stiffer medium. Also to be observed are the indications that the response to the shear wave involves considerably greater deformation effects than the corresponding response to a dilatational wave. For example, note the sharpness of the peak response on curve Sa-S, and also the tendency for the stress to continue to oscillate afterward.

80

The influence of wave form on the response to an incident shear wave is shown in Fig. 24. The liner and medium parameters are the same as those for which the results of Fig. 13 were obtained for the incident dilatational wave. The major stress response is that of the hoop stress, $\tau_{\theta\theta}$, and occurs at

$\bar{\theta} = 45°$ and $135°$, with the maximum being reached earlier at $\bar{\theta} = 135°$. The general character of the response is similar to that for the case of an incident dilatational wave. The most severe response again occurs when the incident wave form is that of a step pulse; and, again, for the parameters considered, the linear rise-exponential decay wave form induces a hoop stress response of greater magnitude, for comparable times — after the passage of the peak of the incident wave — than does a triangular wave form. The steeper character of the shear wave response has already been mentioned in connection with previous figures. The abrupt change in curvature of the response curve at $\bar{\theta} = 135°$, for the case of the step pulse, before the maximum is reached should be noted. The curves at $\bar{\theta} = 135°$ corresponding to the other wave histories exhibit a similar but more pronounced trend. In particular, the curve associated with the linear rise-exponential decay pulse shows a well-defined double peak.

8. Results Obtained by the Present Analysis for the Cylinder Response to an Incident Shear Wave in a Viscoelastic Medium

The numerical results for the response of the elastic cylinder to an incident shear wave, where the cylinder is embedded in a viscoelastic medium, are presented in Figs. 25 through 30. They were obtained for the same cylinder and viscoelastic media as in the case of the incident dilatational wave (Section VI.5). The histories of the incident shear waves are also the same as for the dilatational waves. They are described in Fig. 24. To assess the influence of the viscoelasticity of the medium, results for the elastic-unrelaxed medium are included as a limiting case. These results have already been presented in Figs. 23 and 24, and discussed in the preceding section.

The major stress response in the liner, $\tau_{\theta\theta}$ at the inner surface and $\bar{\theta} = 45°$ and $135°$, is shown in Fig. 25 for the case of the incident step pulse and in Fig. 26 for the case of the triangular pulse. In general, these results indicate that the principal effect of viscoelasticity in the surrounding medium is again to magnify the stress response as compared to that associated with the elastic-unrelaxed medium. The trends at $\bar{\theta} = 45°$ — increasing

stress response with decreasing relaxation time and also with ratios of relaxed to unrelaxed elastic properties — are very similar to those at $\bar{\theta} = 90°$ relating to the incident dilatational wave. Therefore, the discussion in Section VI.5 pertaining to Figs. 14 and 16 applies equally to the curves for $\bar{\theta} = 45°$ in Figs. 25 and 26a. In Fig. 25a, the per cent increase in stress at $c_{tm}\bar{t}/2b = 2.5$ resulting from the decrease in the relaxation time of the medium is practically identical with that observed previously in Fig. 14a at $c_{dm}\bar{t}/2b = 2.5$.

Again, the ratio of the peak stress associated with the elastic-relaxed medium to that associated with the elastic-unrelaxed increases from a value of about 3 in the case $\tau_1/\Omega_1 = \tau_2/\Omega_2 = .25$ (Fig. 25a), to a value of about 5 in the case $\tau_1/\Omega_1 = \tau_2/\Omega_2 = .10$ (Fig. 25b). The hoop stress response at $\bar{\theta} = 135°$, however, departs significantly from that at $\bar{\theta} = 45°$ in the case of both an incident step pulse and an incident triangular pulse. In both these cases, a complete reversal of the trends of stress magnification with viscoelasticity in the medium occurs at $\bar{\theta} = 135°$ during a time interval after the arrival of the pulse. In the cases where $\tau_1/\Omega_1 = \tau_2/\Omega_2 = .25$ (Figs. 25a and 26a), this decrease in the stress response with decreasing relaxation time stops before the stress associated with the elastic-unrelaxed medium has reached its maximum $(c_{tm}\bar{t}/2b = 2)$ and gives way to the more prevalent trend of increasing stress response. However, it is seen in Fig. 25b, where $\tau_1/\Omega_1 = \tau_2/\Omega_2 = .1$, that the hoop stress at $\bar{\theta} = 135°$ in the case of the elastic-relaxed medium remains considerably below the peak stress for the elastic-unrelaxed medium until about a half transit past this peak. This indicates that, at least for the case of an incident step pulse, the effect of decreasing the ratios τ_1/Ω_1 and τ_2/Ω_2 is not only to magnify the trend itself but also its duration. As $c_{dm}/\Omega_2 b \to 0$, a peculiarity associated with this trend at $\bar{\theta} = 135°$ is the appearance in Figs. 25a and 26a of a stress of opposite sign for a short time after the arrival of the pulse. This stress, barely noticeable in Figs. 25a and 26a, becomes much more prominent as τ_1/Ω_1 and τ_2/Ω_2 decrease (Fig. 25b).

Other effects of the viscoelasticity of the medium on the stress response at $\bar{\theta} = 135°$ can be seen in Figs. 25 and 26. The curve representing the response to an incident step pulse in the purely elastic (unrelaxed) medium goes through abrupt changes in curvature before reaching its peak. For the case of a triangular pulse (Fig. 26), these changes in curvature are more pronounced,

82

and the curve has what amounts to a double peak. With a decrease in relaxation time, this behavior is progressively less in evidence. It ceases to be noticeable for $c_{dm}/\Omega_2 b \leq 1.0$.

It was also pointed out in the preceding section that the stress response to an incident step pulse in the elastic-unrelaxed medium reaches its maximum earlier at $\bar{\theta} = 135°$ than at $\bar{\theta} = 45°$. It can be seen in Fig. 25 that this is also the case when the elastic-relaxed medium is involved. By contrast, the hoop stress response associated with the viscoelastic media for which $c_{dm}/\Omega_2 b = 1.0$, is never larger at $\bar{\theta} = 135°$ than at $\bar{\theta} = 45°$.

The influence of the shear wave history on the stress response of the liner inner surface at $\bar{\theta} = 45°$ and $135°$ is illustrated in Fig. 27 for the case of the medium for which $c_{dm}/\Omega_2 b = 1.0$.

This influence, when the medium is viscoelastic, can be compared to that when the medium is purely elastic (unrelaxed) by referring back to Fig. 24. For the finite value of the relaxation time considered here, it can be seen that the nature of the differences between the responses to the three distinct pulses described in Section VI.7 is preserved. Again, the effect of viscoelasticity is to magnify these differences. It can also be seen that the disappearance of the double peak for the response at $\bar{\theta} = 135°$ due to the viscoelasticity in the medium occurs in the case of the linear rise-exponential decay incident wave as well as in the case of triangular incident wave. By contrast with the responses shown in Fig. 24 for the case of the purely elastic (unrelaxed) medium, the stress responses at $\bar{\theta} = 45°$ in the case of the viscoelastic medium are almost identical in character with those at $\bar{\theta} = 135°$.

The nondimensional displacement response perpendicular to the path of the incident wave, $2\mu v_\theta/\tau_0 b$, at $\bar{\theta} = 0°$, $90°$ and $180°$, and at the liner inner surface, is presented in Figs. 28 through 30. It is given by $\tilde{v}_\theta$ at $0°$ and $180°$ and $\tilde{v}_r$ at $90°$. Since $\tilde{v}_r$ is an odd function of $\bar{\theta}$, the distance between opposite points along the diameter perpendicular to the path of the incident wave remains unchanged and $\tilde{v}_r$ at $\bar{\theta} = 90°$ — the middle curve in each set of three given in Figs. 28 through 30 — represents the translation of the whole cylinder. When the vertical distances between this curve and the other two curves ($\tilde{v}_\theta$ at $0°$ and $180°$) are equal — as they are for a substantial portion of the response — the diameter of the cylinder aligned

with the path of the wave experiences a pure rotation in addition to a translation equal to that of the perpendicular diameter.

The curves in Figs. 28 through 30 are very similar in character to those shown in Figs. 15, 17, and 19 for the response, $2\mu u_x/\sigma_0 b$, to incident dilatational pulses. They indicate similar trends. For all three incident waves — the step pulse, the triangular pulse, and linear rise-exponential decay pulse — the effect of a decrease in the relaxation time is to increase the translation described by $\tilde{v}_r$ at $\bar{\theta} = 90°$ and the rotation described by the other two displacements. Figure 28 indicates that, at least for the case of an incident step pulse, the same effect is induced by a decrease in the ratios τ_1/Ω_1 and τ_2/Ω_2. The curves in Fig. 29 for the case of an incident triangular pulse indicate that the sharp acceleration of the front of the cylinder, just before the intensity of the incident pulse at this point in the cylinder reduces to zero $(c_{tm}t/2b = 3)$, is at first attenuated by decreasing values of the relaxation time. Figure 30c shows that this trend continues at least until $c_{dm}/\Omega_2 b$ reduces to the value 1.0. However, as implied by the character of the curve for the displacement at $\bar{\theta} = 0°$ in the case of the elastic-relaxed medium, at some value of $c_{dm}/\Omega_2 b$ below unity the acceleration starts to increase again. It also becomes sizable at $\bar{\theta} = 90°$. The very slow recovery of the liner's original shape after the passage of the pulse is again indicated in Fig. 29 for the case $c_{dm}/\Omega_2 b = 1.0$, by the slow convergence of the curves.

Figure 30 illustrates the influence of the incident wave history on the displacement response. Again, a decrease in relaxation time magnifies the differences between the responses to the various pulses. It should be noted that for the case of a viscoelastic medium (Fig. 30c) as well as for the case of the elastic-unrelaxed medium (Fig. 30a), the sharp acceleration experienced by the front of the liner in the case of an incident triangular wave is far less pronounced in the case of the linear rise-exponential decay incident wave.

84

9. **Results Obtained by the Present Analysis for the Superposition of the Cylinder Responses to Incident Dilatational and Shear Waves in an Elastic Medium**

As formulated in Section I, the idealized problem with which the present analysis is concerned, is that of determining the response in a cylindrical liner buried in an infinite medium, the cylinder being subject, in succession, to plane dilatational and shear waves. Results obtained by the present analysis are valid for different physical situations, provided that effects other than those postulated can be neglected. For example, an air-induced ground loading results when a pressure wave, generated by an above-ground burst, travels along the surface of an elastic half space with superseismic velocity, V, where $V > c_{dm}$. Then, the results of Ref. 20 imply that plane dilatational and shear waves are transmitted into the half space. The transmitted wave fronts are inclined to the surface by the angles $\alpha_d = \arcsin (c_{dm}/V)$ and $\alpha_t = \arcsin (c_{tm}/V)$ respectively. These fronts are inclined to each other by the angle φ (see Fig. 1) where $\phi = \alpha_d - \alpha_t$. Thus, the incident shear wave impinges upon the liner at an angle φ with respect to the dilatational wave, and its time of arrival is delayed by an amount depending upon the location of the cylinder with respect to the surface loading. Now, if the liner is located at a depth such that the effects upon its response, of surface waves, as well as reflections from the surface, can be neglected, then the application of the present idealized analysis is justified.

Another physical situation for which the present analysis could be applicable was suggested in Ref. 21 and involves the direct-induced loading case (burst in direct contact with surface). In this case, justification for the use of the present analysis requires the validity of certain approximations. These involve the location of the cylinder with respect to the burst such that, in the ground effects, a spherical dilatational wave front may be replaced by a plane dilatational wave front (the previous assumptions on surface waves and reflections are also required). If the half space is assumed to be homogeneous and isotropic, only the response to an incident dilatational wave is needed to approximate this case. If the liner is assumed to be located in the lower level of a two-layered half space, then dilatational and shear waves will be refracted through the interface (assumed to be plane in this case). The angle between refracted dilatational and shear waves may be calculated in terms of the incident angle and the seismic velocities of the two layers. The delay between

arrival times, at the cylinder, of the refracted dilatational and shear waves may be calculated from the known location of the cylinder with respect to the layered medium interface. Sufficient distance between the liner and interface, so that interface reflections may be neglected, is required.

Two numerical problems, posed in Ref. 21 to illustrate the conditions discussed above, were analyzed. The parameters involved have little significance beyond providing somewhat realistic examples (on empirical grounds, the amplitude of the shear wave was chosen as one-third the amplitude of the dilatational wave).

As an example of air-induced loading, a concrete cylinder, 50 ft in diameter, is regarded as embedded in a homogeneous slow granite environment, at a depth that requires the transmitted waves to travel a distance of 150 ft before contact with the cylinder. The surface wave is assumed to be a step pulse, with velocity $V = 8500$ ft/sec. From the analysis of Ref. 20, it may be deduced that σ_0 and τ_0 are negative with respect to the cylinder coordinate systems of Fig. 1. Results obtained for this case are illustrated in Fig. 31. From the data presented on these figures, the angle φ between wave fronts is 19.7°, and the time of arrival of the shear wave, with respect to the arrival of the dilatational wave, $c_{dm}\delta t/b$, is calculated as $c_{dm}\delta t/b = 4.38$. On these figures are shown the components of the hoop stress response at the inner surface to the dilatational and shear waves, as well as the total response. Because the amplitude of the dilatational wave dominates, the maximum response for the points we computed is obtained at $\theta = 90°$, even though at this angle the effect of the shear wave response is to reduce the stress. At $\theta = 64.7°$, corresponding to $\bar{\theta} = 45°$, the shear wave response also reduces the stress, while at $\theta = 154.7°$ $(\bar{\theta} = 135°)$, an addition to the dilatational response occurs after the arrival of the shear wave.

As an example of a direct induced loading, a steel cylinder, 50 ft in diameter, is regarded as embedded in a fast granite layer, separated by a plane interface from a layer having a seismic dilatational velocity $c_{dm} = 6000$ ft/sec. A plane dilatational wave (the approximation to the spherical wave) impinges on the interface at an angle of incidence $\varphi'_d = 15°$. The cylinder is assumed to be located in the fast granite layer at a depth such that the refracted waves travel 100 ft before impinging on it. Denoting the refraction angles for the transmitted dilatational and shear waves as φ_{dm} and φ_{tm}, the angle φ between the

86

transmitted wave fronts may be found by utilizing the data in Fig. 32, along with the relations $\sin \varphi'_d / c_{dm} = \sin \varphi_{dm} / c_{dm} = \sin \varphi_{tm} / c_{tm}$. In this manner the angle φ is found to be $\varphi = 22°$. The delay time of the refracted shear wave with respect to the refracted dilatational wave is found to be $c_{dm} \delta t / b = 2.92$. Results for this case are presented in Fig. 32 in which component dilatational and shear responses, as well as their superposition, are shown. It should be noted that the dilatational component is identical with that shown in Fig. 12. The shear component represents that shown in Fig. 23, with a different abscissa scale, $c_{dm} t / b$, rather than the corresponding shear wave parameter, $c_{tm} t / b$. Again, because of the dominance of the dilatational wave amplitude, the maximum hoop stress for the points we computed occurs at $\theta = 90°$.

REFERENCES

(1) Baron, M.L., Bleich, H.H., and Weidlinger, P., "Theoretical Studies on Ground Shock Phenomena," Technical Report of the Mitre Corporation, SR-19, October 1960.

(2) Baron, M.L., and Matthews, A.T., "Diffraction of a Pressure Wave by a Cylindrical Cavity in an Elastic Medium," *Journal of Applied Mechanics*, Sept. 1961.

(3) Baron, M.L., and Parnes, R., "Displacement and Velocities Produced by the Diffraction of a Pressure Wave by a Cylindrical Cavity in an Elastic Medium," *Journal of Applied Mechanics*, June 1962.

(4) Paul, S.L., and Robinson, A.R., "Interaction of Plane Elastic Waves with a Cylindrical Cavity," RTD-TDR-63-3021 Air Force Weapons Laboratory, Kirtland Air Force Base, New Mexico, June 1963.

(5) Logcher, R.D., "A Method for the Study of Failure Mechanisms in Cylindrical Rock Cavities Due to the Diffraction of a Pressure Wave," School of Engineering, Massachusetts Institute of Technology, Technical Report T62-5, July 1962.

(6) Baron, M.L., and Parnes, R., "Diffraction of a Pressure Wave by a Cylindrical Shell in an Elastic Medium," *Proceedings of the Fourth U.S. National Congress of Applied Mechanics*, June 1962.

(7) Baron, M.L., and Parnes, R., "Diffraction of a Pressure Wave by an Elastically Lined Cylindrical Cavity in an Elastic Medium," The Mitre Corporation, Report SR-44, Dec. 1961; "Further Studies on the Diffraction of a Pressure Wave by an Elastically Lined Cylindrical Cavity in an Elastic Medium," The Mitre Corporation, Report SR-72, September 1962.

(8) Bisplinghoff, R.L., Isakson, G., and Pian, T.H., "Methods in Transient Stress Analysis," *Journal of the Aeronautical Sciences*, Vol. 17, No. 5, May 1950.

(9) Redwood, M., *Mechanical Waveguides*, Pergamon Press, 1960.

(10)   Sternberg, E., "On the Integration of the Equations of
       Motion in the Classical Theory of Elasticity," *Archives
       for Rational Mechanics and Analysis*, Vol. 6, No. 1, 1960.

(11)   Mow, C.C., and McCabe, W.L., "Dynamic Stresses in an
       Elastic Cylindrical Lining of Arbitrary Thickness in an
       Elastic Medium," The Mitre Corporation, Report SR-57,
       August 1962, *Proceedings ASCE*, Vol. 89, No. EM-3, Part 1,
       June 1963.

(12)   Garnet, H., and Kayel, R., "Sound Scattering of a Steady
       State Plane Wave by a Hollow Cylinder of Arbitrary Thick-
       ness," Office of Naval Research Contract NOnr-346(00) FBM
       Technical Rept. No. 4, and Grumman Research Dept. Memoran-
       dum RM-223, September 1963.

(13)   McLachlan, N.W., *Bessel Functions for Engineers*, Oxford
       Press, 2nd edition, 1955.

(14)   Bland, D.R., *The Theory of Linear Viscoelasticity*, Pergamon
       Press, 1960.

(15)   Harkin, J.B., "Theoretical Study of Energy Distribution in
       a Half-Space Under Dynamic Loads," AFSWC-TDR-62-43, July
       1962, Section 4.

(16)   Nolan, F., *Dynamic Stresses in a Thick Elastic Cylinder
       Subject to Transient Pressure Loadings*, Vol. II: Dis-
       cussion of Computer Program, Air Force Weapons Laboratory
       Report WL TR 65-20, 1965.

(17)   Hamming, R.W., *Numerical Methods for Scientists and Engi-
       neers*, McGraw Hill Book Company, New York, 1962, pp. 297-300.

(18)   Timoshenko, S. and Goodier, J.N., *Theory of Elasticity*, Second
       edition, New York: McGraw Hill Book Co., 1951, p. 80.

(19)   Baron, M.L., and Matthews, A.T., "Diffraction of a Shear
       Wave by a Cylindrical Cavity in an Elastic Medium,"
       Journal of Applied Mechanics, March 1962.

(20)   Cole, J.D., and Huth, J.H., "Stresses Produced in a Half
       Plane by Moving Loads," *Jour. of Applied Mechanics*, Vol. 25
       December 1958.

(21) Private Communications from Lt. J. Johnson, Project Officer,
      Contract AF29(601)-5993, Kirtland Air Force Base.

(22) Erdélyi, A., Magnus, W., Oberhettinger, F., and Tricomi, F.G.,
      <u>Higher Transcendental Functions</u>, Bateman Manuscript Project,
   Vol. 2, McGraw Hill Book Co., New York, 1953.
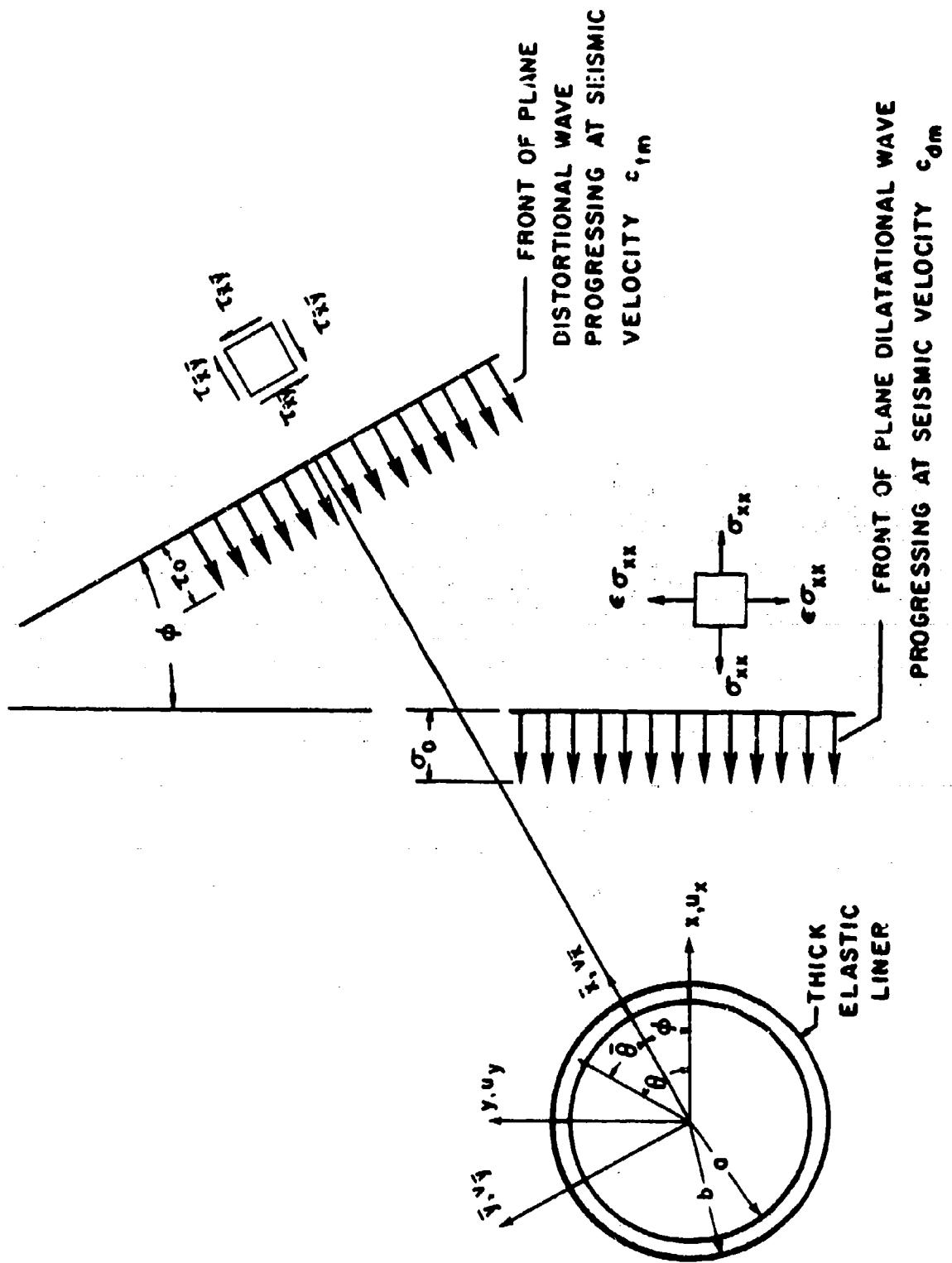
Fig. 1 CYLINDRICAL LINER, COORDINATE SYSTEMS, AND INCOMING PLANE WAVES.

91
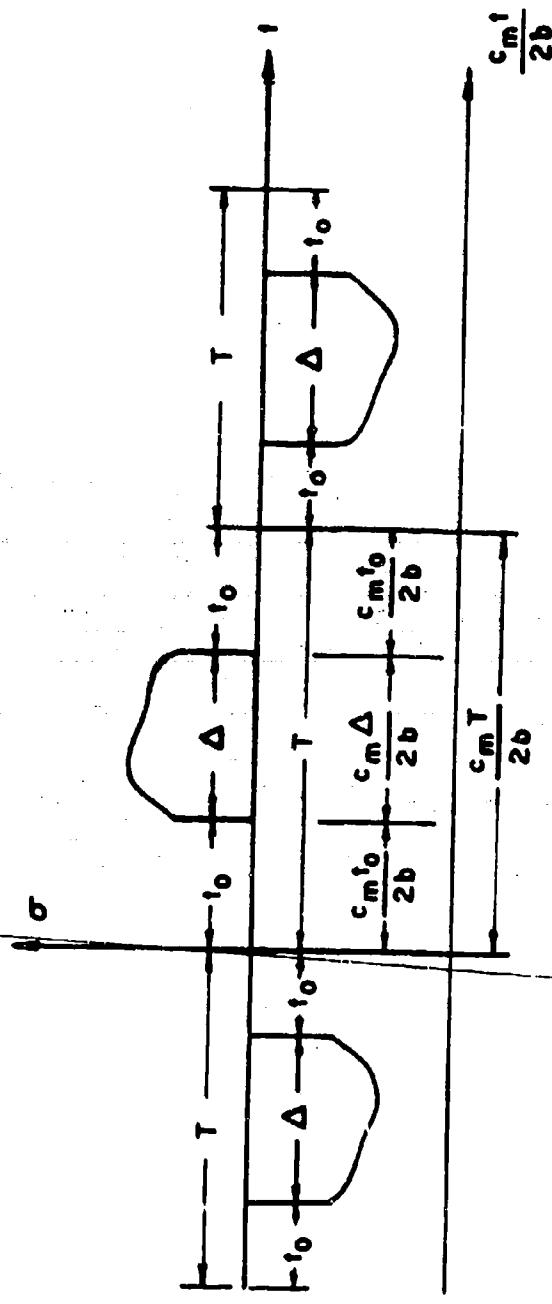
$$c_m, \sigma = \begin{cases} c_{dm}, \sigma_{xx} \text{ for incoming dilatational wave} \\ c_{im}, \tau_{ij} \text{ for incoming shear wave} \end{cases}$$

Fig. 2a   TRAVELING WAVES IN REAL TIME AND NON-DIMENSIONAL TRANSIT TIME COORDINATES.

RECTANGULAR WAVE FORM
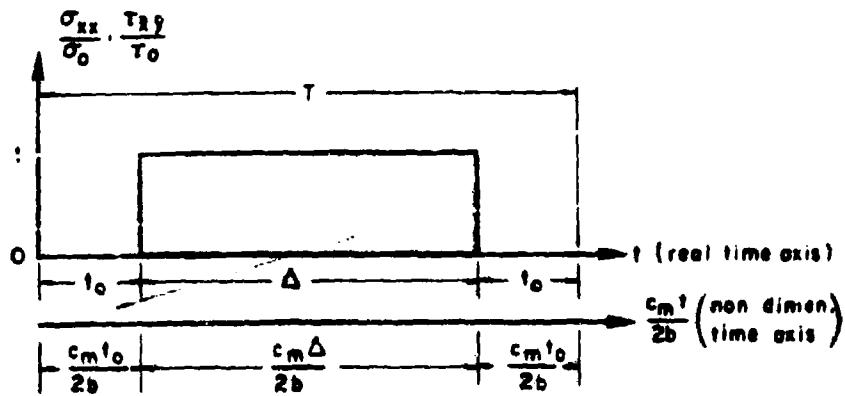
TRIANGULAR WAVE FORM
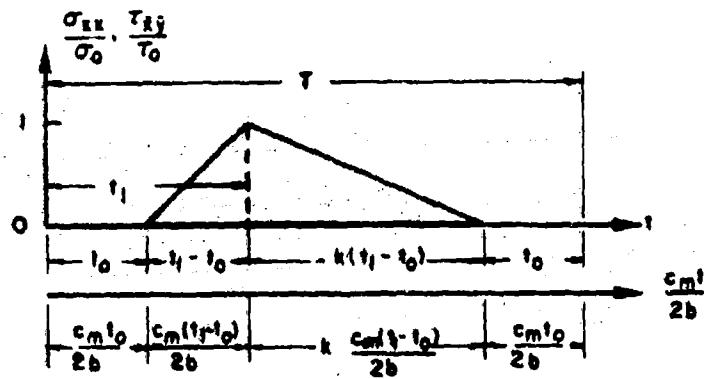
LINEAR RISE-EXPONENTIAL DECAY WAVE FORM
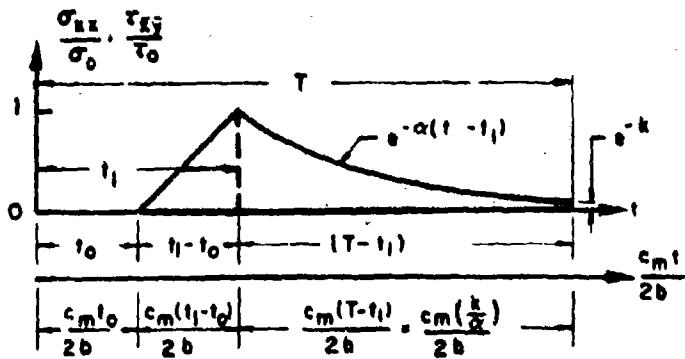
$$c_m = \begin{cases} c_{dm} & \text{for incoming dilatational wave} \\ c_{tm} & \text{for incoming shear wave} \end{cases}$$

Note: k is selected so that the incident stress is negligeably small at t = T

Fig. 2b. RECTANGULAR, TRIANGULAR, AND LINEAR RISE-EXPONENTIAL DECAY WAVE FORMS

ELEMENT OF LINER
SHOWING STRESS
NOTATION

THICK
ELASTIC
LINER
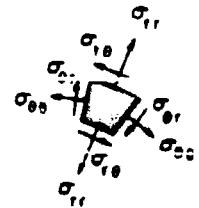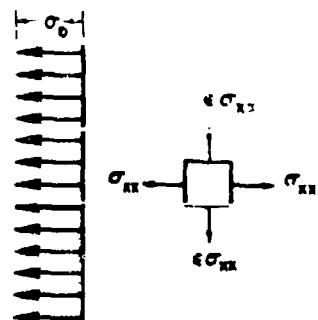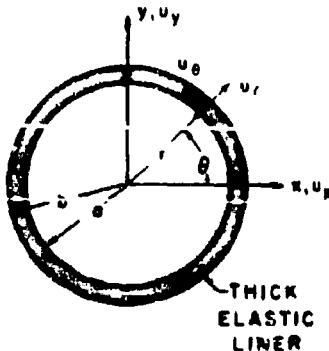
FRONT OF PLANE
DILATATIONAL WAVE
PROGRESSING WITH
SEISMIC VELOCITY
c_{dm}

(a) DILATATIONAL WAVE

ELEMENT OF LINER
SHOWING STRESS
NOTATION

THICK
ELASTIC
LINER
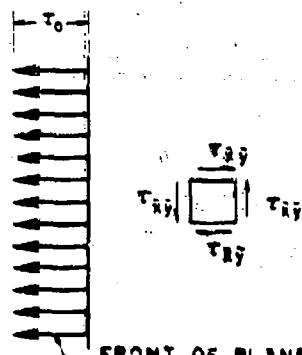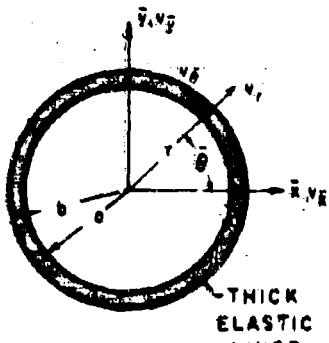
FRONT OF PLANE
SHEAR WAVE
PROGRESSING WITH
SEISMIC VELOCITY
c_{sm}

(b) SHEAR WAVE

Fig.3. CYLINDRICAL LINER, INCOMING WAVES, COORDINATE SYSTEM,
STRESS AND DISPLACEMENT NOTATION.

94
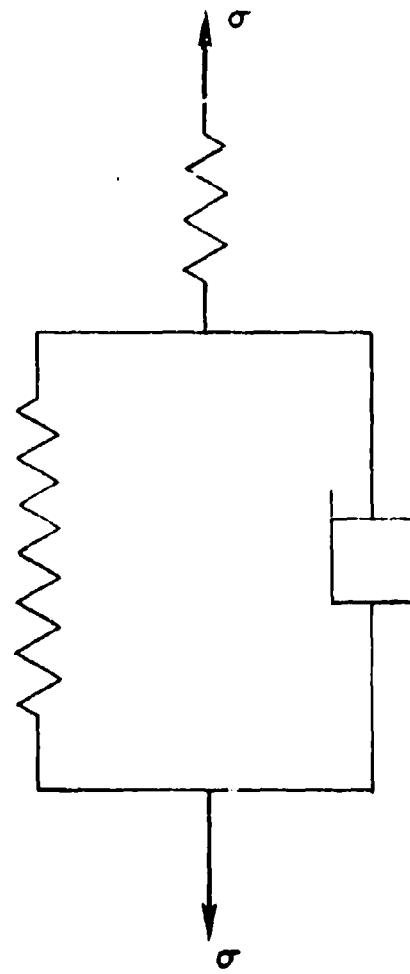
Fig. 4   MECHANICAL MODEL OF A STANDARD LINEAR SOLID.

LINER CONCRETE, $E = 2.5 \times 10^6$ psi, $\nu = .2$, $\gamma = 4.5$ slugs/ft.^{3}

MEDIUM: SLOW GRANITE, $E_m = 1.0 \times 10^6$ psi, $\nu_m = .25$, $\gamma_m = 5.2$ slugs/ft.^{3}

○ Computed points illustrating satisfaction of initial conditions criteria.
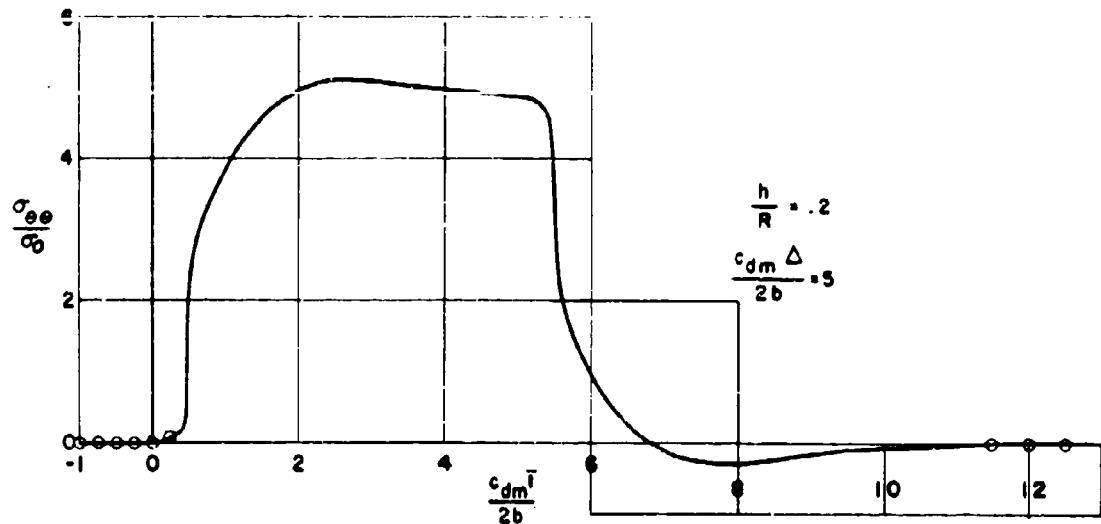
(a) HOOP STRESS AT $\theta = 90°$
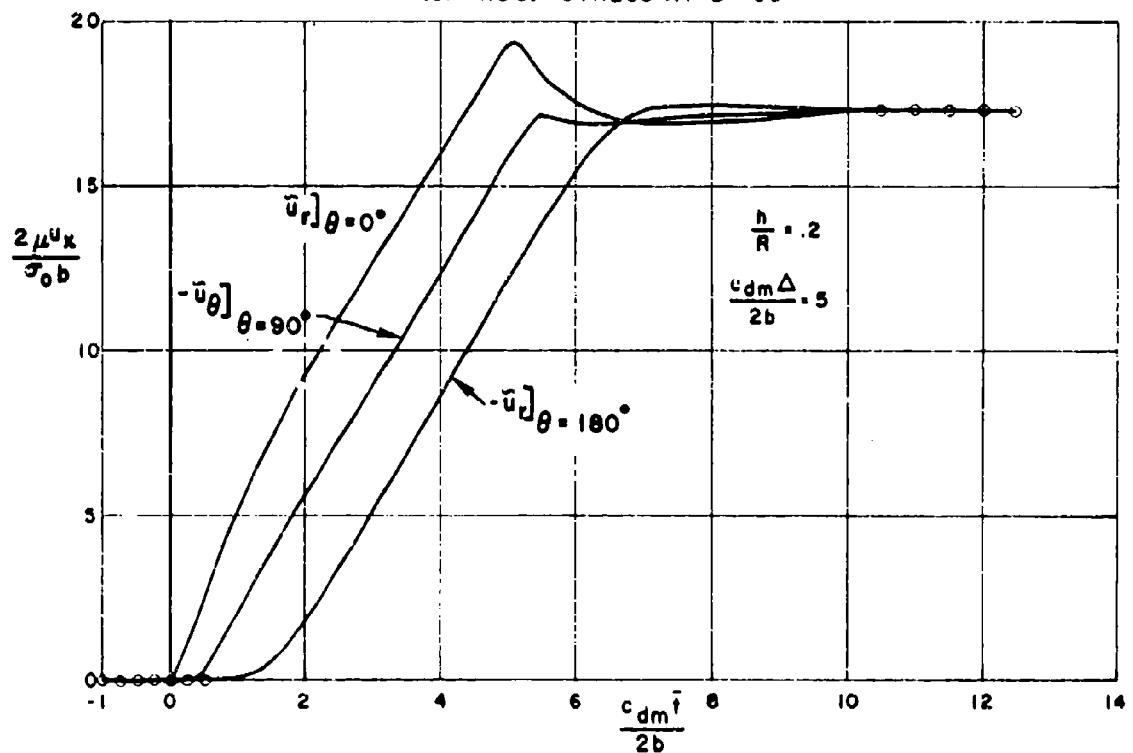
(b) DISPLACEMENTS

Fig. 5   RESPONSE OF LINER INNER SURFACE TO INCIDENT
DILATATIONAL RECTANGULAR WAVE (Elastic medium)

96

⊙ △ ▢ Points obtained by present analysis.
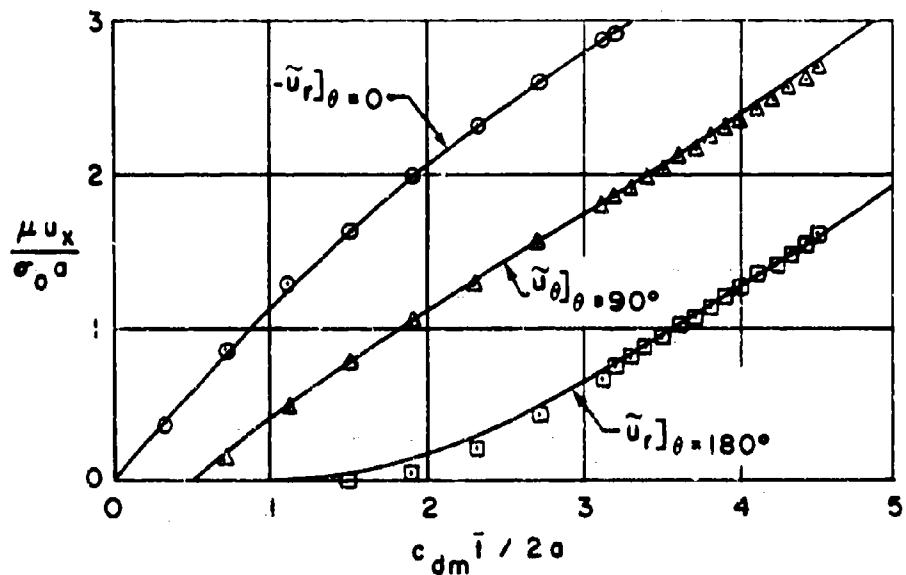
Note : Curves reproduced from Ref. 3.

Fig. 6. COMPARISON OF CAVITY DISPLACEMENTS WITH
THOSE OBTAINED BY REF. 3.
(ELASTIC MEDIUM)

⊙ Results obtained by present method, using number of modes
   required by convergence criteria

△ Results obtained by present method, using n = 0,1,2
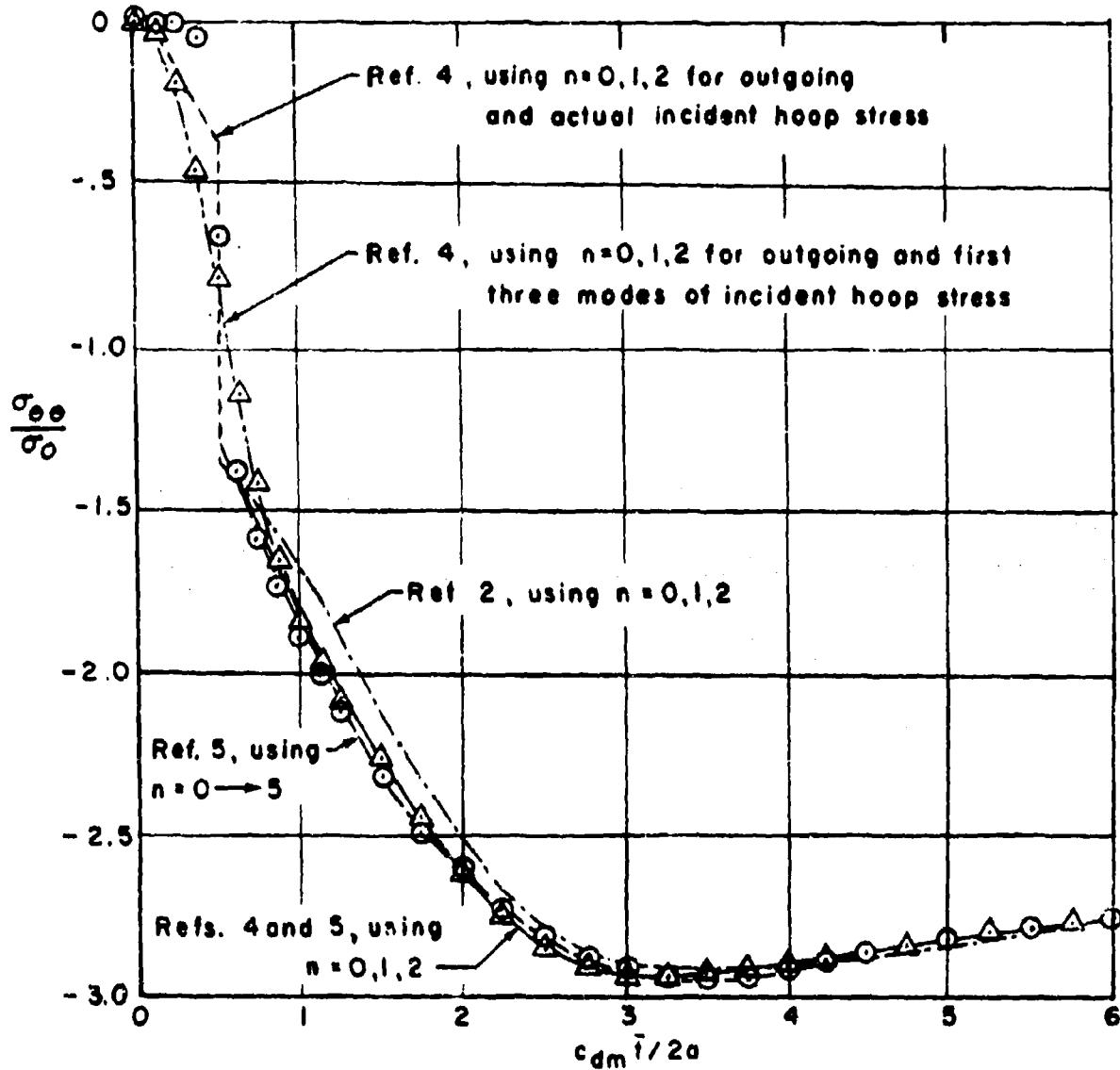
Note   Curves reproduced from Ref. 4

Fig. 7a. COMPARISON OF PRESENT COMPUTATIONS WITH THOSE OF
REFS. 2,4 AND 5 FOR HOOP STRESS AT $\theta = 90°$ DUE TO INCIDENT
DILATATIONAL STEP PULSE, AT BOUNDARY OF CAVITY IN ELASTIC
MEDIUM, $\epsilon = 1/3$

98

⊙ Results obtained by present method, using number of modes required by convergence criteria

△ Results obtained by present method, using n = 0,1,2
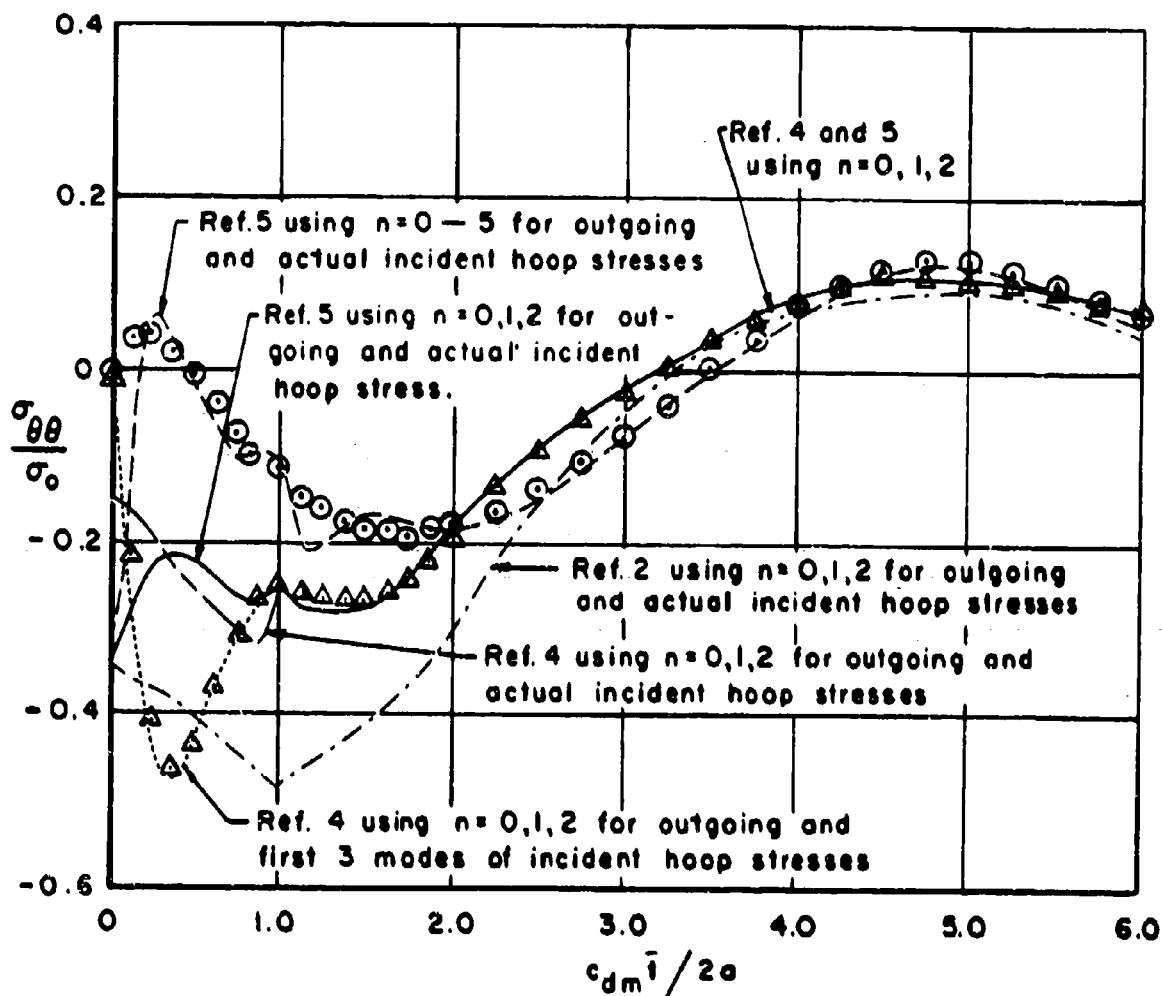
Note: Curves reproduced from Ref. 4

Fig. 7b   COMPARISON OF PRESENT COMPUTATIONS WITH THOSE OF REFS. 2,4, AND 5 FOR HOOP STRESS AT θ = 0° DUE TO INCIDENT DILATATIONAL STEP PULSE, AT BOUNDARY OF CAVITY IN ELASTIC MEDIUM, ϵ = 1/3.
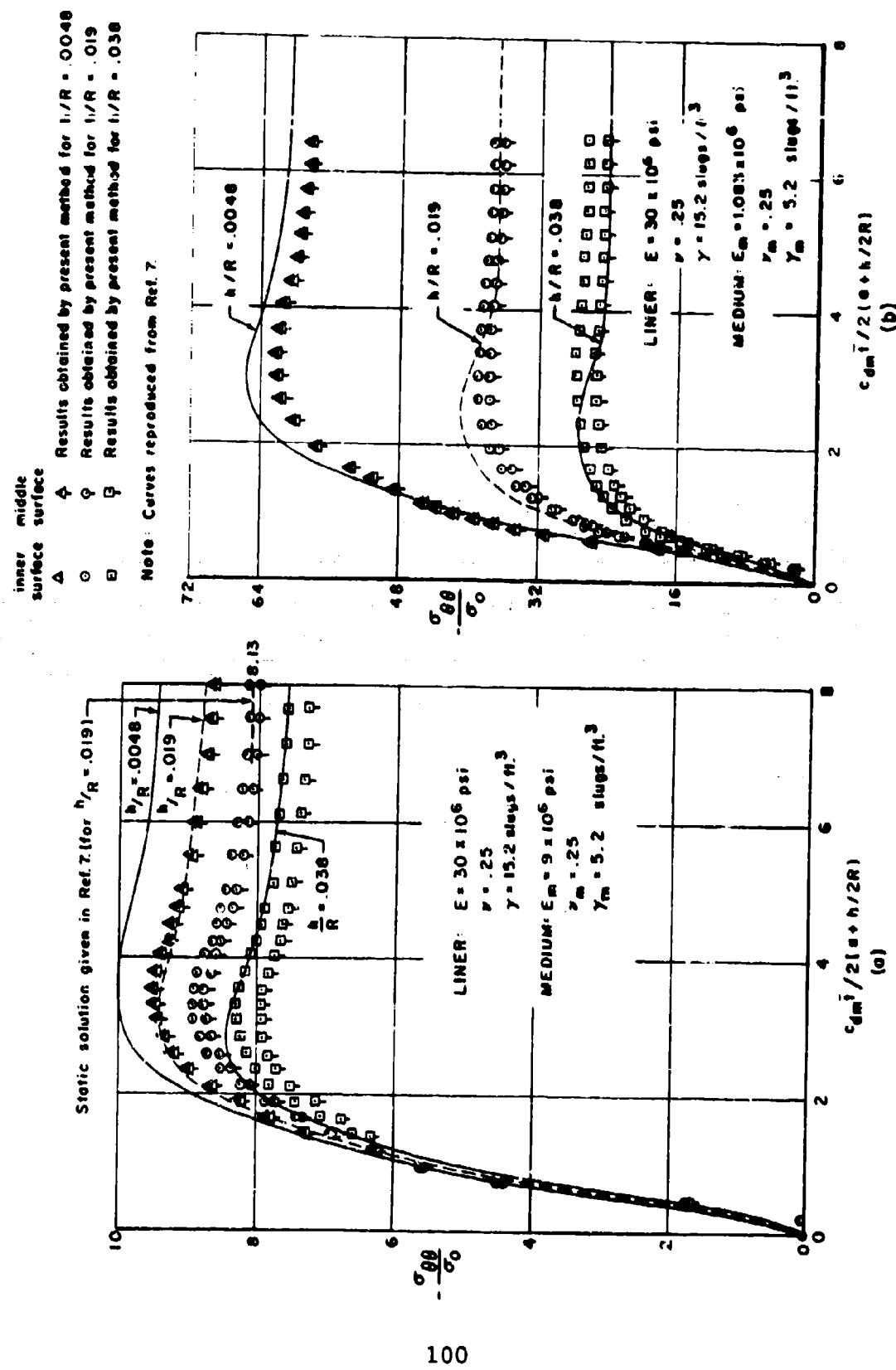
Fig. 8 COMPARISON OF HOOP STRESSES, CALCULATED AT $\theta = 90°$ BY PRESENT METHOD, WITH THOSE GIVEN IN REF. 7 FOR DILATATIONAL STEP PULSE IMPINGING UPON THIN SHELL IN ELASTIC MEDIUM.

100

LINER: $\frac{h}{R} = .019$, $E = 30 (10^6)$ psi, $\nu = .25$ $\gamma = 15.2$ slugs/ft.^{3}

MEDIUM: $E_m = 9(10^6)$ psi, $\nu_m = .25$, $\gamma_m = 5.2$ slugs/ft.^{3}

□ △ Results obtained by present method, at C° and 90° using number of modes required by convergence criteria.

▽ ⊙ Results obtained by present method, at 0° and 90°, using n = 0,1,2
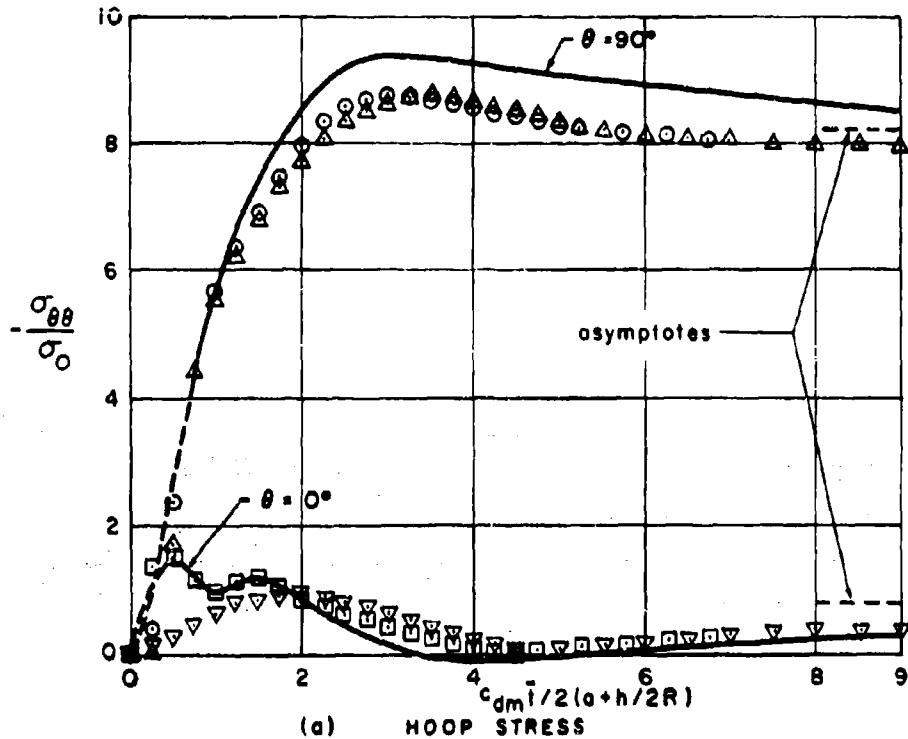
(a) HOOP STRESS

⊙ △ □ Results obtained by present method for n = 0,1, and 2.
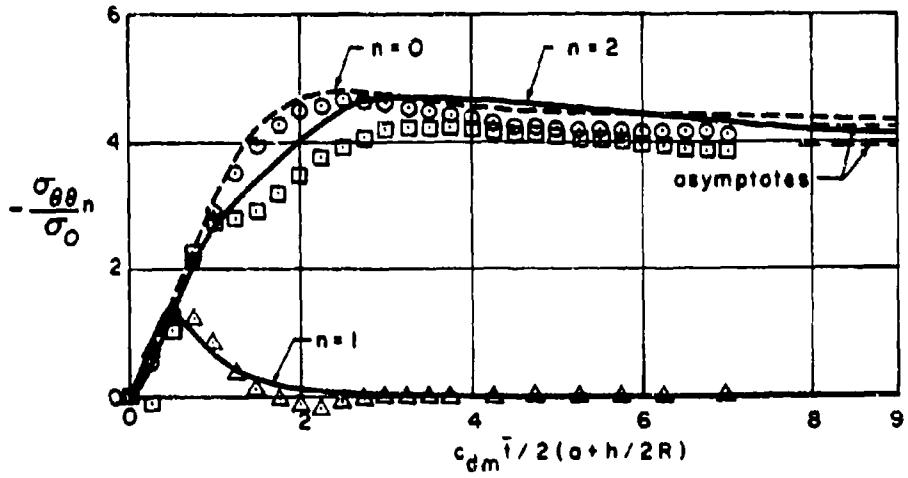
(b) MODAL CONTRIBUTIONS

Note: Curves and asymptotes reproduced from Ref. 7

Fig 9 COMPARISON OF HOOP STRESS AND ITS MODAL CONTRI-
BUTIONS, AT LINER MIDDLE SURFACE, WITH THOSE GIVEN
IN REF. 7.

101

LINER: CONCRETE; $E = 2.5 \times 10^6$ psi, $\nu = .2$, $\gamma = 4.5$ slugs/ft.^{3}

MEDIUM

———— SLOW GRANITE, $E = 1.0 \times 10^6$ psi, $\nu_m = .25$, $\gamma_m = 5.2$ slugs/ft.^{3}

— · — · — FAST GRANITE, $E = 9.0 \times 10^6$ psi, $\nu_m = .25$, $\gamma_m = 5.2$ slugs/ft.^{3}
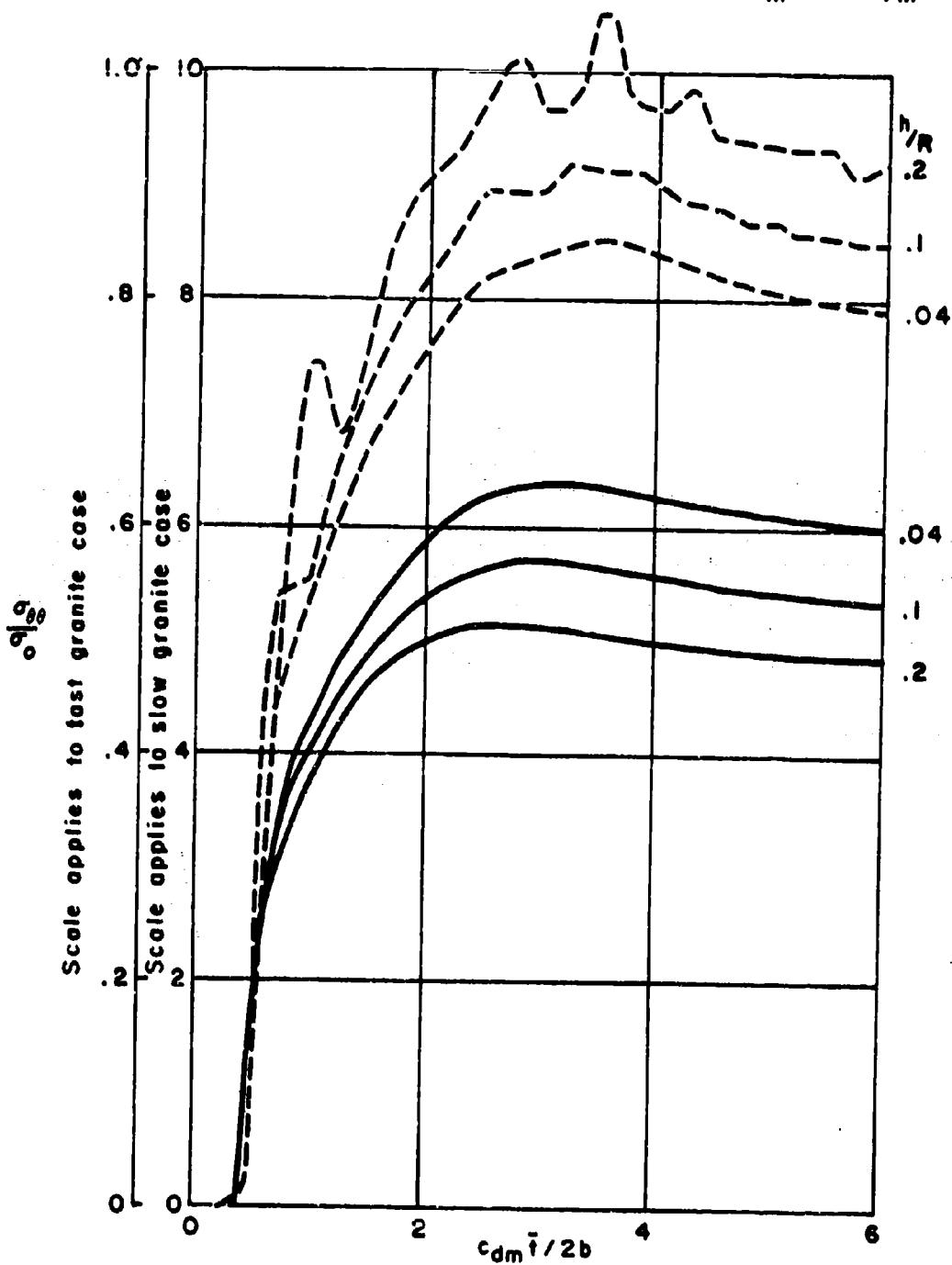
Fig. 10 EFFECT OF LINER THICKNESS ON THE MAXIMUM STRESS ($\sigma_{\theta\theta}$ at inner surface and $\theta = 90°$) FOR AN INCIDENT DILATATIONAL STEP PULSE IN ELASTIC MEDIUM.

102

LINER: CONCRETE, $E = 2.5 \times 10^6$ psi, $\nu = 2$, $\gamma = 4.5$ slugs/ft.³

MEDIUM: SLOW GRANITE, $E_m = 1.0 \times 10^6$ psi, $\nu_m = .25$, $\gamma_m = 5.2$ slugs/ft.³
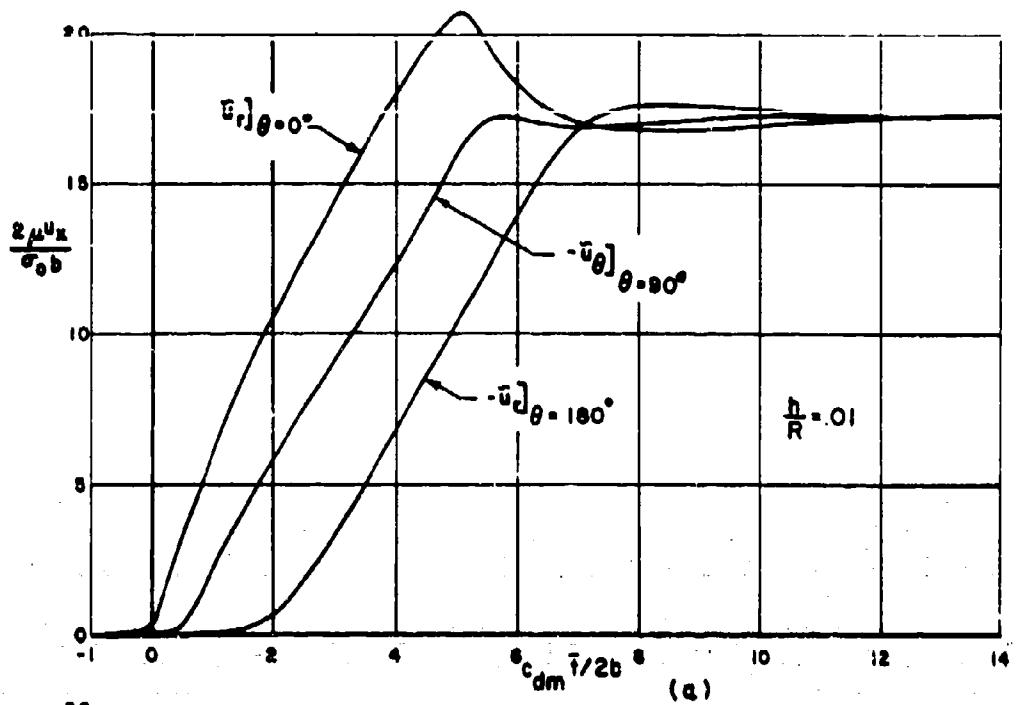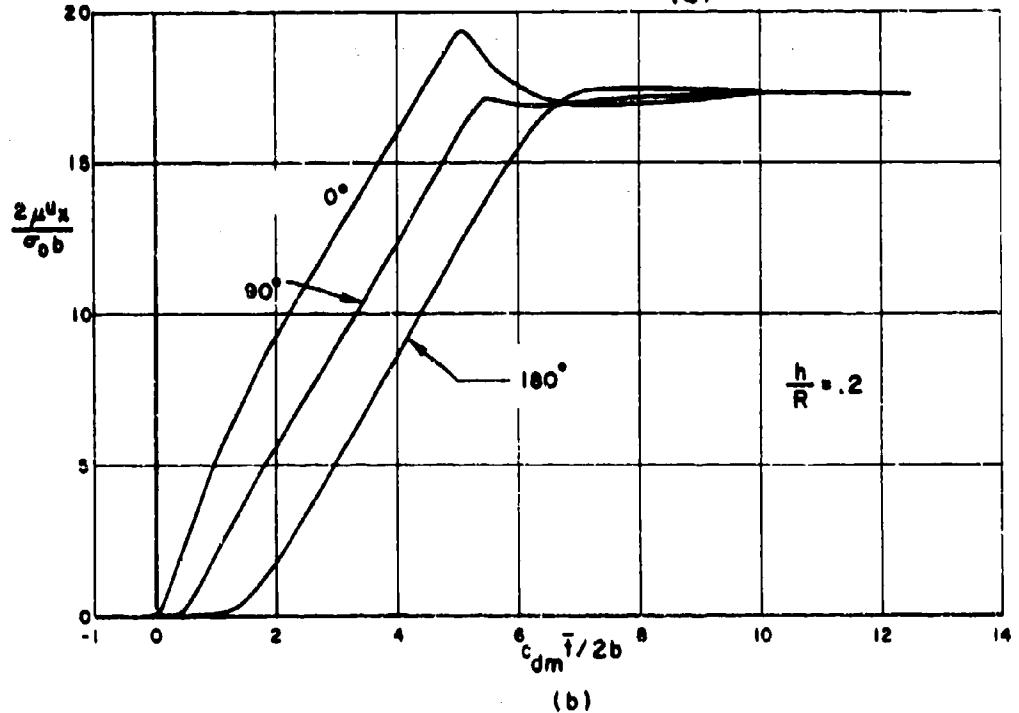
Fig. II DISPLACEMENT RESPONSE AT LINER INNER SURFACE TO INCIDENT DILITATIONAL RECTANGULAR WAVE, $\frac{c_{dm}\Delta}{2b} = 5$

(Elastic medium)

103

LINER· CONCRETE, $E = 2.5 \times 10^6$ psi, $\nu = .2$, $\gamma = 4.5$ slugs/ft.^{3}
MEDIUM·FAST GRANITE, $E_m = 9.0 \times 10^6$ psi, $\nu_m = .25$, $\gamma_m = 5.2$ slugs/ft.^{3}

——————————— $h/R = .01$
– – – – – – – – – – – – $h/R = .2$

$\tilde{u}_r]_{\theta = 0°}$

$-\tilde{u}_r]_{\theta = 90°}$

$-\tilde{u}_r]_{\theta = 180°}$

$\dfrac{2\mu u_x}{\sigma_0 b}$

$\dfrac{c_{dm} \Delta}{2b} = 5$

$c_{dm} \tilde{t}/2b$
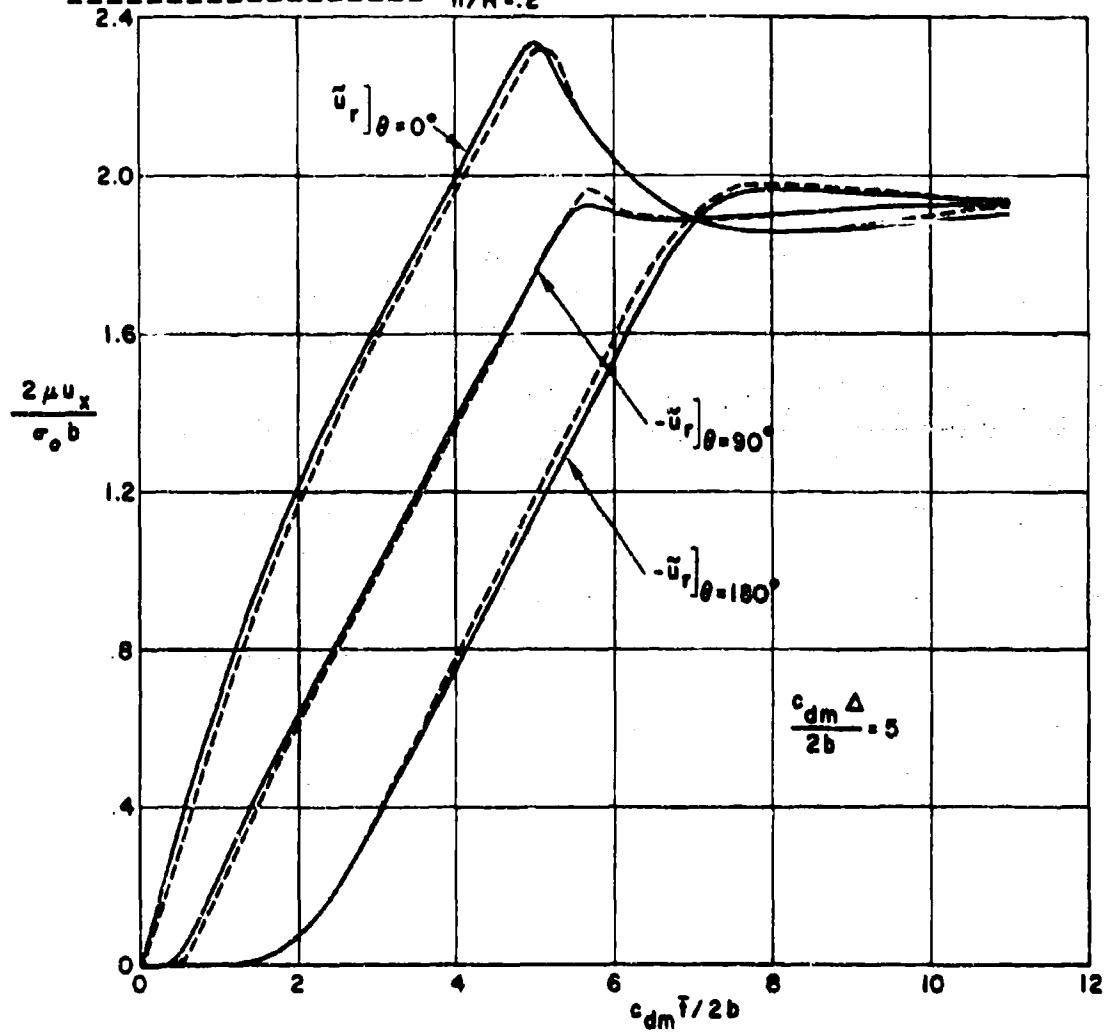
Fig. IIc DISPLACEMENT RESPONSE AT LINER INNER SURFACE TO INCIDENT
DILATATIONAL RECTANGULAR WAVE (Elastic medium)

104
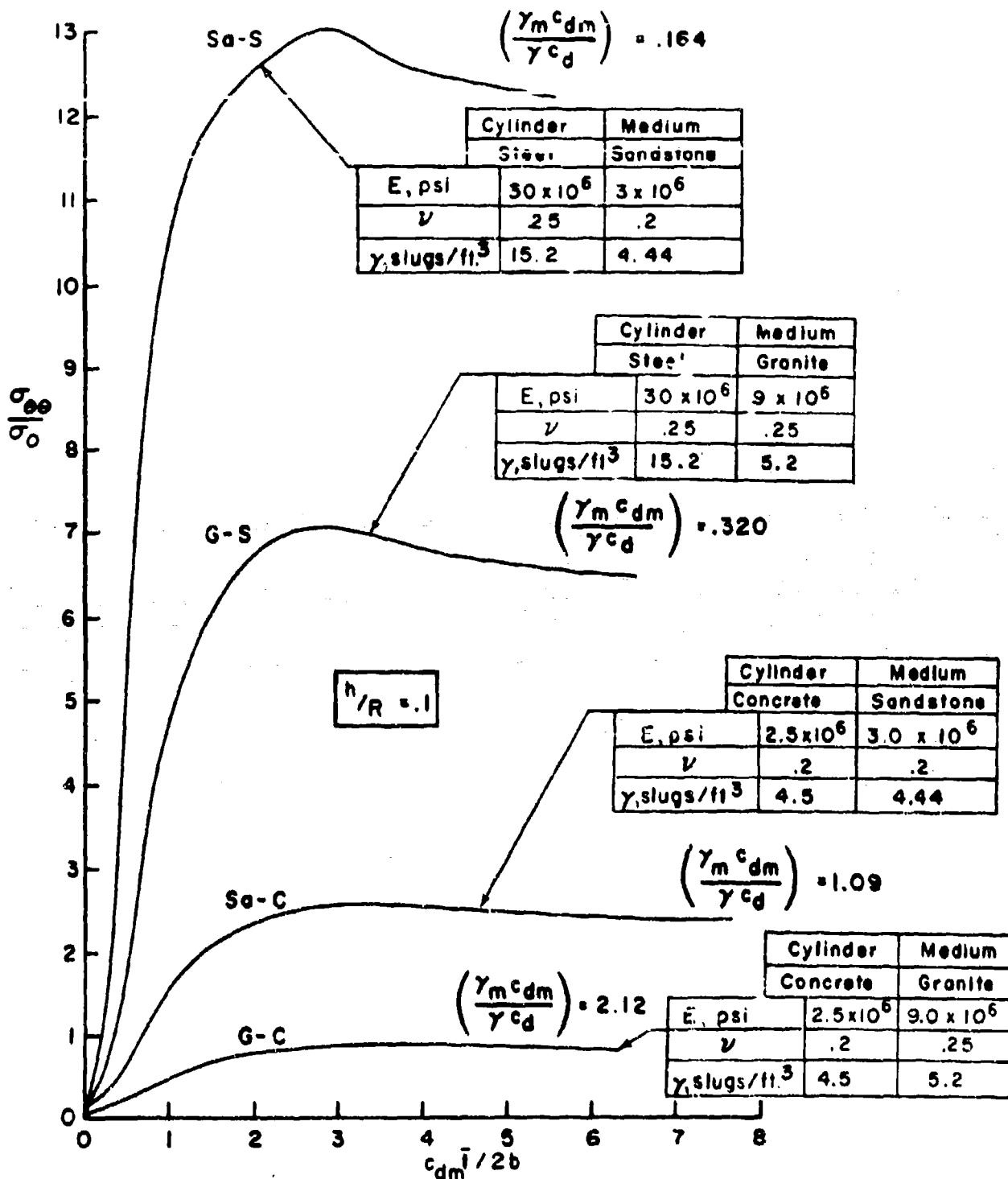
Fig.12 INFLUENCE OF CYLINDER-MEDIUM IMPEDANCE MISMATCH ON MAXIMUM STRESS IN THE CYLINDER ($\sigma_{\theta\theta}$ at $\theta = 90°$ and inner surface) FOR AN INCIDENT DILATATIONAL STEP PULSE IN AN ELASTIC MEDIUM.

105

LINER: CONCRETE; $h/R = .10$; $E = (2.5)(10^6)$ psi; $\nu = .20$; $\gamma = 4.5$ slugs/ft³

MEDIUM: POROUS SANDSTONE; $E_m = (3)(10^5)$ psi; $\nu_m = .20$; $\gamma_m = 4.44$ slugs/ft³

Step-Pulse

Triangular Wave

Linear Rise-Exponential Decay
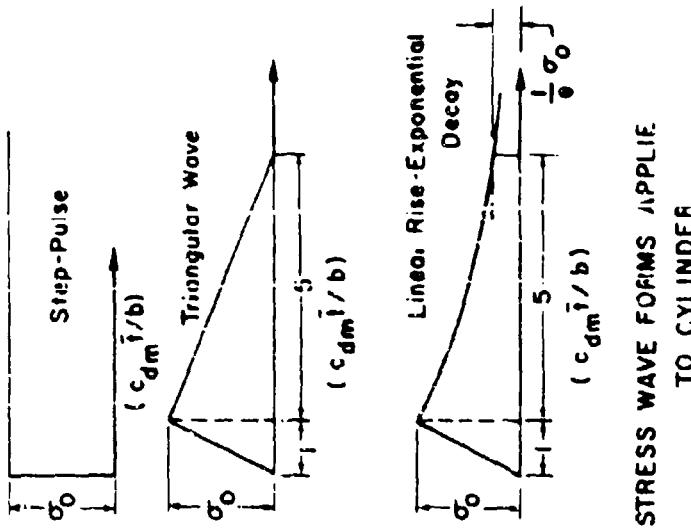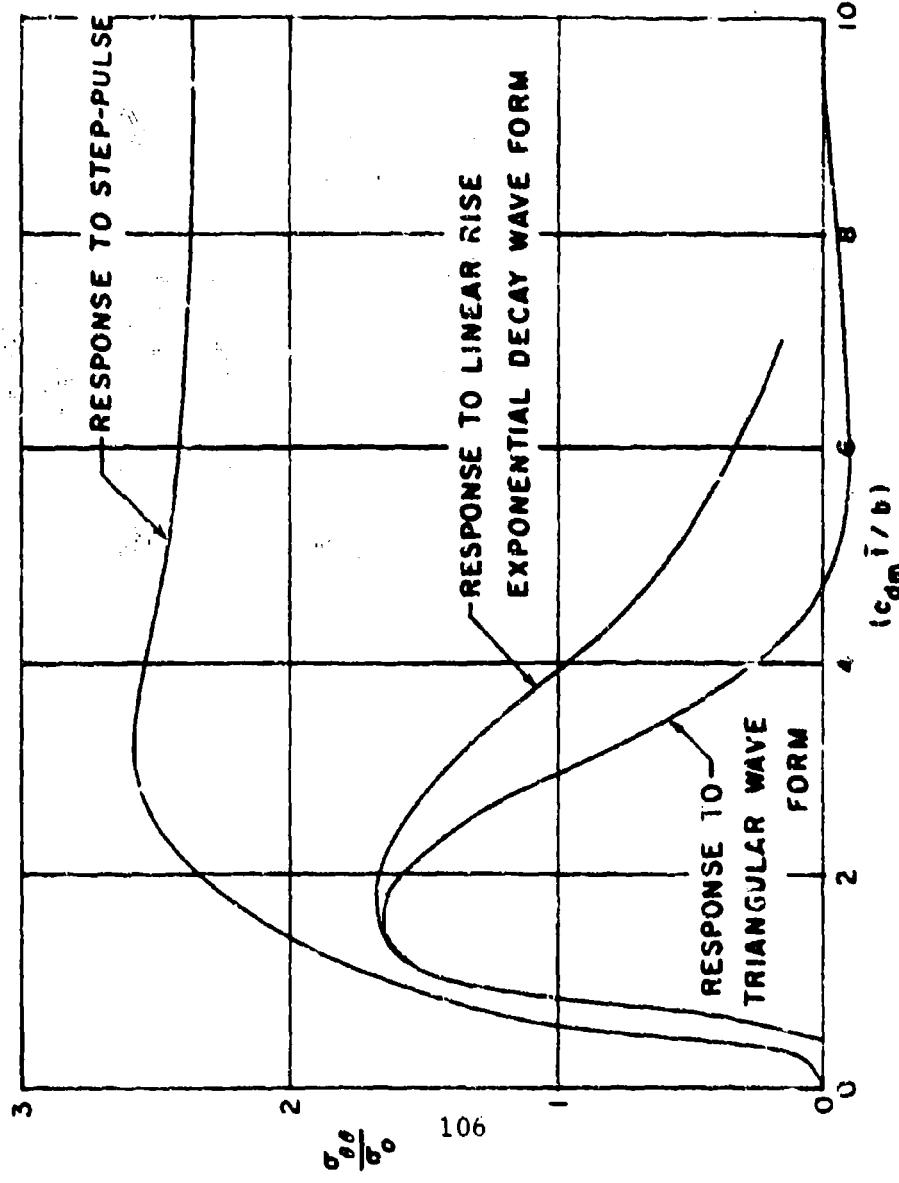
STRESS WAVE FORMS APPLIED TO CYLINDER

RESPONSE TO STEP-PULSE

RESPONSE TO LINEAR RISE EXPONENTIAL DECAY WAVE FORM

RESPONSE TO TRIANGULAR WAVE FORM

$(c_{dm} \bar{t}/b)$

$\sigma_{\theta\theta}/\sigma_0$

106

Fig 13 EFFECT OF INCIDENT DILATATIONAL WAVE FORM ON MAXIMUM STRESS ($\sigma_{\theta\theta}$) at inner surface and $\theta = 90°$) OR LINER IN ELASTIC MEDIUM
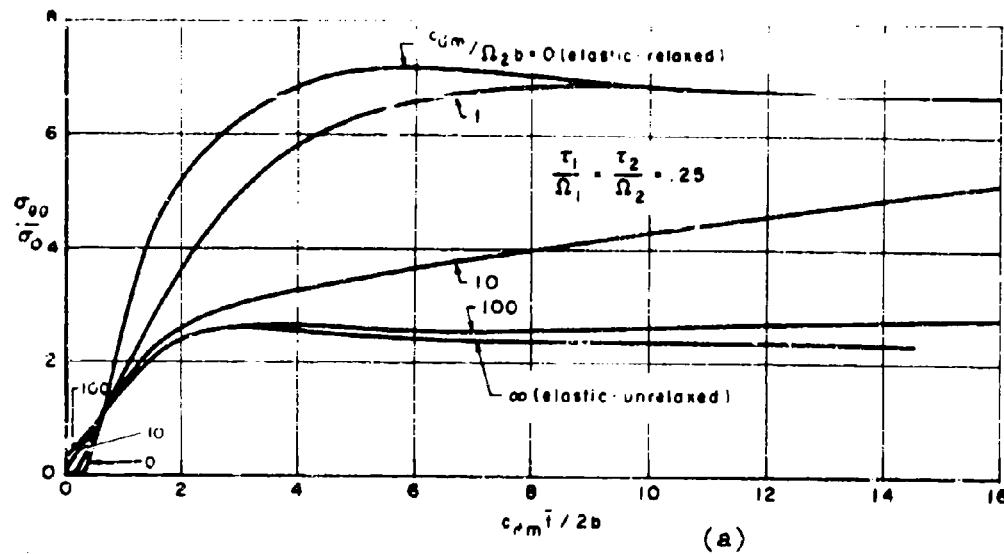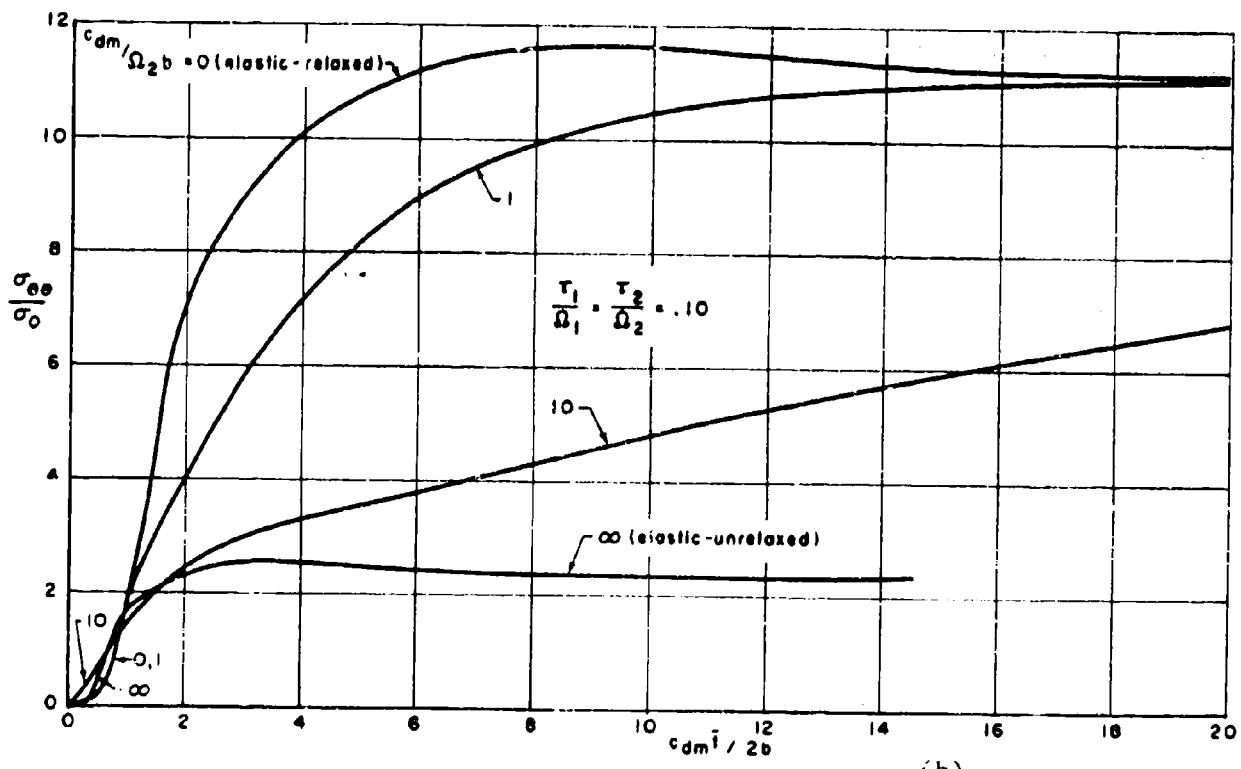
Fig. 14 EFFECT OF SURROUNDING MEDIUM VISCOELASTICITY ON MAXIMUM STRESS ($\sigma_{\theta\theta}$ at 90° and inner surface) IN LINER FOR INCIDENT DILATATIONAL STEP PULSE

107

LINER: CONCRETE; $\frac{h}{R} = .10$, $E = (2.5)(10^6)$ psi, $\nu = .20$, $\gamma = 4.5$ slugs/ft^3.

MEDIUM: $\frac{\Omega_1}{\Omega_2} = 1$, $\frac{\tau_1}{\Omega_1} = \frac{\tau_2}{\Omega_2} = .25$, $E_m = (31)(10^6)$ psi, $\nu_m = .20$, $\gamma_m = 4.44$ slugs/ft^3.

$$\frac{c_{dm}}{\Omega_2 b} = 0$$

$$\frac{c_{dm}}{\Omega_2 b} = 10$$

$$\frac{c_{dm}}{\Omega_2 b} = \infty$$

$\tilde{u}_r]_{\theta=0}$

$\tilde{u}_\theta]_{\theta=90°}$

$\tilde{u}_r]_{\theta=180°}$

$\frac{2\mu u_x}{\sigma_0 b}$

$c_{dm}\tilde{t}/2b$
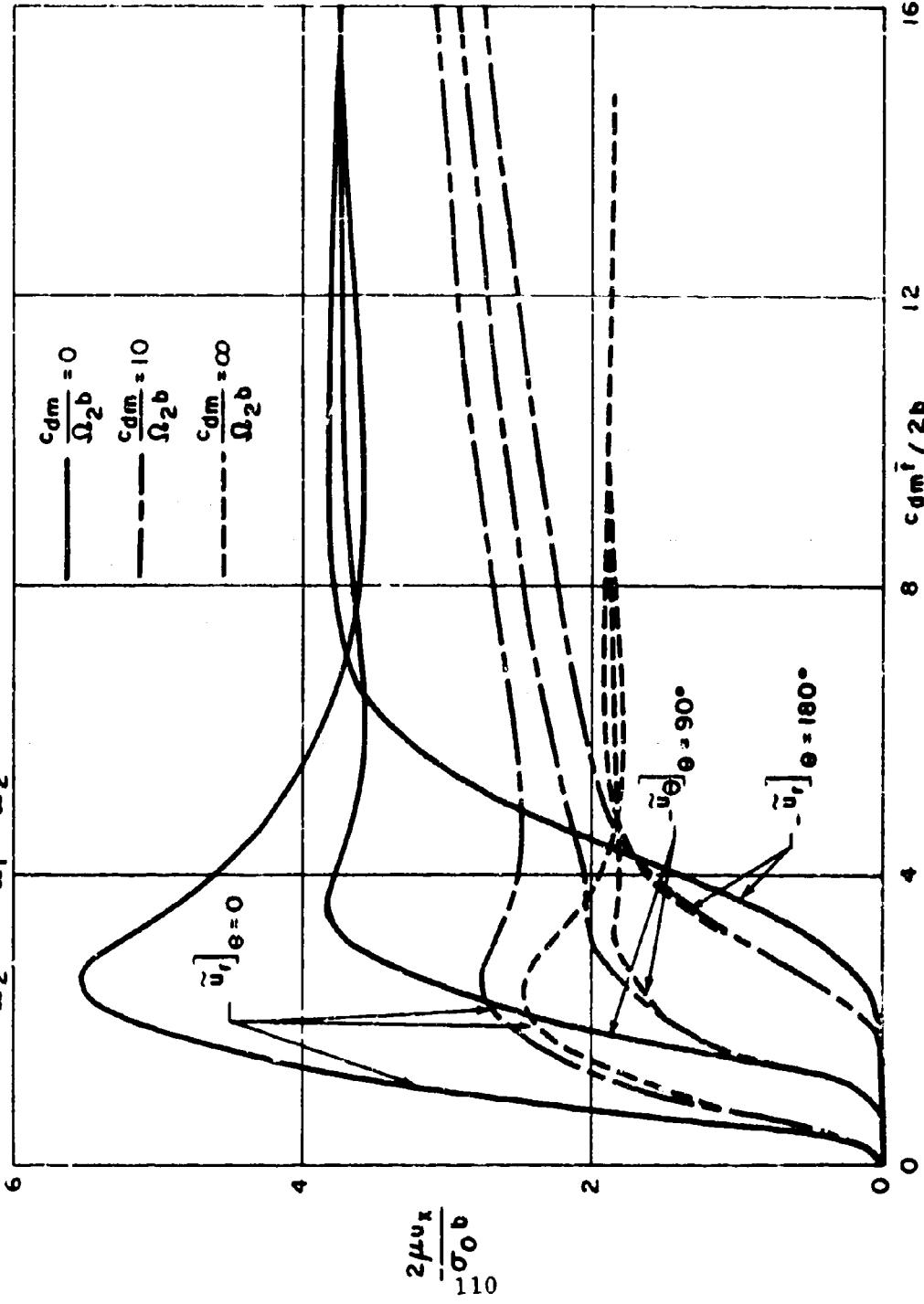
Fig. 17 EFFECT OF SURROUNDING MEDIUM VISCOELASTICITY ON DISPLACEMENT RESPONSE OF LINER INNER SURFACE TO INCIDENT DILATATIONAL TRIANGULAR WAVE.

110

LINER: CONCRETE, $\frac{h}{R} = 10$, $E = (25)(10^6)$ psi, $\nu = .20$, $\gamma = 4.5$ slugs/ft^3

MEDIUM $\frac{a_1}{a_2} = 1$, $\frac{\tau_1}{a_1}$, $\frac{\tau_2}{a_2} = 25$, $E_m = (3 \times 10^6)$ psi, $\nu_m = .20$, $\gamma_m = 4.44$ slugs/ft^3

——— Response to step pulse
——— Response to triangular wave
——— Response to linear rise exponential decay wave

(a) Elastic - unrelaxed medium

(b) Viscoelastic medium

(c) Viscoelastic medium

(d) Elastic-relaxed medium
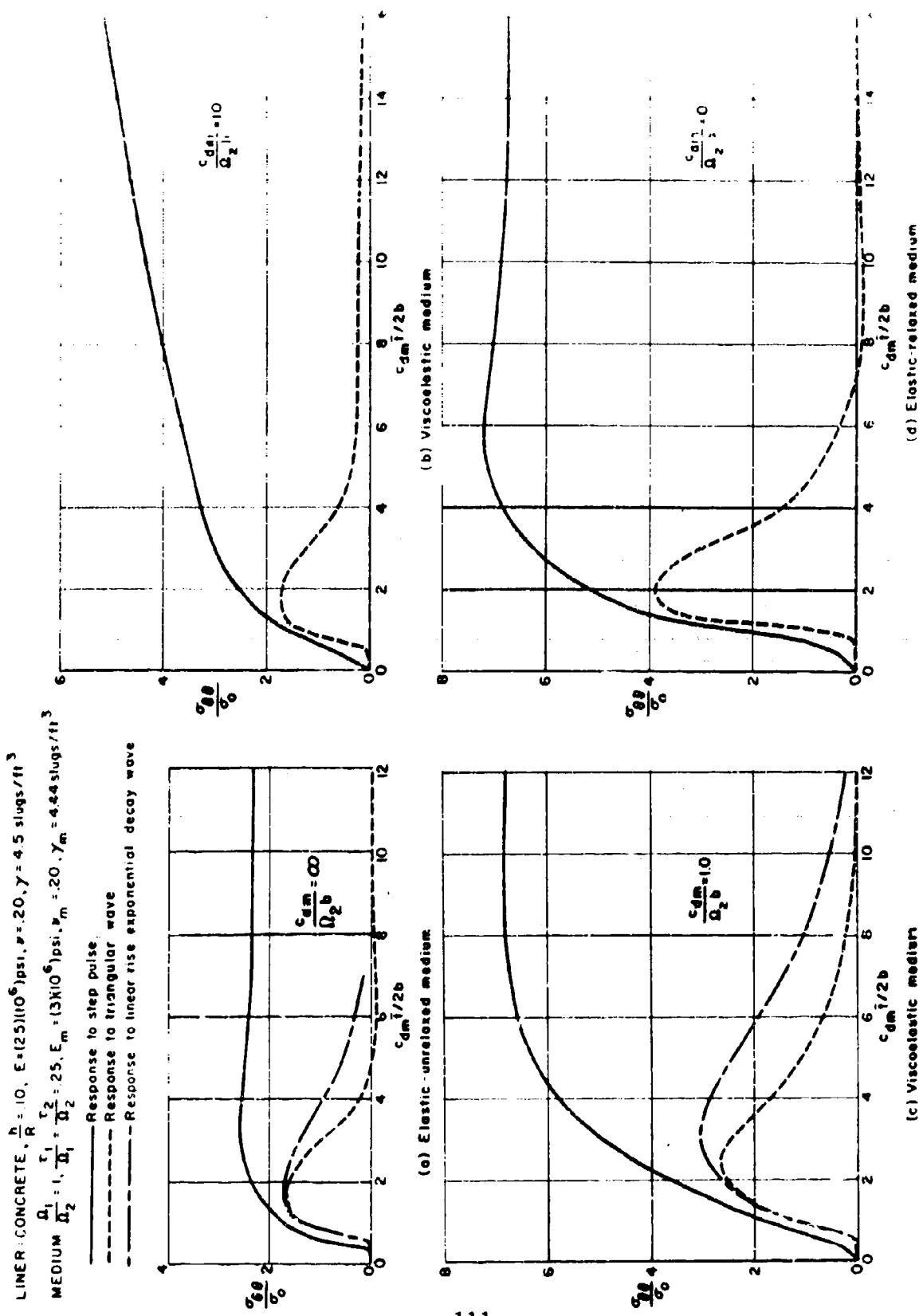
Fig. 18 EFFECT OF INCIDENT DILATATIONAL WAVE FORM ON LINER MAXIMUM STRESS ($\sigma_{\theta\theta}$ at $\theta = 90°$ and inner surface)

111
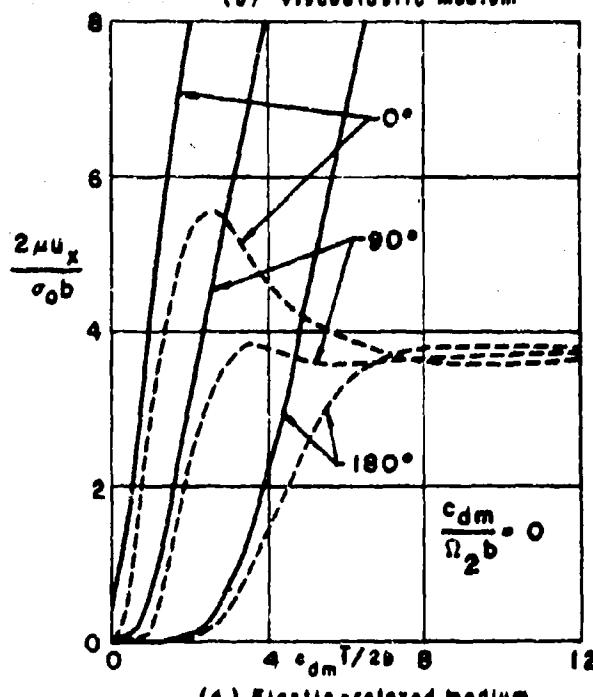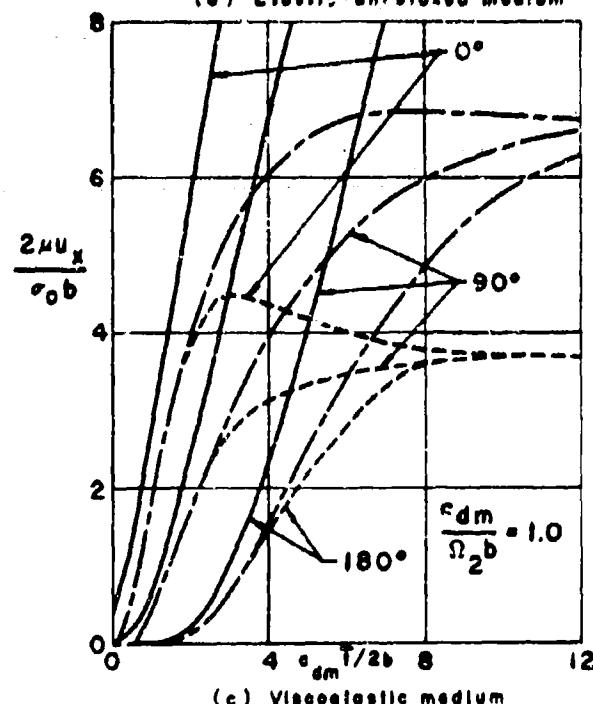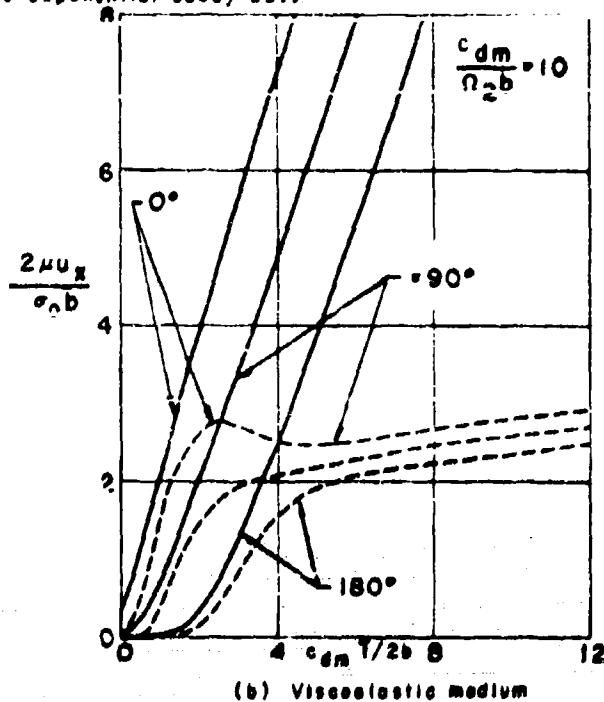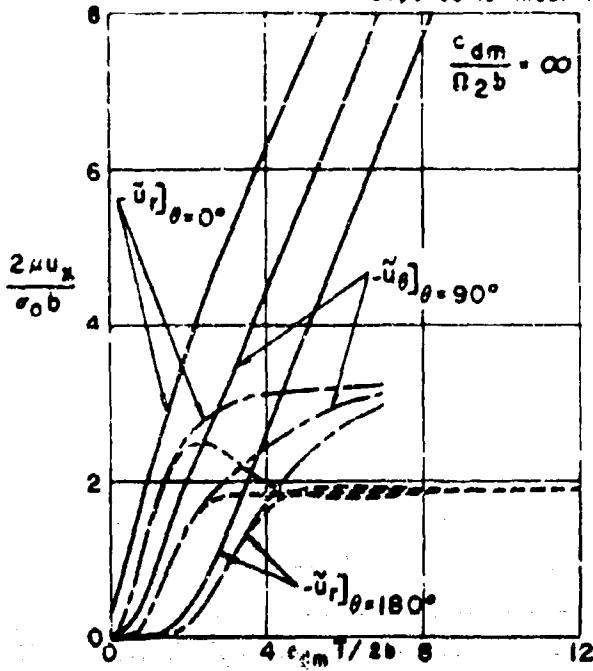
Fig. 19 EFFECT OF INCIDENT DILATATIONAL WAVE FORM ON DISPLACEMENT RESPONSE AT INNER SURFACE OF LINER IN VISCOELASTIC MEDIUM.

112
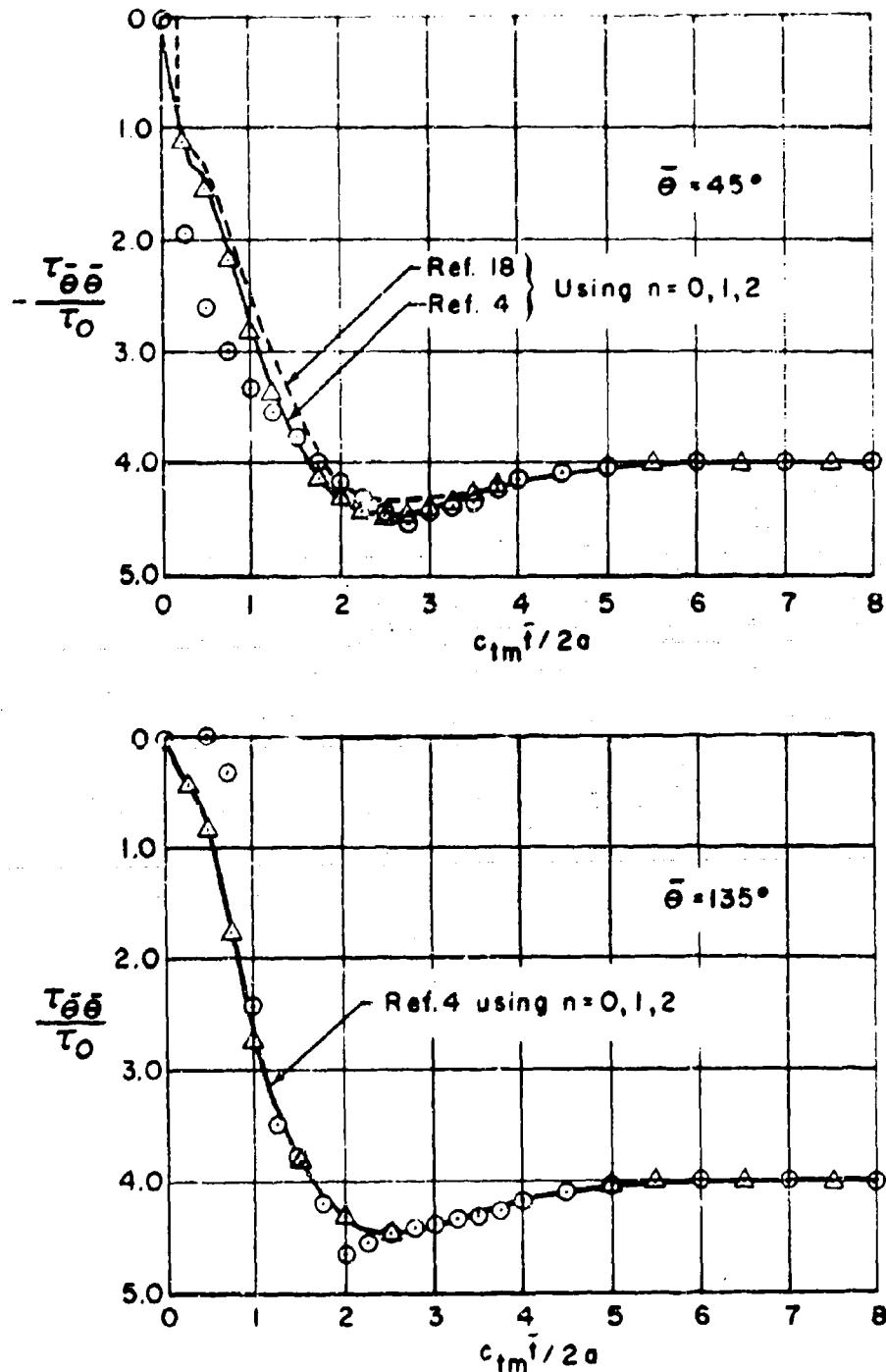
Fig. 20. COMPARISON OF PRESENT COMPUTATIONS WITH THOSE OF REFS. 4 AND 18 FOR HOOP STRESS (at $\bar{\theta}$ = 45° and 135°) DUE TO INCIDENT SHEAR STEP PULSE, AT BOUNDARY OF CAVITY IN ELASTIC MEDIUM, ϵ = 1/3

113

LINER CONCRETE: $E = 25 \times 10^6$ psi, $\nu = 2$, $\gamma = 45$ slugs/ft.³

MEDIUM

——————————— SLOW GRANITE: $E_m = 1.0 \times 10^6$ psi, $\nu_m = .25$ $\gamma_m = 5.2$ slugs/ft.³

— - — - — - — - — - FAST GRANITE, $E_m = 9.0 \times 10^6$ psi, $\nu_m = .25$, $\gamma_m = 5.2$ slugs/ft.³
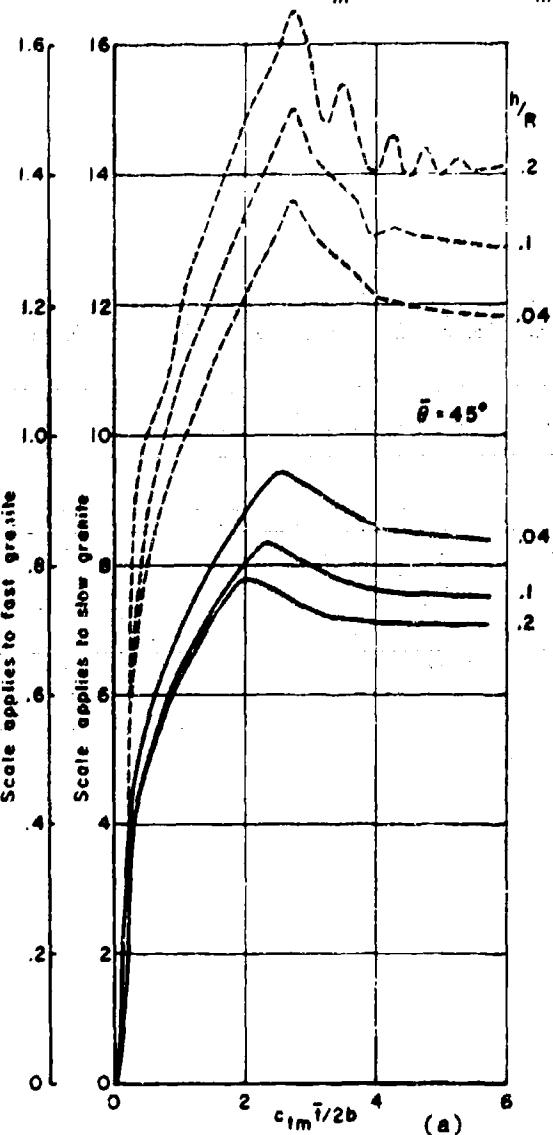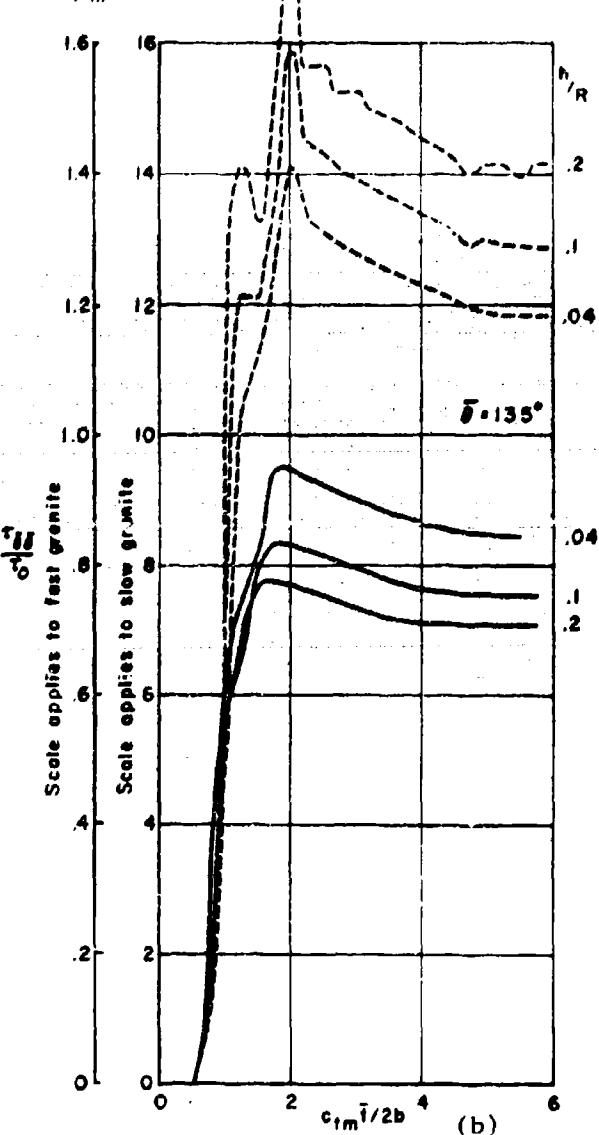
Fig. 21 EFFECT OF LINER THICKNESS ON MAJOR STRESS RESPONSE ($\tau_{\bar{\theta}\bar{\theta}}$ at inner surface and $\bar{\theta} = 45°, 135°$) FOR AN INCIDENT SHEAR STEP PULSE IN AN ELASTIC MEDIUM.

114

LINER CONCRETE , $E = 2.5 \times 10^6$ psi, $\nu = 2$, $\gamma = 4.5$ slugs/ft^3

MEDIUM · SLOW GRANITE , $E_m = 10 \times 10^6$ psi, $\nu_m = 25$, $\gamma_m = 5.2$ slugs/ft^3
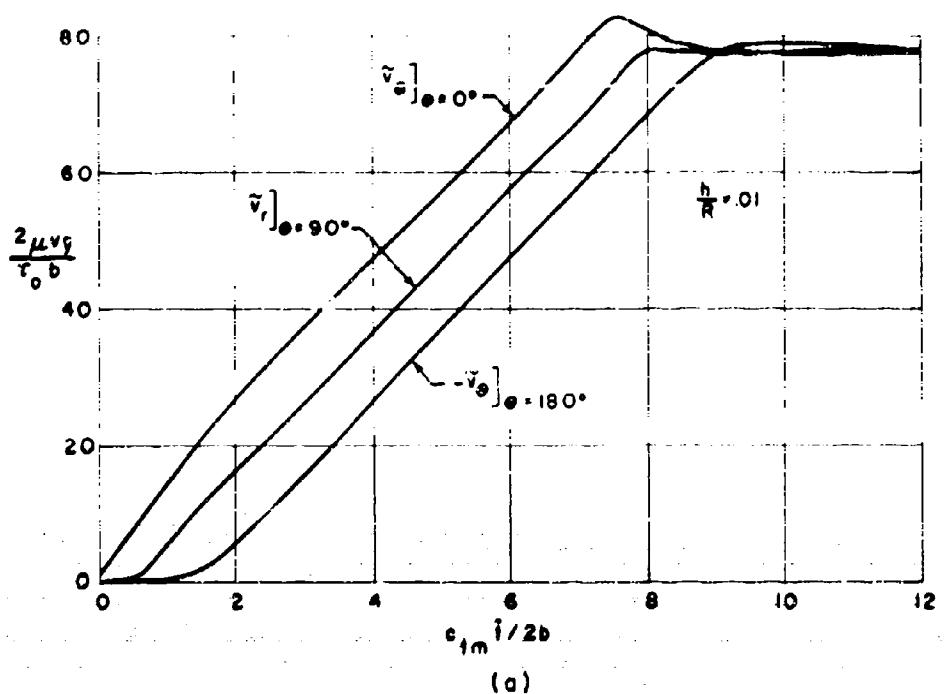
(a)
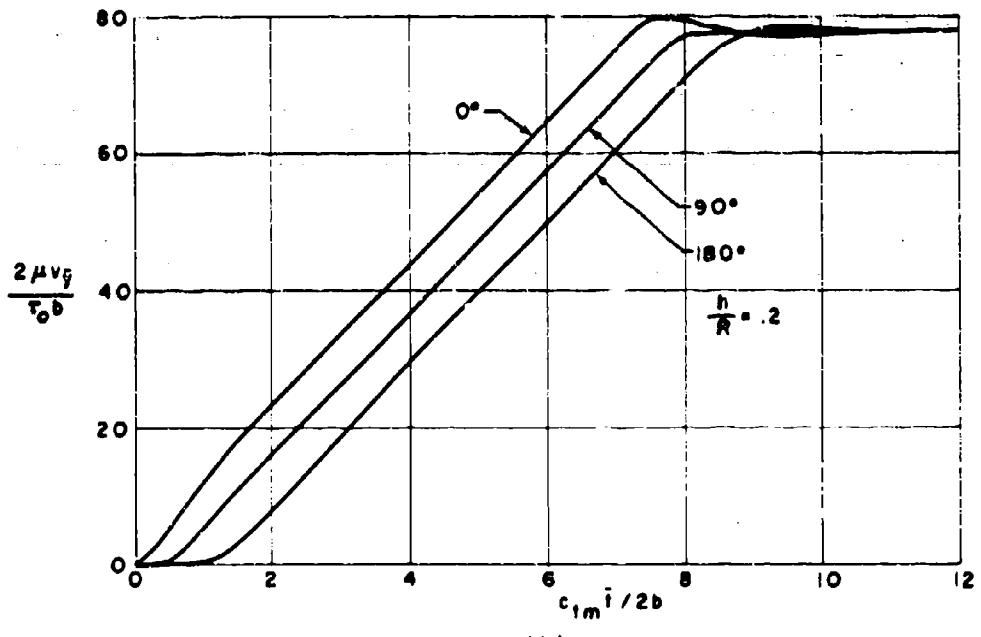
(b)

Fig. 22   EFFECT OF LINER THICKNESS ON DISPLACEMENT RESPONSE OF THE LINER
INNER SURFACE FOR THE CASE OF A INCIDENT SHEAR RECTANGULAR WAVE.
(elastic medium) $c_{1m} \Delta / 2b = 7.5$

115
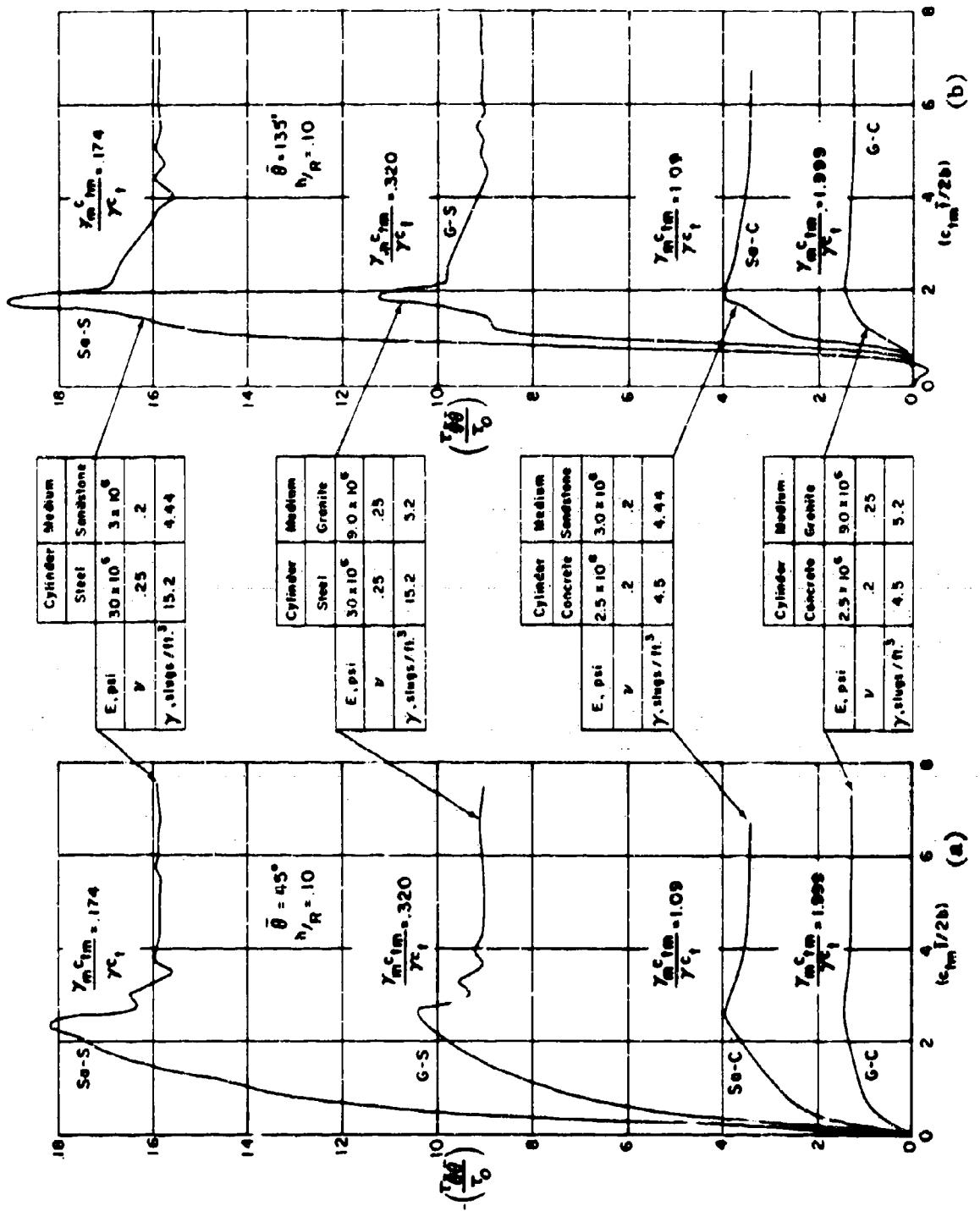
Fig. 23. INFLUENCE OF CYLINDER-MEDIUM IMPEDANCE MISMATCH ON CYLINDER STRESS RESPONSE $\tau_{\bar{\theta}\bar{\theta}}$ at inner surface) FOR INCIDENT SHEAR STEP PULSE IN ELASTIC MEDIUM.

116
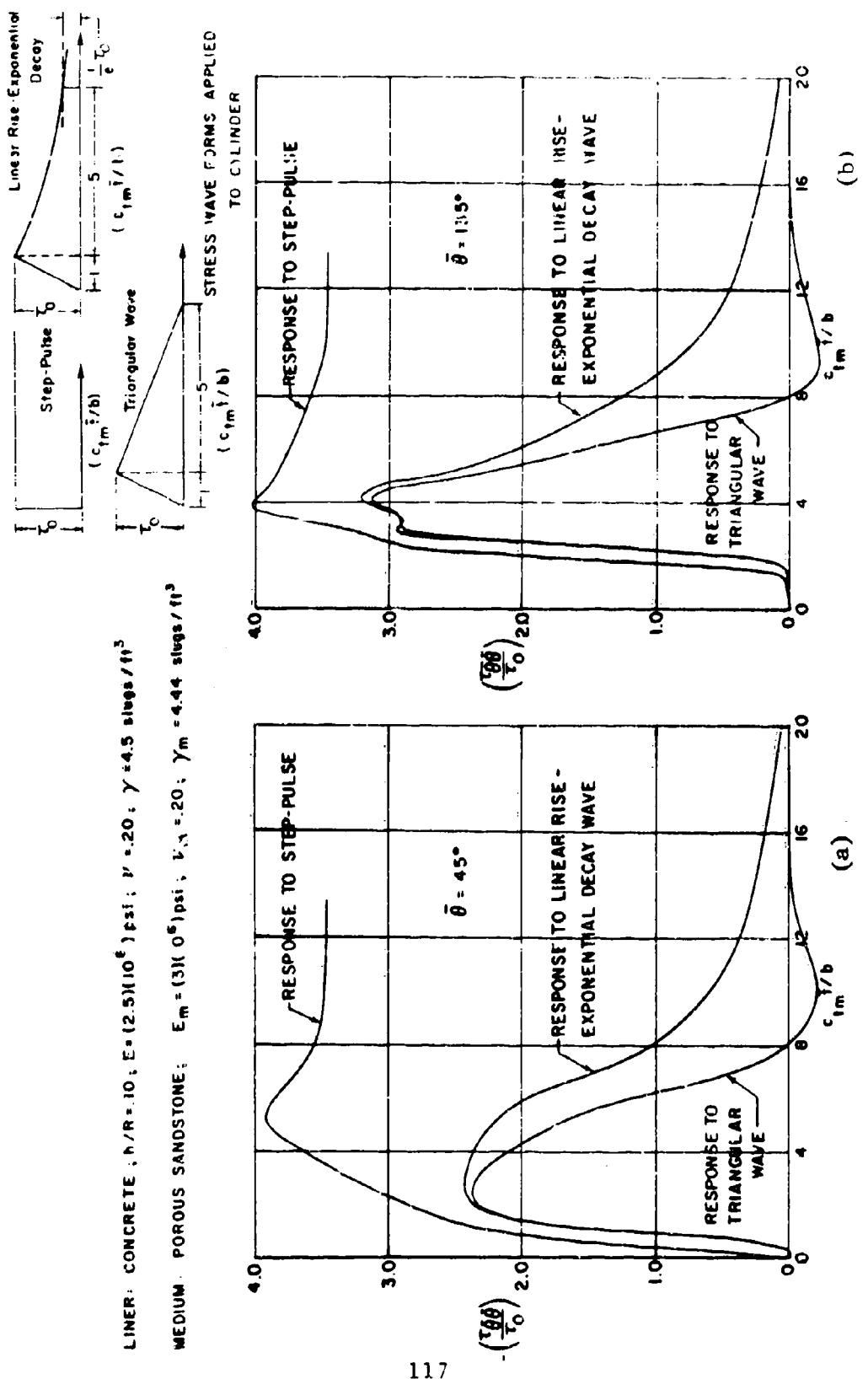
Fig. 24. EFFECT OF STRESS WAVE FORM ON CYLINDER STRESS RESPONSE ($T_{\bar{\theta}\theta}$ at inner surface) FOR INCIDENT SHEAR STEP PULSE IN ELASTIC MEDIUM.

117

Note: Incident wave form given in Fig. 24

Fig. 25   EFFECT OF SURROUNDING MEDIUM VISCOELASTICITY ON HOOP STRESS AT INNER SURFACE OF LINER FOR INCIDENT SHEAR STEP PULSE.

118

LINER: CONCRETE, $\frac{h}{R} = .10$, $E = (2.5)(10^6)$ psi, $\nu = .20$, $\gamma = 4.5$ slugs/ft.^{3}

MEDIUM: $\frac{\Omega_1}{\Omega_2} = 1$, $\frac{T_1}{\Omega_1} = \frac{T_2}{\Omega_2} = .25$, $E_m = (3)(10^6)$ psi, $\nu_m = .20$

$\gamma_m = 4.44$ slugs/ft.^{3}

Note: Incident wave form given in Fig. 24.

Fig. 26. EFFECT OF SURROUNDING MEDIUM VISCOELASTICITY ON
HOOP STRESS AT INNER SURFACE OF LINER FOR
INCIDENT TRIANGULAR SHEAR WAVE.

119

LINER·CONCRETE, $\frac{h}{R} = .10$, $E = (25)(10^6)$psi, $\nu = .20$, $\gamma = 4.5$ slugs/ft^3

MEDIUM $\frac{\Omega_1}{\Omega_2} = 1$, $\frac{\tau_1}{\Omega_1} = \frac{\tau_2}{\Omega_2} = .25$, $E_m = (3)(10^6)$psi, $\nu_m = .20$, $\gamma_m = 4.44$ slugs/ft^3

————————— Response to step pulse

— — — — — — Response to triangular wave

— · — · — · — Response to linear rise exponential decay wave

$\tau_{\bar\theta\bar\theta}/\tau_0$

$\bar\theta = 45°$

$c_{tm}t/2b$

(a)

$\tau_{\bar\theta\bar\theta}/\tau_0$

$\bar\theta = 135°$

$c_{tm}t/2b$

(b)

Note: Incident wave forms given in Fig. 24

Fig. 27 EFFECT OF INCIDENT SHEAR WAVE FORM ON HOOP STRESS AT INNER
SURFACE OF LINER IN VISCOELASTIC MEDIUM WITH $c_{dm}/\Omega_2 b = 1.0$

120

LINER·CONCRETE $\frac{h}{R} = .10$, $E = (2.5)(10^6)$psi, $\nu = .20$, $\gamma = 4.5$ slugs/ft

MEDIUM·$\frac{\Omega_1}{\Omega_2} = 1$, $E_m = (3)(10^6)$psi, $\nu_m = .20$, $\gamma_m = 4.44$ slugs/ft.

——— $\frac{\tau_1}{\Omega_1} = \frac{\tau_2}{\Omega_2} = .25$

- - - - $\frac{\tau_1}{\Omega_1} = \frac{\tau_2}{\Omega_2} = .10$
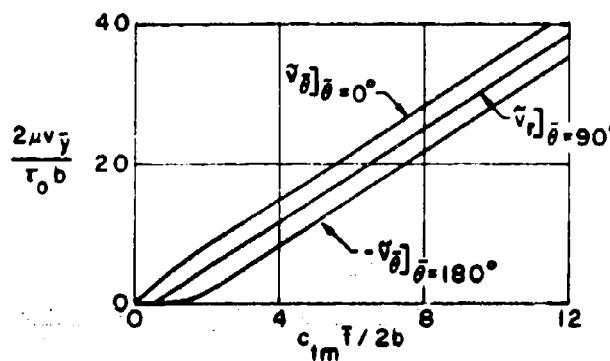
(a) Elastic-unrelaxed medium
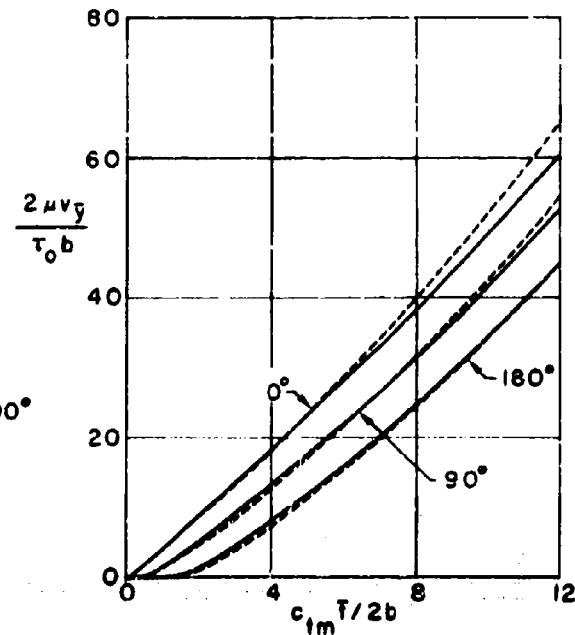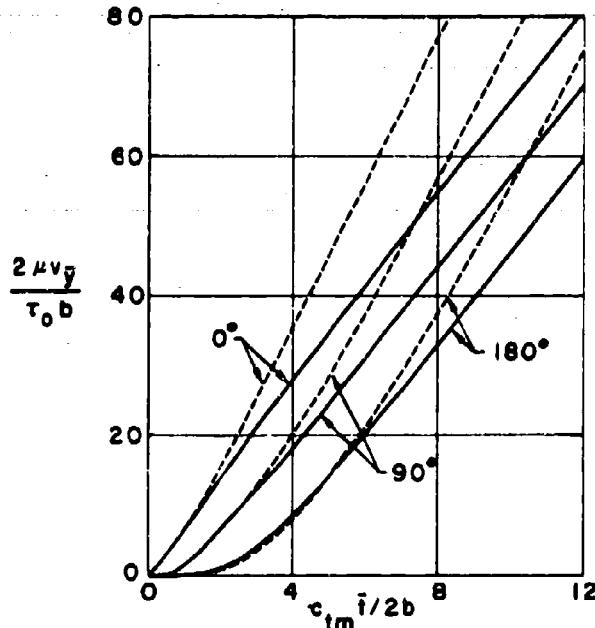
(b) Viscoelastic medium

(c) Viscoelastic medium
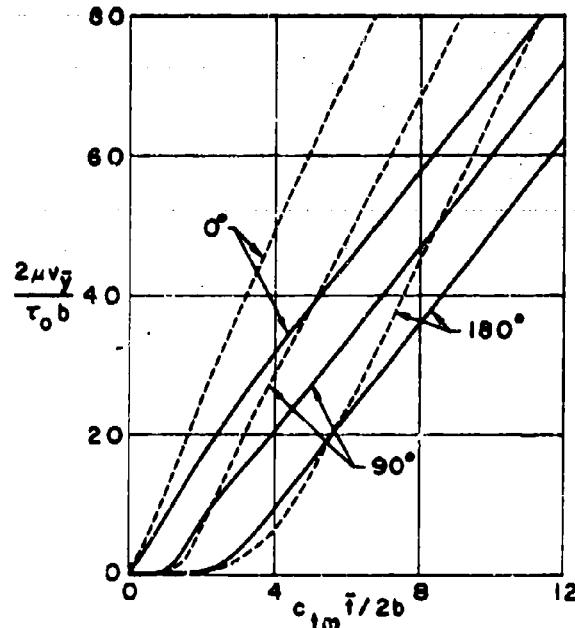
(d) Elastic-relaxed medium

Note: Incident wave form given in Fig. 24

Fig. 28 EFFECT OF SURROUNDING MEDIUM VISCOELASTICITY ON DISPLACE-
MENT RESPONSE OF LINER INNER SURFACE TO INCIDENT SHEAR
STEP PULSE. 121

LINER : CONCRETE, $\frac{h}{R} = .10$, $E = (25)(10^6)$psi, $\nu = .20$, $\gamma = 4.5$ slugs/ft.^{3}

MEDIUM : $\frac{\Omega_1}{\Omega_2} = 1$, $\frac{\tau_1}{\Omega_1} = \frac{\tau_2}{\Omega_2} = .25$, $E_m = (3)(10^6)$psi, $\nu_m = .20$, $\gamma_m = 4.44$ slugs/ft.^{3}
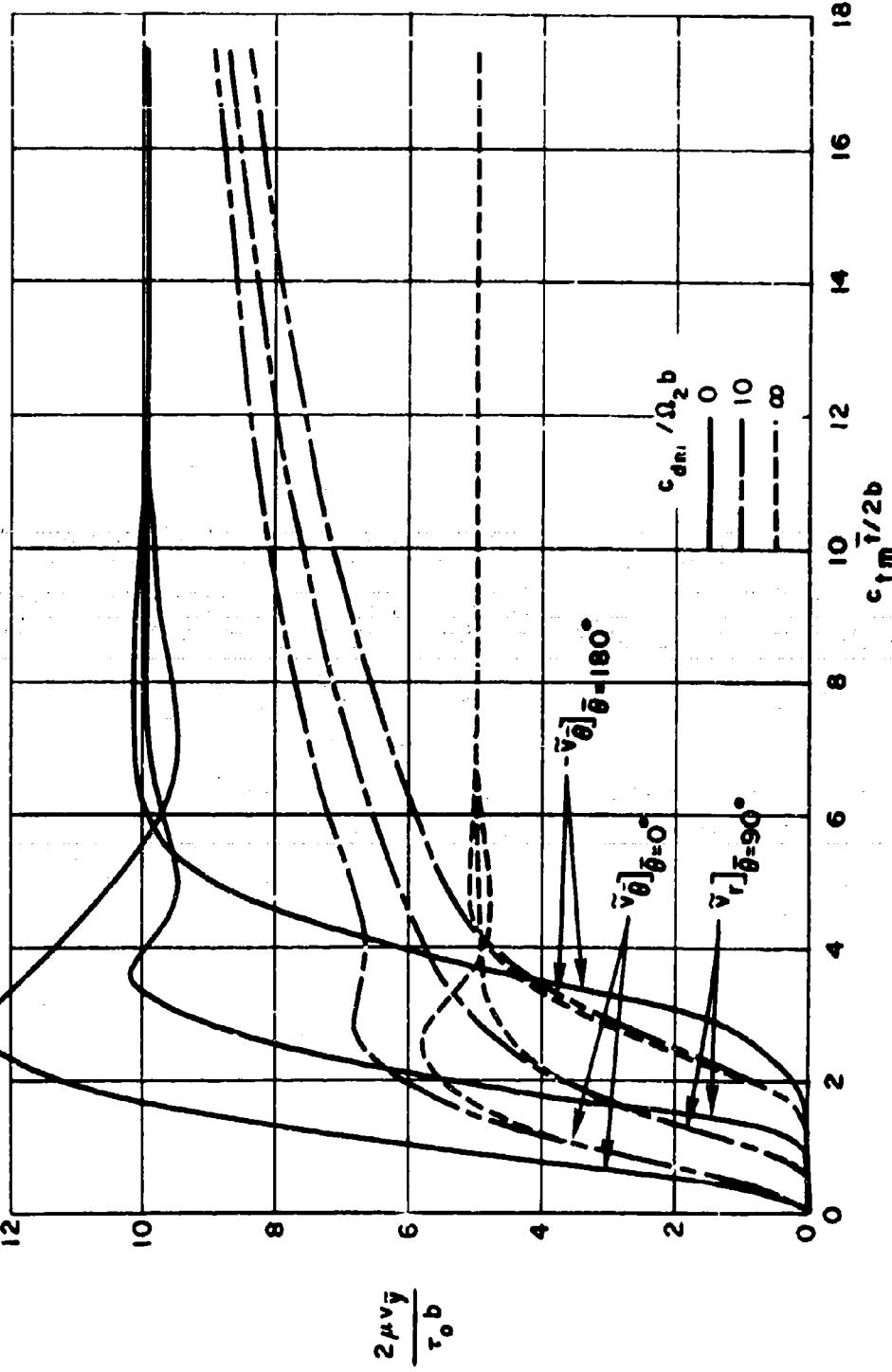
Note: Incident wave form given in Fig. 24

Fig. 29. EFFECT OF SURROUNDING MEDIUM VISCOELASTICITY ON DISPLACEMENT RESPONSE OF LINER INNER SURFACE TO INCIDENT TRIANGULAR SHEAR WAVE.

122

LINER   CONCRETE $\frac{h}{R} = .10$, $E = (2.5)(10^6)$ psi, $\nu = 20$, $\gamma = 4.5$ slugs/ft.^{3}

MEDIUM $\frac{\Omega_1}{\Omega_2} = 1$, $\frac{T_1}{\Omega_1} = \frac{T_2}{\Omega_2} = .25$, $E_m = (3)(10^6)$p· , $\nu_m = .20$, $\gamma_m = 4.44$ slugs/ft^3

——————————— Response to step pulse
- - - - - - - - - - - - Response to triangular wave
—·—·—·—·—·—·— Response to linear rise exponential decay wave
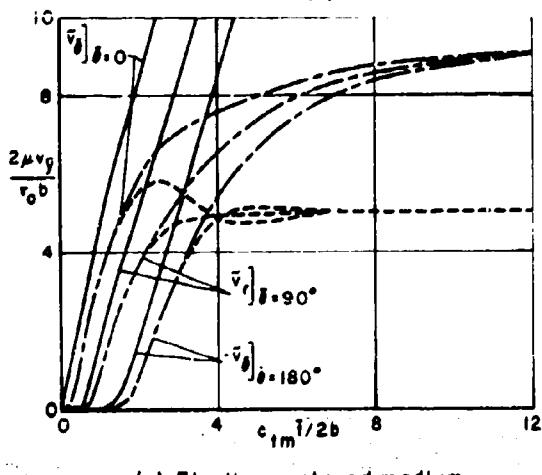
(a) Elastic-unrelaxed medium
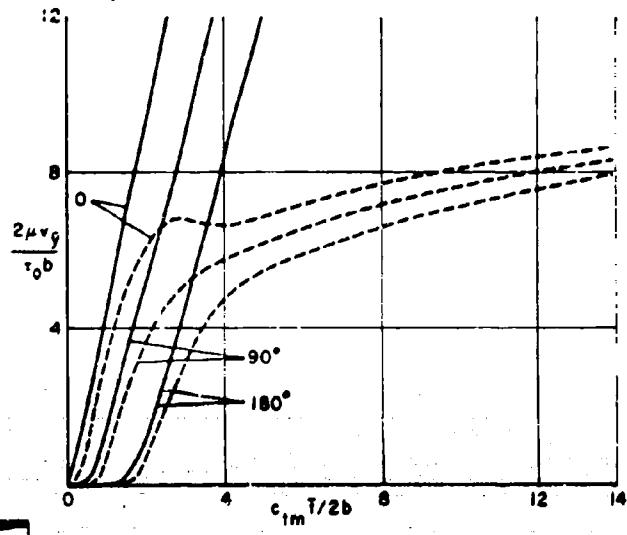
(b) Viscoelastic medium
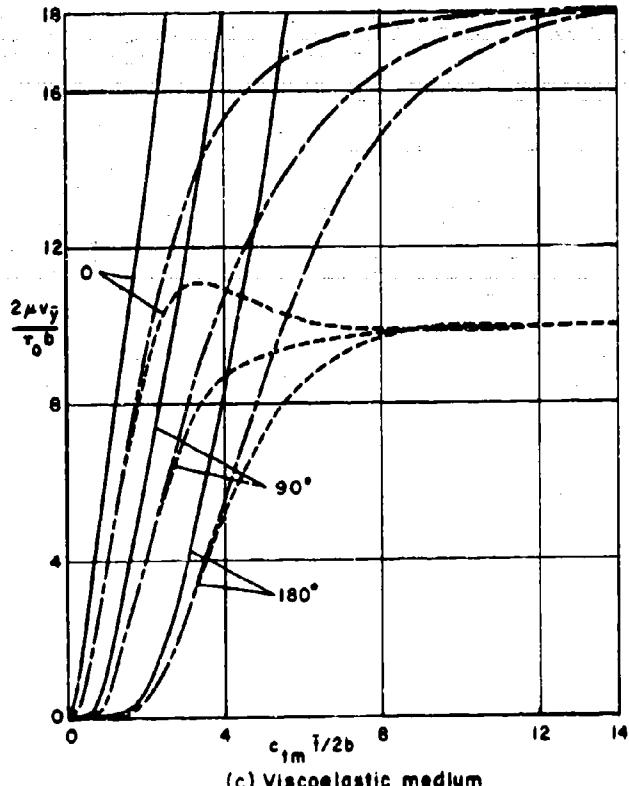
(c) Viscoelastic medium
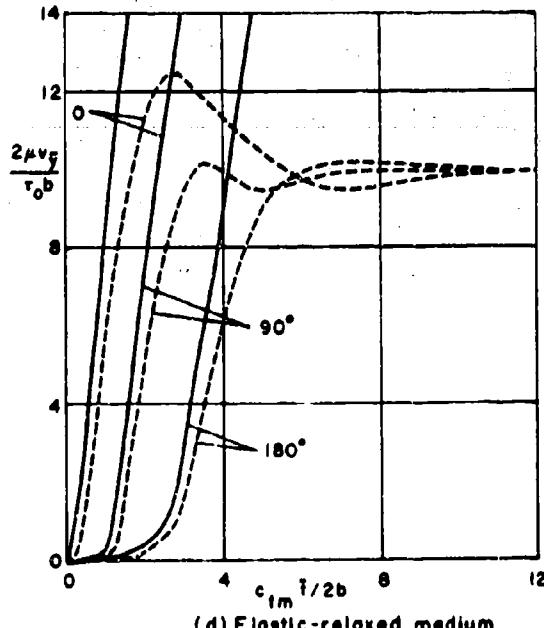
(d) Elastic-relaxed medium

Note Incident wave forms given in Fig. 24

Fig. 30 EFFECT OF INCIDENT SHEAR WAVE FORM ON DISPLACEMENT RESPONSE AT INNER SURFACE
OF LINER IN VISCOELASTIC MEDIUM.

123

Fig.31 SUPERPOSITION OF CYLINDER RESPONSE (Hoop stresses at inner boundary) TO INCIDENT DILATATIONAL AND SHEAR WAVES IN AN ELASTIC MEDIUM.

124

Fig.32 SUPERPOSITION OF CYLINDER RESPONSE (Hoop stresses at inner boundary) TO INCIDENT DILATIONAL AND SHEAR WAVES IN AN ELASTIC MEDIUM.

125

APPENDICES

A. Transformations Employed to Facilitate the Computation

B. Representation of the Fourier Coefficients Associated with
    the Incident Wave

126

APPENDIX A

In this appendix a number of transformations are introduced to facilitate the computational effort involved in performing the inversions of the boundary condition matrix equations (3.8.2) and (4.5.2). For ease of reference, we rewrite these equations omitting the indices of summation p and n, but understanding dependence upon them. For the case of an incident dilatational wave, we have Eq. (3.8.2),

$$\left[C_{ij} \right] \left\{ Z_j \right\} = \left\{ D_i \right\} , \qquad (A.1)$$

and for the case of an incident shear wave we have Eq. (4.4.2),

$$\left[c_{ij} \right] \left\{ \zeta_j \right\} = \left\{ \beta_i \right\} . \qquad (A.2)$$

The stresses and displacements associated with the response to the incident dilatational and incident shear waves, Eqs. (3.8.3) and (4.5.3), respectively, will now be put in nondimensional form. As an intermediate step in this direction, we define

$$\left\{ \begin{array}{c} \bar{\sigma}_{ij} \\ \bar{\tau}_{ij} \end{array} \right\} = \left(\frac{b^2}{2\mu} \right) \left\{ \begin{array}{c} \sigma_{ij} \\ \tau_{ij} \end{array} \right\} \qquad \begin{array}{c} i = r, \theta \\ j = r, \theta \end{array}, \qquad (A.3a)$$

$$\left\{ \begin{array}{c} \bar{u}_i \\ \bar{v}_i \end{array} \right\} = b \left\{ \begin{array}{c} u_i \\ v_i \end{array} \right\} \qquad i = r, \theta , \qquad (A.3b)$$

where (σ_{ij}, u_i) are presumed to be calculated by Eq. (3.8.3) and (τ_{ij}, v_i) by Eq. (4.5.3).

127

When introduced into (A.1) and (A.2), the transformation (A.3) nondimensionalizes the matrix elements on the left-hand sides, and (A.1) and (A.2) may be written in the form

$$\left[\overline{C}_{ij}\right] \left\{z_j\right\} = \left(\frac{b^2 \sigma_0}{2\mu}\right) \left\{\overline{D}_i\right\} , \qquad (A.4)$$

$$\left[\overline{c}_{ij}\right] \left\{\zeta_j\right\} = \left(\frac{b^2 \sigma_0}{2\mu}\right) \left\{\mathcal{D}_i\right\} , \qquad (A.5)$$

where σ_0 and τ_0 are the amplitudes of stress in the incident dilatational and shear waves, respectively, and where $\overline{C}_{ij}$ and $\overline{c}_{ij}$ are nondimensional. Then, if we let

$$z_j = \left(\frac{b^2 \sigma_0}{2\mu}\right)\overline{z}_j ,$$

$$\qquad (A.6)$$

$$\zeta_j = \left(\frac{b^2 \tau_0}{2\mu}\right)\overline{\zeta}_j .$$

The boundary conditions become

$$\left[\overline{C}_{ij}\right] \left\{\overline{z}_j\right\} = \left\{\overline{D}_i\right\} , \qquad (A.7)$$

and

$$\left[\overline{c}_{ij}\right] \left\{\overline{\zeta}_j\right\} = \left\{\overline{\mathcal{D}}_i\right\} , \qquad (A.8)$$

where $\overline{D}_i$ and $\overline{\mathcal{D}}_i$ are nondimensional. Referring to the expressions in Sections III and IV by which the stresses and displacements are represented, we note that they are linearly homogeneous in the z_j and ζ_j. Thus, from (A.6), when the solution vectors to (A.7) and (A.8) are introduced into the expressions defined by (A.3), we obtain the nondimensional stress and displacement

128

$$\tilde{\sigma}_{ij} = \frac{\sigma_{ij}}{\sigma_0} \quad , \quad \tilde{u}_i = \frac{2\mu}{\sigma_0} \frac{u_i}{b} \qquad \text{(A.9a)}$$

in the case of the incident dilatational wave, and

$$\tilde{\tau}_{ij} = \frac{\tau_{ij}}{\tau_0} \quad , \quad \tilde{v}_i = \frac{2\mu}{\tau_0} \frac{u_i}{b} \qquad \text{(A.9b)}$$

in the case of the incident shear wave.

In principle, (A.7), (A.8), and (A.9) may be used directly to determine the nondimensional stresses and displacements. However, it has been found that the form of these equations may lead to computational difficulties. The numerical behavior of the Bessel functions $J_n(z)$, $Y_n(z)$, which are constituents of the matrix elements $\bar{C}_{ij}$, $\bar{c}_{ij}$, necessitates a further modification. For fixed z, as n becomes large, the $J_n(z)$ becomes small and the $Y_n(z)$ becomes large. To keep the elements of (A.7) and (A.8) within the bounds of the IBM 7094 computer, and to ensure calculations of a well behaved character, we modify the construction of Eqs. (A.7) and (A.8). To emphasize that the elements of these matrices and the solution vectors depend upon the indices of summation p and n, we again let these integers appear explicitly. Then we modify the elements in columns 1 and 3 by letting

$$\tilde{c}_{ij,pn} = \frac{2^n n!}{|q_k|^n} \bar{c}_{ij,pn} \quad , \quad \tilde{c}_{ij,pn} = \frac{2^n n!}{|q_k|^n} \bar{c}_{ij,pn} \quad ,\text{(A.10a)}$$

$$\tilde{z}_{j,pn} = \frac{|q_k|^n}{2^n n!} \bar{z}_{j,pn} \quad , \quad \tilde{\zeta}_{j,pn} = \frac{|q_k|^n}{2^n n!} \bar{\zeta}_{j,pn} \quad , \qquad \text{(A.10b)}$$

where

$$k = 1 \quad \text{when} \quad j = 1 \; ,$$

$$k = 2 \quad \text{when} \quad j = 3 \; .$$

129

We modify the elements in columns 2, 4, 5, and 6 by letting

$$\tilde{c}_{ij,pn} = \frac{|q_k|^n}{2^n n!}\, \bar{c}_{ij,pn} \quad , \quad \tilde{\mathcal{C}}_{ij,pn} = \frac{|q_k|^n}{2^n n!}\, \bar{\mathcal{C}}_{ij,pn} \quad , \qquad \text{(A.10c)}$$

$$\tilde{z}_{j,pn} = \frac{2^n n!}{|q_k|^n}\, \bar{z}_{j,pn} \quad , \quad \tilde{\zeta}_{j,pn} = \frac{2^n n!}{|q_k|^n}\, \bar{\zeta}_{j,pn} \quad , \qquad \text{(A.10d)}$$

where

$$k = 1 \qquad \text{when} \quad j = 2\,,$$

$$k = j - 2 \quad \text{when} \quad j = 4,\ 5,\ 6\,.$$

After the definitions (A.10) are imposed, (A.7) and (A.8) become

$$\left[\tilde{c}_{ij}\right]\left\{\tilde{z}_j\right\} = \left\{\bar{D}_i\right\}\,, \qquad\qquad \text{(A.11)}$$

$$\left[\tilde{\mathcal{C}}_{ij}\right]\left\{\tilde{\zeta}_j\right\} = \left\{\bar{\mathcal{D}}_i\right\}\,. \qquad\qquad \text{(A.12)}$$

Note that the substitutions defined by (A.10) have modified only the left-hand sides. The right-hand sides have not been altered.

Because of (A.10), instead of computing the $J_n(z)$ and $Y_n(z)$, in columns 1 through 4, we compute the functions defined by

$$\tilde{J}_n(z) = \frac{2^n n!}{|q_k|^n}\, J_n(z) \quad , \quad \tilde{Y}_n(z) = \frac{|q_k|^n}{2^n n!}\, Y_n(z)\,, \qquad \text{(A.13a)}$$

where $k = 1$ in columns 1 and 2; and $k = 2$ in columns 3 and 4.

In columns 5 and 6, we compute

$$\tilde{J}_n(z) = \frac{2^n n!}{|z|^n} J_n(z) \quad , \quad \tilde{Y}_n(z) = \frac{|z|^n}{2^n n!} Y_n(z) \tag{A.13b}$$

The elements composing the left- and right-hand sides of (A.11) and (A.12) are given in Appendices B and C.

For computational purposes, Eqs. (A.11) and (A.12), which represent sets of six by six complex equations, were cast respectively into the following form, which represents sets of twelve simultaneous real equations:

$$\left[\tilde{L}_{ij}\right] \left\{\tilde{X}_j\right\} = \left\{\bar{M}_i\right\} , \tag{A.14}$$

$$\left[\tilde{\ell}_{ij}\right] \left\{\tilde{X}_j\right\} = \left\{\bar{m}_i\right\} , \tag{A.15}$$

where, using superscripts R and I to denote real and imaginary parts, (A.14) is constructed from (A.11) as follows:

$$\tilde{L}_{ij} = \tilde{C}_{ij}^R \qquad (1 \le i \le 6), \ (1 \le j \le 6)$$

$$\tilde{L}_{ij} = - \tilde{C}_{ij}^I \qquad (1 \le i \le 6), \ (7 \le j \le 12)$$

$$\tilde{L}_{i+6,j+6} = \tilde{L}_{ij} \qquad (1 \le i \le 6), \ (1 \le j \le 6)$$

$$\tilde{L}_{i+6,j} = - \tilde{L}_{ij} \qquad (1 \le i \le 6), \ (1 \le j \le 6)$$

$$\tilde{X}_j = \tilde{Z}_j^R \qquad (1 \le j \le 6)$$

$$\tilde{X}_{j+6} = \tilde{Z}_j^I \qquad (1 \le j \le 6)$$

$$\bar{M}_i = \bar{D}_i^R \qquad (1 \leq i \leq 6)$$

$$\bar{M}_{i+6} = \bar{D}_i^I \qquad (1 \leq i \leq 6) \ .$$

Similarly (A.15) is constructed from (A.12) in the following manner:

$$\tilde{\mathcal{L}}_{ij} = \tilde{\mathcal{C}}_{ij}^R \qquad (1 \leq i \leq 6), \ (1 \leq j \leq 6)$$

$$\tilde{\mathcal{L}}_{ij} = -\tilde{\mathcal{C}}_{ij}^I \qquad (1 \leq i \leq 6), \ (7 \leq j \leq 12)$$

$$\tilde{\mathcal{L}}_{i+6,j+6} = \tilde{\mathcal{L}}_{ij} \qquad (1 \leq i \leq 6), \ (1 \leq j \leq 6)$$

$$\tilde{\mathcal{L}}_{i+6,j} = -\tilde{\mathcal{L}}_{ij} \qquad (1 \leq i \leq 6), \ (1 \leq j \leq 6)$$

$$\tilde{\chi}_j = \tilde{\zeta}_j^R \qquad (1 \leq j \leq 6)$$

$$\tilde{\chi}_{j+6} = \tilde{\zeta}_j^I \qquad (1 \leq j \leq 6)$$

$$\bar{m}_i = \tilde{\mathcal{B}}_i^R \qquad (1 \leq i \leq 6)$$

$$\bar{m}_{i+6} = \tilde{\mathcal{B}}_i^I \qquad (1 \leq i \leq 6) \ .$$

We recall the discussion in Section IV.1 and note that $\tilde{L}_{ij}$ and $\tilde{\mathcal{L}}_{ij}$ stem from the response to incident dilatational and shear waves, respectively. Thus, these elements may be given in the same form if we regard $\bar{n} = n$ as pertaining to L_{ij} and $\bar{n} = -n$ as pertaining to $\tilde{\mathcal{L}}_{ij}$. Then, the real matrix elements are given by

132

$$\tilde{L}_{1,1} = - q_1^2 \left\{ \left[\frac{1}{2}\left(\frac{\lambda}{\mu}\right) - \left\{\frac{n(n-1)}{(q_1\beta)^2} - 1\right\}\right]\tilde{J}_n(q_1\beta) - \frac{1}{2(n+1)\beta}\,\tilde{J}_{n+1}(q_1\beta)\right\}$$

$$\tilde{L}_{1,2} = - q_1^2 \left\{ \left[\frac{1}{2}\left(\frac{\lambda}{\mu}\right) - \left\{\frac{n(n-1)}{(q_1\beta)^2} - 1\right\}\right]\tilde{Y}_n(q_1\beta) - \frac{2(n+1)}{q_1^2\beta}\,\tilde{Y}_{n+1}(q_1\beta)\right\}$$

$$\tilde{L}_{1,3} = \frac{\bar{n}}{\beta^2}\left[(n-1)\tilde{J}_n(q_2\beta) - \frac{q_2^2\beta}{2(n+1)}\,\tilde{J}_{n+1}(q_2\beta)\right]$$

$$\tilde{L}_{1,4} = \frac{\bar{n}}{\beta^2}\left[(n-1)\tilde{Y}_n(q_2\beta) - 2\beta(n+1)\tilde{Y}_{n+1}(q_2\beta)\right]$$

$$\tilde{L}_{1,5} = \tilde{L}_{1,6} = \cdots = \tilde{L}_{1,12} = 0$$

$$\tilde{L}_{2,1} = \frac{\bar{n}}{\beta^2}\left[\frac{q_1^2\beta}{2(n+1)}\,\tilde{J}_{n+1}(q_1\beta) - (n-1)\tilde{J}_n(q_1\beta)\right]$$

$$\tilde{L}_{2,2} = \frac{\bar{n}}{\beta^2}\left[2\beta(n+1)\tilde{Y}_{n+1}(q_1\beta) - (n-1)\tilde{Y}_n(q_1\beta)\right]$$

$$\tilde{L}_{2,3} = - \frac{q_2^2}{2}\left[\left(\frac{2n(n-1)}{(q_2\beta)^2} - 1\right)\tilde{J}_n(q_2\beta) + \frac{1}{\beta(n+1)}\,\tilde{J}_{n+1}(q_2\beta)\right]$$

$$\tilde{L}_{2,4} = - \frac{q_2^2}{2}\left[\left(\frac{2n(n-1)}{(q_2\beta)^2} - 1\right)\tilde{Y}_n(q_2\beta) + \frac{4(n+1)}{q_2^2\beta}\,\tilde{Y}_{n+1}(q_2\beta)\right]$$

$$\tilde{L}_{2,5} = \tilde{L}_{2,6} = \cdots = \tilde{L}_{2,12} = 0$$

133

$$\tilde{L}_{3,1} = -q_1^2 \left\{ \left[\frac{1}{2}\left(\frac{\tilde{\lambda}}{\mu}\right) - \left\{ \frac{n(n-1)}{q_1^2} - 1 \right\} \right] \tilde{J}_n(q_1) - \frac{1}{2(n+1)} \tilde{J}_{n+1}(q_1) \right\}$$

$$\tilde{L}_{3,2} = -q_1^2 \left\{ \left[\frac{1}{2}\left(\frac{\tilde{\lambda}}{\mu}\right) - \left\{ \frac{n(n-1)}{q_1^2} - 1 \right\} \right] \tilde{Y}_n(q_1) - \frac{2(n+1)}{q_1^2} \tilde{Y}_{n+1}(q_1) \right\}$$

$$\tilde{L}_{3,3} = \bar{n} \left[(n-1)\tilde{J}_n(q_2) - \frac{q_2^2}{2(n+1)} \tilde{J}_{n+1}(q_2) \right]$$

$$\tilde{L}_{3,4} = \bar{n} \left[(n-1)\tilde{Y}_n(q_2) - 2(n+1)\tilde{Y}_{n+1}(q_2) \right]$$

$$\tilde{L}_{3,5} = \left(\frac{q_{3e}^n}{2^n n!}\right)^2 \left\{ (\bar{q}_3^2 - \tilde{q}_3^2)\left[\left[\frac{1}{2}\left(\frac{\bar{\lambda}}{\mu}\right) + \left(\frac{\bar{\mu}}{\mu}\right)\right]\widetilde{J}_{n3}^R - \left[\frac{1}{2}\left(\frac{\tilde{\lambda}}{\mu}\right) + \left(\frac{\tilde{\mu}}{\mu}\right)\right]\widetilde{J}_{n3}^I \right] \right.$$

$$- \frac{q_{3e}}{2(n+1)} \bar{q}_3 \left[\left(\frac{\tilde{\mu}}{\mu}\right)\widetilde{J}_{(n+1)3}^R - \left(\frac{\tilde{\mu}}{\mu}\right)\widetilde{J}_{(n+1)3}^I \right]$$

$$- \frac{q_{3e}}{2(n+1)} \tilde{q}_3 \left[\left(\frac{\tilde{\mu}}{\mu}\right)\widetilde{J}_{(n+1)3}^R + \left(\frac{\bar{\mu}}{\mu}\right)\widetilde{J}_{(n+1)3}^I \right]$$

$$+ 2\bar{q}_3\tilde{q}_3 \left[\left[\frac{1}{2}\left(\frac{\tilde{\lambda}}{\mu}\right) + \left(\frac{\tilde{\mu}}{\mu}\right)\right]\widetilde{J}_{n3}^R + \left[\frac{1}{2}\left(\frac{\bar{\lambda}}{\mu}\right) + \left(\frac{\bar{\mu}}{\mu}\right)\right]\widetilde{J}_{n3}^I \right] - (n)(n-1)\left[\left(\frac{\bar{\mu}}{\mu}\right)\widetilde{J}_{n3}^R - \left(\frac{\tilde{\mu}}{\mu}\right)\widetilde{J}_{n3}^I \right] \right\}$$

$$- 2\bar{q}_3\tilde{q}_3 \left[\left[\frac{1}{2}\left(\frac{\bar{\lambda}}{\mu}\right) + \left(\frac{\bar{\mu}}{\mu}\right)\right]\widetilde{Y}_{n3}^R - \left[\frac{1}{2}\left(\frac{\tilde{\lambda}}{\mu}\right) + \left(\frac{\tilde{\mu}}{\mu}\right)\right]\widetilde{Y}_{n3}^I \right]$$

$$+ (\bar{q}_3^2 - \tilde{q}_3^2) \left[\left[\frac{1}{2}\left(\frac{\tilde{\lambda}}{\mu}\right) + \left(\frac{\tilde{\mu}}{\mu}\right)\right]\widetilde{Y}_{n3}^R + \left[\frac{1}{2}\left(\frac{\bar{\lambda}}{\mu}\right) + \left(\frac{\bar{\mu}}{\mu}\right)\right]\widetilde{Y}_{n3}^I \right]$$

$$- \left(\frac{\bar{\mu}}{\mu}\right)\left\{ (n)(n-1)\widetilde{Y}_{n3}^I + \frac{2(n+1)}{q_{3e}}\left[\bar{q}_3\widetilde{Y}_{(n+1)3}^I - \tilde{q}_3\widetilde{Y}_{(n+1)3}^R \right] \right\}$$

$$- \left(\frac{\tilde{\mu}}{\mu}\right)\left\{ (n)(n-1)\widetilde{Y}_{n3}^R + \frac{2(n+1)}{q_{3e}}\left[\bar{q}_3\widetilde{Y}_{(n+1)3}^R + \tilde{q}_3\widetilde{Y}_{(n+1)3}^I \right] \right\}$$

134

$$\tilde{L}_{3,6} = \bar{n}\left[\left(\frac{\bar{\mu}}{\mu}\right)R_{rr}^{s} - \left(\frac{\tilde{\mu}}{\mu}\right)I_{rr}^{s}\right]$$

where

$$R_{rr}^{s} = -\left(\frac{q_{4e}^{n}}{2^{n}n!}\right)^{2}\left\{(n-1)\tilde{J}_{n4}^{R} - \left(\frac{q_{4e}}{2(n+1)}\right)\left[\bar{q}_{4}\tilde{J}_{(n+1)4}^{R} + \tilde{q}_{4}\tilde{J}_{(n+1)4}^{I}\right]\right\}$$

$$- (n-1)\tilde{Y}_{n4}^{I} + \frac{2(n+1)}{q_{4e}}\left[\bar{q}_{4}\tilde{Y}_{(n+1)4}^{I} - \tilde{q}_{4}\tilde{Y}_{(n+1)4}^{R}\right]$$

$$I_{rr}^{s} = -\left(\frac{q_{4e}^{n}}{2^{n}n!}\right)^{2}\left\{(n-1)\tilde{J}_{n4}^{I} - \left(\frac{q_{4e}}{2(n+1)}\right)\left[\bar{q}_{4}\tilde{J}_{(n+1)4}^{I} - \tilde{q}_{4}\tilde{J}_{(n+1)4}^{R}\right]\right\}$$

$$+ (n-1)\tilde{Y}_{n4}^{R} - \frac{2(n+1)}{q_{4e}}\left[\bar{q}_{4}\tilde{Y}_{(n+1)4}^{R} + \tilde{q}_{4}\tilde{Y}_{(n+1)4}^{I}\right]$$

$$\tilde{L}_{3,7} = \tilde{L}_{3,8} = \tilde{L}_{3,9} = \tilde{L}_{3,10} = 0$$

$$\tilde{L}_{3,11} = -\left(\frac{q_{3e}^{n}}{2^{n}n!}\right)^{2}\left\{(\bar{q}_{3}^{2} - \tilde{q}_{3}^{2})\left[\left[\tfrac{1}{2}\left(\frac{\bar{\lambda}}{\mu}\right) + \left(\frac{\bar{\mu}}{\mu}\right)\right]\tilde{J}_{n3}^{I} + \left[\tfrac{1}{2}\left(\frac{\tilde{\lambda}}{\mu}\right) + \left(\frac{\tilde{\mu}}{\mu}\right)\right]\tilde{J}_{n3}^{R}\right]\right.$$

$$- \frac{q_{3e}}{2(n+1)}\,\bar{q}_{3}\left[\left(\frac{\tilde{\mu}}{\mu}\right)\tilde{J}_{(n+1)3}^{R} + \left(\frac{\bar{\mu}}{\mu}\right)\tilde{J}_{(n+1)3}^{I}\right]$$

$$+ \frac{q_{3e}}{2(n+1)}\,\tilde{q}_{3}\left[\left(\frac{\bar{\mu}}{\mu}\right)\tilde{J}_{(n+1)3}^{R} - \left(\frac{\tilde{\mu}}{\mu}\right)\tilde{J}_{(n+1)3}^{I}\right]$$

$$- 2\bar{q}_{3}\tilde{q}_{3}\left[\left[\tfrac{1}{2}\left(\frac{\bar{\lambda}}{\mu}\right) + \left(\frac{\bar{\mu}}{\mu}\right)\right]\tilde{J}_{n3}^{R} - \left[\tfrac{1}{2}\left(\frac{\tilde{\lambda}}{\mu}\right) + \left(\frac{\tilde{\mu}}{\mu}\right)\right]\tilde{J}_{n3}^{I}\right]$$

$$- n(n-1)\left[\left(\frac{\bar{\mu}}{\mu}\right)\tilde{J}_{n3}^{I} + \left(\frac{\tilde{\mu}}{\mu}\right)\tilde{J}_{n3}^{R}\right]\right\}$$

$$- (\bar{q}_{3}^{2} - \tilde{q}_{3}^{2})\left[\left[\tfrac{1}{2}\left(\frac{\bar{\lambda}}{\mu}\right) + \left(\frac{\bar{\mu}}{\mu}\right)\right]\tilde{Y}_{n3}^{R} - \left[\tfrac{1}{2}\left(\frac{\tilde{\lambda}}{\mu}\right) + \left(\frac{\tilde{\mu}}{\mu}\right)\right]\tilde{Y}_{n3}^{I}\right]$$

$$L_{3,1} = \pi\left[2(n+1)\tilde{Y}_{n+1}(q_1) - (n-1)\tilde{Y}_n(q_1)\right]$$

$$L_{3,2} = \frac{q^2}{2}\left[\frac{2n(n+1)}{q_2^2} - 1\right]Y_n(q_2) + \frac{1}{(n+1)}\tilde{J}_{n+1}(q_2)$$

$$L_{3,3} = \frac{q^2}{2}\left[\frac{n(n-1)}{q_2^2} - 1\right]Y_n(q_2) + \frac{n(n+1)}{q_2^2}\tilde{Y}_{n+1}(q_2)$$

$$I_{r\theta}^d = -\left(\frac{q_{3e}^n}{2^n n!}\right)^2 \left\{\left(\frac{q_{3e}}{2(n+1)}\right)\left[\bar{q}_3 \tilde{J}_{(n+1)3}^I - \tilde{q}_3 \tilde{J}_{(n+1)3}^R\right] - (n-1)\tilde{J}_{n3}^I\right\}$$

$$+ \frac{2(n+1)}{q_{3e}}\left[\bar{q}_3 \tilde{Y}_{(n+1)3}^R + \tilde{q}_3 \tilde{Y}_{(n+1)3}^I\right] - (n-1)\tilde{Y}_{n3}^R$$

$$\tilde{L}_{4,6} = \left(\frac{\bar{\mu}}{\mu}\right)R_{r\theta}^s - \left(\frac{\tilde{\mu}}{\mu}\right)I_{r\theta}^s$$

where

$$R_{r\theta}^s = \frac{1}{2}\left|\left(\frac{q_{4e}^n}{2^n n!}\right)^2 \left\{\left[2n(n-1) - (\bar{q}_4^2 - \tilde{q}_4^2)\right]\tilde{J}_{n4}^R - 2\bar{q}_4 \tilde{q}_4 \tilde{J}_{n4}^I\right.\right.$$

$$+ \frac{q_{4e}}{(n+1)}\left[\bar{q}_4 \tilde{J}_{(n+1)4}^R + \tilde{q}_4 \tilde{J}_{(n+1)4}^I\right]\right\}$$

$$+ \left[2n(n-1) - (\bar{q}_4^2 - \tilde{q}_4^2)\right]\tilde{Y}_{n4}^I + 2\bar{q}_4 \tilde{q}_4 \tilde{Y}_{n4}^R$$

$$+ \left.\frac{4(n+1)}{q_{4e}}\left[\bar{q}_4 \tilde{Y}_{(n+1)4}^I - \tilde{q}_4 \tilde{Y}_{(n+1)4}^R\right]\right|$$

$$I_{r\theta}^s = \frac{1}{2}\left|\left(\frac{q_{4e}^n}{2^n n!}\right)^2 \left\{\left[2n(n-1) - (\bar{q}_4^2 - \tilde{q}_4^2)\right]\tilde{J}_{n4}^I + 2\bar{q}_4 \tilde{q}_4 \tilde{J}_{n4}^R\right.\right.$$

$$+ \frac{q_{4e}}{(n+1)}\left[\bar{q}_4 \tilde{J}_{(n+1)4}^I - \tilde{q}_4 \tilde{J}_{(n+1)4}^R\right]\right\}$$

$$- \left[2(n)(n-1) - (\bar{q}_4^2 - \tilde{q}_4^2)\right]\tilde{Y}_{n4}^R + 2\bar{q}_4 \tilde{q}_4 \tilde{Y}_{n4}^I$$

$$- \left.\frac{4(n+1)}{q_{4e}}\left[\bar{q}_4 \tilde{Y}_{(n+1)4}^R + \tilde{q}_4 \tilde{Y}_{(n+1)4}^I\right]\right|$$

$$\tilde{L}_{4,7} = \tilde{L}_{4,8} = \tilde{L}_{4,9} = \tilde{L}_{4,10} = 0$$

137

$$\tilde{L}_{4,11} = -\bar{n}\left[\left(\frac{\tilde{\mu}}{\mu}\right)R_{r\theta}^d + \left(\frac{\bar{\mu}}{\mu}\right)I_{r\theta}^d\right]$$

$$\tilde{L}_{4,12} = -\left[\left(\frac{\tilde{\mu}}{\mu}\right)R_{r\theta}^s + \left(\frac{\bar{\mu}}{\mu}\right)I_{r\theta}^s\right]$$

$$\tilde{L}_{5,1} = n\tilde{J}_n(q_1) - \frac{q_1^2}{2(n+1)}\tilde{J}_{n+1}(q_1)$$

$$\tilde{L}_{5,2} = n\tilde{Y}_n(q_1) - 2(n+1)\tilde{Y}_{n+1}(q_1)$$

$$\tilde{L}_{5,3} = \bar{n}\tilde{J}_n(q_2)$$

$$\tilde{L}_{5,4} = \bar{n}\tilde{Y}_n(q_2)$$

$$\tilde{L}_{5,5} = \left[\left(\frac{q_{3e}^n}{2^n n!}\right)^2\left\{n\tilde{J}_{n3}^R - \left(\frac{q_{3e}}{2(n+1)}\right)\left[\bar{q}_3\tilde{J}_{(n+1)3}^R + \tilde{q}_3\tilde{J}_{(n+1)3}^I\right]\right\} + n\tilde{Y}_{n3}^I\right.$$
$$\left. - \frac{2(n+1)}{q_{3e}}\left[\bar{q}_3\tilde{Y}_{(n+1)3}^I - \tilde{q}_3\tilde{Y}_{(n+1)3}^R\right]\right]$$

$$\tilde{L}_{5,6} = -\bar{n}\left\{\left(\frac{q_{4e}^n}{2^n n!}\right)^2\tilde{J}_{n4}^R + \tilde{Y}_{n4}^I\right\}$$

$$\tilde{L}_{5,7} = \tilde{L}_{5,8} = \tilde{L}_{5,9} = \tilde{L}_{5,10} = 0$$

138

$$\tilde{L}_{5,11} = - \left[\left(\frac{q_{3e}^n}{2^n n!} \right)^2 \left\{ n \tilde{J}_{n3}^I - \left(\frac{q_{3e}}{2(n+1)} \right) \left[\bar{q}_3 \tilde{J}_{(n+1)3}^I - \tilde{q}_3 \tilde{J}_{(n+1)3}^R \right] \right\} - n \tilde{Y}_{n3}^R \right.$$

$$\left. + \frac{2(n+1)}{q_{3e}} \left[\bar{q}_3 \tilde{Y}_{(n+1)3}^R + \tilde{q}_3 \tilde{Y}_{(n+1)3}^I \right] \right]$$

$$\tilde{L}_{5,12} = \bar{n} \left\{ \left(\frac{q_{4e}^n}{2^n n!} \right)^2 \tilde{J}_{n4}^I - \tilde{Y}_{n4}^R \right\}$$

$$\tilde{L}_{6,1} = - \bar{n} \tilde{J}_n(q_1)$$

$$\tilde{L}_{6,2} = - \bar{n} \tilde{Y}_n(q_1)$$

$$\tilde{L}_{6,3} = - n \tilde{J}_n(q_2) + \frac{q_2^2}{2(n+1)} \tilde{J}_{n+1}(q_2)$$

$$\tilde{L}_{6,4} = - n \tilde{Y}_n(q_2) + 2(n+1) \tilde{Y}_{n+1}(q_2)$$

$$\tilde{L}_{6,5} = \bar{n} \left\{ \left(\frac{q_{3e}^n}{2^n n!} \right)^2 \tilde{J}_{n3}^R + \tilde{Y}_{n3}^I \right\}$$

$$\tilde{L}_{6,6} = \left(\frac{q_{4e}^n}{2^n n!} \right)^2 \left\{ n \tilde{J}_{n4}^R - \left(\frac{q_{4e}}{2(n+1)} \right) \left[\bar{q}_4 \tilde{J}_{(n+1)4}^R + \tilde{q}_4 \tilde{J}_{(n+1)4}^I \right] \right\}$$

$$+ n \tilde{Y}_{n4}^I - \frac{2(n+1)}{q_{4e}} \left[\bar{q}_4 \tilde{Y}_{(n+1)4}^I - \tilde{q}_4 \tilde{Y}_{(n+1)4}^R \right]$$

$$\tilde{L}_{6,7} = \tilde{L}_{6,8} = \tilde{L}_{6,9} = \tilde{L}_{6,10} = 0$$

139

$$\tilde{L}_{6,11} = -\bar{n}\left\{\left(\frac{q_{3e}^{n}}{2^{n}n!}\right)^{2}\tilde{J}_{n3}^{I} - \tilde{Y}_{n3}^{R}\right\}$$

$$\tilde{L}_{6,12} = -\left(\frac{q_{4e}^{n}}{2^{n}n!}\right)^{2}\left\{n\tilde{J}_{n4}^{I} - \left(\frac{q_{4e}}{2(n+1)}\right)\left[\bar{q}_{4}\tilde{J}_{(n+1)4}^{I} - \tilde{q}_{4}\tilde{J}_{(n+1)4}^{R}\right]\right\}$$

$$- n\tilde{Y}_{n}^{R} + \frac{2(n+1)}{q_{4e}}\left[\bar{q}_{4}\tilde{Y}_{(n+1)4}^{R} + \tilde{q}_{4}\tilde{Y}_{(n+1)4}^{I}\right]$$

and

$$\tilde{L}_{ij} = -\tilde{L}_{i-6,\,j+6} \qquad \begin{array}{l} 7 \leq i \leq 12 \\ 1 \leq j \leq 6 \end{array}$$

$$\tilde{L}_{ij} = \tilde{L}_{i-6,\,j-6} \qquad \begin{array}{l} 7 \leq i \leq 12 \\ 7 \leq j \leq 12 \end{array}$$

In the preceding equations,

$$\tilde{J}_{nk} = \tilde{J}_{n}(q_{k})$$

$$k = 3, 4 .$$

$$\tilde{Y}_{nk} = \tilde{Y}_{n}(q_{k})$$

The expressions, in real form, for the stresses and displacements associated with the responses to incident dilatational and shear waves will be given now. The transformations leading to Eq. (A.9), in conjunction with the results (A.10b) and (A.13), yield — when applied to the appropriate terms in the expressions defined by Eqs. (3.8.3) and (4.5.3) — the following formulation of the stresses and displacements associated with the response to an incident dilatational wave. Note that the components of the solution vector entering into these terms are those obtained from

140

Eq. (A.14). In addition, the rigid body contributions discussed
in Section V.1, have been removed by taking account of Eqs. (5.1.6)
and (5.1.9), and the variable t/T is to be regarded as computed
with respect to the time of arrival of the incident wave as

$$\left(\frac{t}{T}\right) = \left(\frac{c_{dm}\bar{t}}{b}\right)\left(\frac{b}{c_{dm}T}\right) + \left(\frac{c_{dm}t_0}{b}\right)\left(\frac{b}{c_{dm}T}\right) .$$

Thus,

$$
\begin{aligned}
\tilde{\sigma}_{rr}^{pn} = - \cos n\theta \Bigg| \Bigg\{ &q_1^2\left[\left\{\tfrac{1}{2}\left(\tfrac{\lambda}{\mu}\right) - \left(\tfrac{n(n-1)}{(q_1\rho)^2} - 1\right)\right\}\tilde{J}_n(q_1\rho) - \tfrac{1}{2(n+1)\rho}J_{n+1}(q_1\rho)\right]\tilde{X}_1 \\
+ &q_1^2\left[\left\{\tfrac{1}{2}\left(\tfrac{\lambda}{\mu}\right) - \left(\tfrac{n(n-1)}{(q_1\rho)^2} - 1\right)\right\}\tilde{Y}_n(q_1\rho) - \tfrac{2(n+1)}{q_1^2\rho}\tilde{Y}_{n+1}(q_1\rho)\right]\tilde{X}_2 \\
- &\tfrac{\bar{n}}{\rho^2}\left[(n-1)\tilde{J}_n(q_2\rho) - \tfrac{q_2^2\rho}{2(n+1)}\tilde{J}_{n+1}(q_2\rho)\right]\tilde{X}_3 \\
- &\tfrac{\bar{n}}{\rho^2}\left[(n-1)\tilde{Y}_n(q_2\rho) - 2(n+1)\rho\tilde{Y}_{n+1}(q_2\rho)\right]\tilde{X}_4 \Bigg\} \cos p\pi\left(\tfrac{t}{T}\right) \\
- \Bigg\{ &q_1^2\left[\left\{\tfrac{1}{2}\left(\tfrac{\lambda}{\mu}\right) - \left(\tfrac{n(n-1)}{(q_1\rho)^2} - 1\right)\right\}\tilde{J}_n(q_1\rho) - \tfrac{1}{2(n+1)\rho}\tilde{J}_{n+1}(q_1\rho)\right]\tilde{X}_7 \\
+ &q_1^2\left[\left\{\tfrac{1}{2}\left(\tfrac{\lambda}{\mu}\right) - \left(\tfrac{n(n-1)}{(q_1\rho)^2} - 1\right)\right\}\tilde{Y}_n(q_1\rho) - \tfrac{2(n+1)}{q_1^2\rho}\tilde{Y}_{n+1}(q_1\rho)\right]\tilde{X}_8 \\
- &\tfrac{\bar{n}}{\rho^2}\left[(n-1)\tilde{J}_n(q_2\rho) - \tfrac{q_2^2\rho}{2(n+1)}\tilde{J}_{n+1}(q_2\rho)\right]\tilde{X}_9 \\
- &\tfrac{\bar{n}}{\rho^2}\left[(n-1)\tilde{Y}_n(q_2\rho) - 2(n+1)\rho\tilde{Y}_{n+1}(q_2\rho)\right]\tilde{X}_{10} \Bigg\} \sin p\pi\left(\tfrac{t}{T}\right) \Bigg|
\end{aligned}
$$

141

$$
\tilde\sigma_{\theta\theta}^{pn} = - \cos n\theta \left[\left\{ \left[\left\{ \frac{1}{2}\left(\frac{\lambda}{\mu}\right)q_1^2 + \frac{n(n-1)}{\rho^2} \right\} \tilde J_n(q_1\rho) + \frac{q_1^2}{2(n+1)} \frac{\tilde J_{n+1}(q_1\rho)}{\rho} \right] \tilde X_1 \right. \right.
$$

$$
+ \left[\left\{ \frac{1}{2}\left(\frac{\lambda}{\mu}\right)q_1^2 + \frac{n(n-1)}{\rho^2} \right\} \tilde Y_n(q_1\rho) + \frac{2(n+1)}{\rho} \tilde Y_{n+1}(q_1\rho) \right] \tilde X_2
$$

$$
+ \frac{n}{\rho^2} \left[(n-1)\tilde J_n(q_2\rho) - \frac{q_2^2\rho}{2(n+1)} \tilde J_{n+1}(q_2\rho) \right] \tilde X_3
$$

$$
\left. + \frac{n}{\rho^2} \left[(n-1)\tilde Y_n(q_2\rho) - 2(n+1)\rho\tilde Y_{n+1}(q_2\rho) \right] \tilde X_4 \right\} \cos p\pi\left(\frac{t}{T}\right)
$$

$$
- \left\{ \left[\left\{ \frac{1}{2}\left(\frac{\lambda}{\mu}\right)q_1^2 + \frac{n(n-1)}{\rho^2} \right\} \tilde J_n(q_1\rho) + \frac{q_1^2}{2(n+1)} \frac{\tilde J_{n+1}(q_1\rho)}{\rho} \right] \tilde X_7 \right.
$$

$$
+ \left[\left\{ \frac{1}{2}\left(\frac{\lambda}{\mu}\right)q_1^2 + \frac{n(n-1)}{\rho^2} \right\} \tilde Y_n(q_1\rho) + \frac{2(n+1)}{\rho} \tilde Y_{n+1}(q_1\rho) \right] \tilde X_8
$$

$$
+ \frac{n}{\rho^2} \left[(n-1)\tilde J_n(q_2\rho) - \frac{q_2^2\rho}{2(n+1)} \tilde J_{n+1}(q_2\rho) \right] \tilde X_9
$$

$$
\left. \left. + \frac{n}{\rho^2} \left[(n-1)\tilde Y_n(q_2\rho) - 2(n+1)\rho\tilde Y_{n+1}(q_2\rho) \right] \tilde X_{10} \right\} \sin p\pi\left(\frac{t}{T}\right) \right]
$$

$$
\tilde{\sigma}_{r\theta}^{pn} = \sin n\theta \left[\left\{ \frac{\bar{n}}{\rho^2} \left[\frac{q_1^2 \rho}{2(n+1)} \tilde{J}_{n+1}(q_1\rho) - (n-1)\tilde{J}_n(q_1\rho) \right] \tilde{X}_1 \right. \right.
$$

$$
+ \frac{\bar{n}}{\rho^2} \left[2(n+1)\rho\tilde{Y}_{n+1}(q_1\rho) - (n-1)\tilde{Y}_n(q_1\rho) \right] \tilde{X}_2
$$

$$
- \frac{q_2^2}{2} \left[\left\{ \frac{2n(n-1)}{(q_2\rho)^2} - 1 \right\} \tilde{J}_n(q_2\rho) + \frac{1}{(n+1)\rho} \tilde{J}_{n+1}(q_2\rho) \right] \tilde{X}_3
$$

$$
\left. - \frac{q_2^2}{2} \left[\left\{ \frac{2n(n-1)}{(q_2\rho)^2} - 1 \right\} \tilde{Y}_n(q_2\rho) + \frac{4(n+1)}{q_2^2\rho} \tilde{Y}_{n+1}(q_2\rho) \right] \tilde{X}_4 \right\} \cos p\pi \frac{t}{T}
$$

$$
- \left\{ + \frac{\bar{n}}{\rho^2} \left[\frac{q_1^2 \rho}{2(n+1)} \tilde{J}_{n+1}(q_1\rho) - (n-1)\tilde{J}_n(q_1\rho) \right] \tilde{X}_7 \right.
$$

$$
+ \frac{\bar{n}}{\rho^2} \left[2(n+1)\rho\tilde{Y}_{n+1}(q_1\rho) - (n-1)\tilde{Y}_n(q_1\rho) \right] \tilde{X}_8
$$

$$
- \frac{q_2^2}{2} \left[\left\{ \frac{2n(n-1)}{(q_2\rho)^2} - 1 \right\} \tilde{J}_n(q_2\rho) + \frac{1}{(n+1)\rho} \tilde{J}_{n+1}(q_2\rho) \right] \tilde{X}_9
$$

$$
\left. \left. - \frac{q_2^2}{2} \left[\left\{ \frac{2n(n-1)}{(q_2\rho)^2} - 1 \right\} \tilde{Y}_n(q_2\rho) + \frac{4(n+1)}{q_2^2\rho} \tilde{Y}_{n+1}(q_2\rho) \right] \tilde{X}_{10} \right\} \sin p\pi \frac{t}{T} \right]
$$

143

$$
\tilde{u}_r^{pn} = \cos n\theta \left\lvert\!\left\{\!\left\{\!\left[\frac{n}{\rho}\tilde{J}_n(q_1\rho) - \frac{q_1^2}{2(n+1)}\tilde{J}_{n+1}(q_1\rho)\right]\tilde{X}_1 \right.\right.\right.
$$

$$
+ \left[\frac{n}{\rho}\tilde{Y}_n(q_1\rho) - 2(n+1)\tilde{Y}_{n+1}(q_1\rho)\right]\tilde{X}_2
$$

$$
+ \left[\frac{\bar{n}}{\rho}\tilde{J}_n(q_2\rho)\right]\tilde{X}_3 + \left[\frac{\bar{n}}{\rho}\tilde{Y}_n(q_2\rho)\right]\tilde{X}_4 \right\}\cos\left[p\pi\left(\frac{t}{T}\right)\right]
$$

$$
- \left\{\!\left[\frac{n}{\rho}\tilde{J}_n(q_1\rho) - \frac{q_1^2}{2(n+1)}\tilde{J}_{n+1}(q_1\rho)\right]\tilde{X}_7 + \left[\frac{n}{\rho}\tilde{Y}_n(q_1\rho) - 2(n+1)\tilde{Y}_{n+1}(q_1\rho)\right]\tilde{X}_8\right.
$$

$$
+ \left[\frac{\bar{n}}{\rho}\tilde{J}_n(q_2\rho)\right]\tilde{X}_9 + \left[\frac{\bar{n}}{\rho}\tilde{Y}_n(q_2\rho)\right]\tilde{X}_{10}\right\}\sin\left[p\pi\left(\frac{t}{T}\right)\right]
$$

$$
- \delta_{n1}\left[\left\{\!\left[\frac{1}{\beta}\tilde{J}_1(q_1\beta) - \frac{q_1^2}{4}\tilde{J}_2(q_1\beta)\right]\tilde{X}_1 + \left[\frac{1}{\beta}\tilde{Y}_1(q_1\beta) - 4\tilde{Y}_2(q_1\beta)\right]\tilde{X}_2\right.\right.
$$

$$
+ \left[\frac{1}{\beta}\tilde{J}_1(q_2\beta)\right]\tilde{X}_3 + \left[\frac{1}{\beta}\tilde{Y}_1(q_2\beta)\right]\tilde{X}_4\right\}\cos\left[p\pi\left(\frac{t^*}{T}\right)\right]
$$

$$
- \left\{\!\left[\frac{1}{\beta}\tilde{J}_1(q_1\beta) - \frac{q_1^2}{4}\tilde{J}_2(q_1\beta)\right]\tilde{X}_7 + \left[\frac{1}{\beta}\tilde{Y}_1(q_1\beta) - 4\tilde{Y}_2(q_1\beta)\right]\tilde{X}_8\right.
$$

$$
\left.\left.\left.\left.+ \left[\frac{1}{\beta}\tilde{J}_1(q_2\beta)\right]\tilde{X}_9 + \left[\frac{1}{\beta}\tilde{Y}_1(q_2\beta)\right]\tilde{X}_{10}\right\}\sin\left[p\pi\left(\frac{t^*}{T}\right)\right]\right]\right\rvert
$$

where $\delta_{n1} = \begin{cases} 0 & \text{if} \quad n \neq 1 \\ 1 & \text{if} \quad n = 1 \end{cases}$

and $\dfrac{t^*}{T} = \left(\dfrac{t_0}{T}\right) - 2\left(\dfrac{b}{c_{dm}T}\right)$

144

$$\tilde{u}_\theta^{pn} = - \sin n\theta \left\{ \left\{ \left[\frac{\bar{n}}{\rho} \tilde{J}_n(q_1\rho) \right] \tilde{X}_1 + \left[\frac{\bar{n}}{\rho} \tilde{Y}_n(q_1\rho) \right] \tilde{X}_2 \right. \right.$$

$$+ \left[\frac{n}{\rho} \tilde{J}_n(q_2\rho) - \frac{q_2^2}{2(n+1)} \tilde{J}_{n+1}(q_2\rho) \right] \tilde{X}_3$$

$$+ \left[\frac{n}{\rho} \tilde{Y}_n(q_2\rho) - 2(n+1)\tilde{Y}_{n+1}(q_2\rho) \right] \tilde{X}_4 \right\} \cos\left[p\pi\left(\frac{t}{T}\right) \right]$$

$$- \left\{ \left[\frac{\bar{n}}{\rho} \tilde{J}_n(q_1\rho) \right] \tilde{X}_7 + \left[\frac{\bar{n}}{\rho} \tilde{Y}_n(q_1\rho) \right] \tilde{X}_8 + \left[\frac{n}{\rho} \tilde{J}_n(q_2\rho) - \frac{q_2^2}{2(n+1)} \tilde{J}_{n+1}(q_2\rho) \right] \tilde{X}_9 \right.$$

$$+ \left[\frac{n}{\rho} \tilde{Y}_n(q_2\rho) - 2(n+1)\tilde{Y}_{n+1}(q_2\rho) \right] \tilde{X}_{10} \right\} \sin\left[p\pi\left(\frac{t}{T}\right) \right]$$

$$- \delta_{n1} \left[\left\{ \left[\frac{1}{\beta} \tilde{J}_1(q_1\beta) \right] \tilde{X}_1 + \left[\frac{1}{\beta} \tilde{Y}_1(q_1\beta) \right] \tilde{X}_2 + \left[\frac{1}{\beta} \tilde{J}_1(q_2\beta) - \frac{q_2^2}{4} \tilde{J}_2(q_2\beta) \right] \tilde{X}_3 \right. \right.$$

$$+ \left[\frac{1}{\beta} \tilde{Y}_1(q_2\beta) - 4\tilde{Y}_2(q_2\beta) \right] \tilde{X}_4 \right\} \cos\left[p\pi \frac{t^*}{T} \right]$$

$$- \left\{ \left[\frac{1}{\beta} \tilde{J}_1(q_1\beta) \right] \tilde{X}_7 + \left[\frac{1}{\beta} \tilde{Y}_1(q_1\beta) \right] \tilde{X}_8 + \left[\frac{1}{\beta} \tilde{J}_1(q_2\beta) - \frac{q_2^2}{4} \tilde{J}_2(q_2\beta) \right] \tilde{X}_9 \right.$$

$$\left. \left. + \left[\frac{1}{\beta} \tilde{Y}_1(q_2\beta) - 4\tilde{Y}_2(q_2\beta) \right] \tilde{X}_{10} \right\} \sin\left[p\pi \frac{t^*}{T} \right] \right] \right\}$$

where
$$\delta_{n1} = \begin{cases} 0 & \text{if} \quad n \neq 1 \\ 1 & \text{if} \quad n = 1 \end{cases}$$

and
$$\frac{t^*}{T} = \left(\frac{t_0}{T}\right) - 2\left(\frac{b}{c_{dm}T}\right)$$

145

The stresses and displacements associated with the response to an incident shear wave are obtained from the preceding expressions by: 1) regarding $\tilde{\sigma}$, $\tilde{u}$, $\tilde{X}_j$ and U as $\tilde{\tau}$, $\tilde{v}$, $\tilde{Y}_j$ and $\tilde{\eta}$, respectively; 2) $\bar{n}$ as equal to $-n$; 3) interchanging $\sin n\bar{\theta}$ and $\cos n\bar{\theta}$; 4) replacing $\frac{t^*}{T}$ by $\frac{\tilde{t}^*}{T} = \frac{t_0}{T} - 2\left(\frac{b}{c_{dm}T}\right)\left(\frac{c_{dm}}{c_{tm}}\right)$; and 5) treating the $n = 0$ case separately for $\tilde{v}_{\bar{\theta}}^{po}$ as

$$\tilde{v}_{\bar{\theta}}^{po} = \left\{\left[\frac{q_2^2}{2}\,\tilde{J}_1(q_2\rho)\right]\tilde{X}_3 + \left[2\tilde{Y}_1(q_2\rho)\right]\tilde{X}_4\right\}\cos\left[p\pi\,\frac{t}{T}\right]$$

$$- \left\{\left[\frac{q_2^2}{2}\,\tilde{J}_1(q_2\rho)\right]\tilde{X}_9 + \left[2\tilde{Y}_1(q_2\rho)\right]\tilde{X}_{10}\right\}\sin\left[p\pi\,\frac{t}{T}\right]$$

$$- \left\{\left[\frac{q_2^2}{2}\,\tilde{J}_1(q_2\beta)\right]\tilde{X}_3 + \left[2\tilde{Y}_1(q_2\beta)\right]\tilde{X}_4\right\}\cos\left[p\pi\,\frac{\tilde{t}^*}{T}\right]$$

$$+ \left\{\left[\frac{q_2^2}{2}\,\tilde{J}_1(q_2\beta)\right]\tilde{X}_9 + \left[2\tilde{Y}_1(q_2\beta)\right]\tilde{X}_{10}\right\}\sin\left[p\pi\,\frac{\tilde{t}^*}{T}\right]$$

APPENDIX B

REPRESENTATION OF THE FOURIER COEFFICIENTS
ASSOCIATED WITH THE INCIDENT WAVE

This appendix contains the explicit representations of the Fourier coefficients that define both the shape of the incident traveling waves and their Fourier expansion in the circumferential direction.

The coefficients a_p define the time history of the incident pulses σ_{xx} and τ_{xy} (see Fig. 2 and Sections III.1 and IV.1), and are determined from the usual expression for the Fourier constants. They are

$$a_p = \frac{2}{T} \int_0^T \sigma_{xx} \sin \omega_p t \, dt \qquad (B.1)$$

in the case of an incident dilatational pulse, and

$$a_p = \frac{2}{T} \int_0^T \tau_{xy} \sin \omega_p t \, dt \qquad (B.2)$$

in the case of an incident distortional pulse.

Since a_p defines the shape of the pulse, identical values of a_p will be obtained in both cases if the shapes of the incoming pulses are identical.

Referring to Fig. 2a for the time histories and associated parameters of the rectangular, triangular, and linear rise-exponential decay pulses, we obtain after integrating (B.1) or (B.2):

147

Rectangular Pulse

$$a_p = \begin{cases} 0 & , \quad p \quad \text{even} \\[2ex] \dfrac{4\sigma_p}{p\pi} \sin\left(\dfrac{p\pi}{2}\right) \sin\left[\dfrac{p\pi}{2}\left(\dfrac{c_m\Delta}{2b}\right) \Big/ \dfrac{c_m T}{2b}\right] & , \quad p \quad \text{odd} \end{cases} \tag{B.3}$$

where c_m is the speed of propagation of dilatational waves when (B.1) is being calculated; and c_m is the speed of propagation of shear waves when (B.2) is being calculated; σ_p is the Lanczos factor discussed previously in Section VI.2.

In this case, any two of the following parameters may be selected arbitrarily: $\left(\dfrac{c_m\Delta}{2b}\right)$, $\left(\dfrac{c_m T}{2b}\right)$, $\left(\dfrac{c_m t_0}{b}\right)$. The remaining one is determined by the relation

$$\frac{c_m T}{2b} = \frac{c_m t_0}{b} + \frac{c_m\left(\frac{k}{\alpha}\right)}{b} \tag{B.4}$$

Triangular Wave

$$a_p = \frac{4\left(\dfrac{c_m T}{2b}\right)}{(p\pi)^2 \left[\dfrac{c_m(t_1-t_0)}{b}\right]} \left[\left(1 + \frac{1}{k}\right) \sin\left\{ \frac{p\pi}{2\left(\dfrac{c_m T}{2b}\right)} \left[\frac{c_m(t_1-t_0)}{b} + \frac{c_m t_0}{b} \right] \right\} \right.$$

$$\left. - \sin\left[\frac{p\pi}{2\left(\dfrac{c_m T}{2b}\right)} \frac{c_m t_0}{b} \right] - \frac{1}{k} \sin\left\{ \frac{p\pi}{2\left(\dfrac{c_m T}{2b}\right)} \left[(k+1) \frac{c_m(t_1-t_0)}{b} + \frac{c_m t_0}{b} \right] \right\} \right] \tag{B.5}$$

148

where the parameters k and $\dfrac{c_m(t_1 - t_0)}{b}$ will, in general be pre-scribed input, and only _one_ of the _two_ parameters $\dfrac{c_m T}{2b}$, $\dfrac{c_m t_0}{b}$ may be chosen arbitrarily, the other being determined by the relation

$$\frac{c_m T}{2b} = \frac{(k+1)}{2}\frac{c_m(t_1 - t_0)}{b} + \left(\frac{c_m t_0}{b}\right) \ . \tag{B.6}$$

Linear Rise-Exponential Decay

$$
\begin{aligned}
a_p = \ & \frac{4\left(\frac{c_m T}{2b}\right)}{(p\pi)^2 \left[\frac{c_m(t_1 - t_0)}{b}\right]} \left[\sin \frac{1}{2}\left[p\pi\left(\frac{c_m t_1}{b}\right) \Big/ \left(\frac{c_m T}{2b}\right)\right]\right. \\[2ex]
& - \sin \frac{1}{2}\left[p\pi\left(\frac{c_m t_0}{b}\right) \Big/ \left(\frac{c_m T}{2b}\right)\right]\Big] \\[2ex]
& - \frac{2}{p\pi}\cos \frac{1}{2}\left[p\pi\left(\frac{c_m t_1}{b}\right) \Big/ \left(\frac{c_m T}{2b}\right)\right] \\[2ex]
& - \frac{2\,e^{-k}}{(\alpha T)^2 + (p\pi)^2}(-1)^p \\[2ex]
& + \frac{2}{(\alpha T)^2 + (p\pi)^2}\left[\alpha T \sin \frac{1}{2}\left[p\pi\left(\frac{c_m t_1}{b}\right) \Big/ \left(\frac{c_m T}{2b}\right)\right]\right. \\[2ex]
& + p\pi \cos \frac{1}{2}\left[p\pi\left(\frac{c_m t_1}{b}\right) \Big/ \left(\frac{c_m T}{2b}\right)\right]\Big] \ ,
\end{aligned} \tag{B.7}
$$

where

$$\alpha T = \frac{k}{\left[1 - \frac{1}{2}\left(\frac{c_m t_1}{b} \Big/ \frac{c_m T}{2b}\right)\right]}$$

$$\frac{c_m t_1}{b} = \frac{c_m(t_1 - t_0)}{b} + \frac{c_m t_0}{b} \ ,$$

149

where the parameters α and $\dfrac{c_m(t_1-t_0)}{b}$ will, in general, be prescribed input; the parameter k is selected so that in the time interval considered, the incident stress will have decayed to a small value (i.e., $e^{-k} \ll 1$); and only one of the two parameters $\dfrac{c_m T}{b}$, $\dfrac{c_m t_0}{b}$ may be chosen arbitrarily, the other being determined by the relation

$$\frac{c_m T}{b} = \frac{c_m t_0}{b} + \frac{c_m(t_1-t_0)}{b} + \frac{c_m(\frac{k}{\alpha})}{b} . \qquad (B.8)$$

The coefficients defining the circumferential expansion, in Fourier series, of the incident pulses will be discussed now. As indicated in Sections III.1, III.6, and IV.2, it is possible to obtain representations of these coefficients in terms of Bessel functions of a complex argument.

An integral representation of the Bessel function of the first kind with complex argument is given by Ref. 22 as

$$(i)^n \pi J_n(z) = \int_0^\pi e^{iz \cos \theta} \cos n\theta\, d\theta , \qquad (n = 0, 1, 2, \ldots) . \quad (B.9)$$

Employing the trigonometric identities

$$\cos r\theta \cos s\theta = \frac{1}{2}\ [\cos(r+s)\theta + \cos(r-s)\theta]$$

$$\sin r\theta \sin s\theta = -\frac{1}{2}\ [\cos(r+s)\theta - \cos(r-s)\theta]$$

in conjunction with (B.9), we are led to the following representation for the Fourier coefficients defined by Eqs. (3.6.4), (3.6.7):

$$A_{pn} = -\ (i)^{n+1}\ e^{-iq_3}\left\{(1+\epsilon)J_n(q_3) - \left(\frac{1-\epsilon}{2}\right)\left[J_{n+2}(q_3) + J_{n-2}(q_3)\right]\right\}$$

$$(B.10a)$$

$$A_{p0} = \frac{(-1)}{2} e^{-iq_3}\left[(1+\epsilon)J_0(q_3) - (1-\epsilon)J_2(q_3)\right] \qquad \text{(B.10b)}$$

$$B_{pn} = (1)^{n+1} e^{-iq_3}\left(\frac{1-\epsilon}{2}\right)\left[J_{n+2}(q_3) - J_{n-2}(q_3)\right] \qquad \text{(B.10c)}$$

$$C_{pn} = (1)^{n+1} e^{-iq_3}\left(\frac{c_{dm}q_3}{\omega_p b}\right)\left[J_{n+1}(q_3) - J_{n-1}(q_3)\right] \qquad \text{(B.10d)}$$

$$C_{p0} = (1) e^{-iq_3}\left(\frac{c_{dm}q_3}{\omega_p b}\right)J_1(q_3) \qquad \text{(B.10e)}$$

$$D_{pn} = (1)^{n+1} e^{-iq_3}\left(\frac{c_{dm}q_3}{\omega_p b}\right)\left[J_{n+1}(q_3) + J_{n-1}(q_3)\right] \qquad \text{(B.10f)}$$

The preceding coefficients are of course complex. For use on the right-hand side of the equivalent real matrix equations discussed in Appendix A, we separate (B.10) into real and imaginary parts (denoted by superscripts R and I, respectively). Thus, recalling the definitions of the complex quantities, q_3 and ϵ [Eqs. (3.4.16) and (3.4.18)], and with the other barred quantities defined subsequently, we obtain

$$A_{pn}^R = e^{-\tilde{q}_3}\left[\bar{A}_{pn}^R \cos \bar{q}_3 + \bar{A}_{pn}^I \sin \bar{q}_3\right]$$

$$A_{pn}^I = e^{-\tilde{q}_3}\left[\bar{A}_{pn}^I \cos \bar{q}_3 - \bar{A}_{pn}^R \sin \bar{q}_3\right]$$

$$B_{pn}^R = e^{-\tilde{q}_3}\left[\bar{B}_{pn}^R \cos \bar{q}_3 + \bar{B}_{pn}^I \sin \bar{q}_3\right]$$

$$B_{pn}^I = e^{-\tilde{q}_3}\left[\bar{B}_{pn}^I \cos \bar{q}_3 - \bar{B}_{pn}^R \sin \bar{q}_3\right]$$

$$\text{(B.11)}$$

$$C_{pn}^R = e^{-\tilde{q}_3}\left[\bar{C}_{pn}^R \cos \bar{q}_3 + \bar{C}_{pn}^I \sin \bar{q}_3\right]$$

$$C_{pn}^I = e^{-\tilde{q}_3}\left[\bar{C}_{pn}^I \cos \bar{q}_3 - \bar{C}_{pn}^R \sin \bar{q}_3\right]$$

$$D_{pn}^R = e^{-\tilde{q}_3}\left[\bar{D}_{pn}^R \cos \bar{q}_3 + \bar{D}_{pn}^I \sin \bar{q}_3\right]$$

$$D_{pn}^I = e^{-\tilde{q}_3}\left[\bar{D}_{pn}^I \cos \bar{q}_3 - \bar{D}_{pn}^R \sin \bar{q}_3\right],$$

where

$$\bar{A}_{pn}^R = \frac{1}{\pi}\left[\tilde{\epsilon}(\bar{I}_n - \bar{I}_{n2}^c) + (1+\bar{\epsilon})\tilde{I}_n + (1-\bar{\epsilon})\tilde{I}_{n2}^c\right]$$

$$\bar{A}_{pn}^I = \frac{1}{\pi}\left[\tilde{\epsilon}(\tilde{I}_n - \tilde{I}_{n2}^c) - (1+\bar{\epsilon})\bar{I}_n - (1-\bar{\epsilon})\bar{I}_{n2}^c\right]$$

$$\bar{A}_{p0}^R = \frac{1}{2}\left\{\tilde{\epsilon}\left[J_0^R(q_3) + J_2^R(q_3)\right] + (1+\bar{\epsilon})J_0^I(q_3) - (1-\bar{\epsilon})J_2^I(q_3)\right\}$$

$$\bar{A}_{p0}^I = \frac{1}{2}\left\{\tilde{\epsilon}\left[J_0^I(q_3) + J_2^I(q_3)\right] - (1+\bar{\epsilon})J_0^R(q_3) + (1-\bar{\epsilon})J_2^R(q_3)\right\}$$

$$\bar{B}_{pn}^R = \frac{1}{\pi}\left[\tilde{\epsilon}\bar{I}_{n2}^s - (1-\bar{\epsilon})\tilde{I}_{n2}^s\right]$$

$$\bar{B}_{pn}^I = \frac{1}{\pi}\left[\tilde{\epsilon}\tilde{I}_{n2}^s + (1-\bar{\epsilon})\bar{I}_{n2}^s\right]$$

$$\bar{C}_{pn}^R = \frac{2}{\pi}\frac{c_{dm}}{\omega_p b}\left[\bar{q}_3\bar{I}_{n1}^c + \tilde{q}_3\tilde{I}_{n1}^c\right] \qquad\qquad \text{(B.12)}$$

$$\bar{C}_{pn}^I = \frac{2}{\pi}\frac{c_{dm}}{\omega_p b}\left[\bar{q}_3\tilde{I}_{n1}^c - \tilde{q}_3\bar{I}_{n1}^c\right]$$

$$\bar{C}_{p0}^R = -\frac{c_{dm}}{\omega_p b}\left[\bar{q}_3 J_1^I(q_3) - \tilde{q}_3 J_1^R(q_3)\right]$$

$$\bar{C}_{p0}^I = \frac{c_{dm}}{\omega_p b}\left[\bar{q}_3 J_1^R(q_3) + \tilde{q}_3 J_1^I(q_3)\right]$$

$$\bar{D}_{pn}^R = -\frac{2}{\pi}\frac{c_{dm}}{\omega_p b}\left[\bar{q}_3\bar{I}_{n1}^s + \tilde{q}_3\tilde{I}_{n1}^s\right]$$

$$\bar{D}_{pn}^I = -\frac{2}{\pi}\frac{c_{dm}}{\omega_p b}\left[\bar{q}_3\tilde{I}_{n1}^s - \tilde{q}_3\bar{I}_{n1}^s\right] \, ,$$

where

$$\left(\frac{c_{dm}}{\omega_p b}\right) - \frac{2}{p\pi}\left(\frac{c_{dm}T}{2b}\right) \, ,$$

and, when n is an even integer,

$$\bar{I}_n = (-1)^{n/2} \, \pi\left[J_n^R(q_3)\right]$$

$$\tilde{I}_n = (-1)^{n/2} \, \pi\left[J_n^I(q_3)\right]$$

$$\bar{I}_{n1}^c = -(-1)^{n/2} \, \frac{\pi}{2}\left[J_{n+1}^I(q_3) - J_{n-1}^I(q_3)\right]$$

$$\tilde{I}_{n1}^c = (-1)^{n/2} \, \frac{\pi}{2}\left[J_{n+1}^R(q_3) - J_{n-1}^R(q_3)\right]$$

$$\bar{I}_{n1}^s = (-1)^{n/2} \, \frac{\pi}{2}\left[J_{n+1}^I(q_3) + J_{n-1}^I(q_3)\right]$$

$$\tilde{I}_{n1}^s = -(-1)^{n/2} \, \frac{\pi}{2}\left[J_{n+1}^R(q_3) + J_{n-1}^R(q_3)\right]$$

$$\bar{I}_{n2}^c = -(-1)^{n/2} \, \frac{\pi}{2}\left[J_{n+2}^R(q_3) + J_{n-2}^R(q_3)\right]$$

$$\tilde{I}_{n2}^c = -(-1)^{n/2} \, \frac{\pi}{2}\left[J_{n+2}^I(q_3) + J_{n-2}^I(q_3)\right]$$

$$\bar{I}_{n2}^s = (-1)^{n/2} \, \frac{\pi}{2}\left[J_{n+2}^R(q_3) - J_{n-2}^R(q_3)\right]$$

$$\tilde{I}_{n2}^s = (-1)^{n/2} \, \frac{\pi}{2}\left[J_{n+2}^I(q_3) - J_{n-2}^I(q_3)\right] \; ;$$

(B.13)

153

whereas, when n is an odd integer,

$$\overline{I}_n = - (-1)^{\frac{n-1}{2}} \pi \left[J_n^I(q_3) \right]$$

$$\widetilde{I}_n = (-1)^{\frac{n-1}{2}} \pi \left[J_n^R(q_3) \right]$$

$$\overline{I}_{n1}^c = (-1)^{\frac{n+1}{2}} \frac{\pi}{2} \left[J_{n+1}^R(q_3) - J_{n-1}^R(q_3) \right]$$

$$\widetilde{I}_{n1}^c = (-1)^{\frac{n+1}{2}} \frac{\pi}{2} \left[J_{n+1}^I(q_3) - J_{n-1}^I(q_3) \right]$$

$$\overline{I}_{n1}^s = - (-1)^{\frac{n+1}{2}} \frac{\pi}{2} \left[J_{n+1}^R(q_3) + J_{n-1}^R(q_3) \right]$$

$$\widetilde{I}_{n1}^s = - (-1)^{\frac{n+1}{2}} \frac{\pi}{2} \left[J_{n+1}^I(q_3) + J_{n-1}^I(q_3) \right]$$

$$\overline{I}_{n2}^c = - (-1)^{\frac{n+1}{2}} \frac{\pi}{2} \left[J_{n+2}^I(q_3) + J_{n-2}^I(q_3) \right]$$

$$\widetilde{I}_{n2}^c = (-1)^{\frac{n+1}{2}} \frac{\pi}{2} \left[J_{n+2}^R(q_3) + J_{n-2}^R(q_3) \right]$$

$$\overline{I}_{n2}^s = (-1)^{\frac{n+1}{2}} \frac{\pi}{2} \left[J_{n+2}^I(q_3) - J_{n-2}^I(q_3) \right]$$

$$\widetilde{I}_{n2}^s = - (-1)^{\frac{n+1}{2}} \frac{\pi}{2} \left[J_{n+2}^R(q_3) - J_{n-2}^R(q_3) \right] .$$

The coefficients defining the circumferential expansion, in Fourier series, of the stresses and displacements associated with the incident shear wave, are given by Eqs. (4.2.16) and (4.2.19). In a manner similar to that employed in the case of the incident dilatational wave, these coefficients are shown to be representable in terms of Bessel functions of a complex argument. Employing Eq. (B.9), and the trigonometric identities written immediately below it, we are led to the following representation for the coefficients defined by Eqs. (4.2.16) and (4.2.19):

$$A_{pn} = - (i)^{n+1} e^{-iq_4} \left[J_{n+2}(q_4) - J_{n-2}(q_4) \right] \tag{B.15a}$$

$$B_{pn} = (i)^{n+1} e^{-iq_4} \left[J_{n+2}(q_4) + J_{n-2}(q_4) \right] \tag{B.15b}$$

$$B_{p0} = i e^{-iq_4} \left[J_2(q_4) \right] \tag{B.15c}$$

$$C_{pn} = - \left(\frac{c_{tm}}{\omega_p b} \right) q_4 e^{-iq_4} (i)^{n+1} \left[J_{n+1}(q_4) + J_{n-1}(q_4) \right] \tag{B.15d}$$

$$D_{pn} = \left(\frac{c_{tm}}{\omega_p b} \right) q_4 e^{-iq_4} (i)^{n+1} \left[J_{n+1}(q_4) - J_{n-1}(q_4) \right] \tag{B.15e}$$

$$D_{p0} = i \left(\frac{c_{tm}}{\omega_p b} \right) q_4 e^{-iq_4} \left[J_1(q_4) \right] , \tag{B.15f}$$

where it is noted that the above coefficients, A_{pn}, B_{pn}, ..., D_{p0}, associated with an incident wave of distortion are defined differently from the corresponding coefficients, Eq. (B.11), associated with an incident wave of dilatation.

As in the case of the coefficients corresponding to the incident shear wave, we separate the above complex coefficients into real and imaginary parts denoted by superscripts R and I, respectively. Recalling the definition of q_4 [Eq. (3.4.16b)], and with the other barred quantities defined subsequently, we obtain expressions similar to those given by Eq. (B.11):

155

$$A_{pn}^{R} = e^{-\tilde{q}_4} \left[\bar{A}_{pn}^{R} \cos \bar{q}_4 + \bar{A}_{pn}^{I} \sin \bar{q}_4 \right]$$

$$A_{pn}^{I} = e^{-\tilde{q}_4} \left[\bar{A}_{pn}^{I} \cos \bar{q}_4 - \bar{A}_{pn}^{R} \sin \bar{q}_4 \right]$$

$$B_{pn}^{R} = e^{-\tilde{q}_4} \left[\bar{B}_{pn}^{R} \cos \bar{q}_4 + \bar{B}_{pn}^{I} \sin \bar{q}_4 \right]$$

$$B_{pn}^{I} = e^{-\tilde{q}_4} \left[\bar{B}_{pn}^{I} \cos \bar{q}_4 - \bar{B}_{pn}^{R} \sin \bar{q}_4 \right]$$

(B.16)

$$C_{pn}^{R} = e^{-\tilde{q}_4} \left[\bar{C}_{pn}^{R} \cos \bar{q}_4 + \bar{C}_{pn}^{I} \sin \bar{q}_4 \right]$$

$$C_{pn}^{I} = e^{-\tilde{q}_4} \left[\bar{C}_{pn}^{I} \cos \bar{q}_4 - \bar{C}_{pn}^{R} \sin \bar{q}_4 \right]$$

$$D_{pn}^{R} = e^{-\tilde{q}_4} \left[\bar{D}_{pn}^{R} \cos \bar{q}_4 + \bar{D}_{pn}^{I} \sin \bar{q}_4 \right]$$

$$D_{pn}^{I} = e^{-\tilde{q}_4} \left[\bar{D}_{pn}^{I} \cos \bar{q}_4 - \bar{D}_{pn}^{R} \sin \bar{q}_4 \right] ,$$

with, in this case,

$$\bar{A}^{\circ}_{pn} = \frac{2}{\pi} \tilde{I}^{\circ}_{n2}$$

$$\bar{A}^{I}_{pn} = - \frac{2}{\pi} \bar{I}^{s}_{n2}$$

$$\bar{B}^{R}_{pn} = \frac{2}{\pi} \tilde{I}^{c}_{n2}$$

$$\bar{B}^{I}_{pn} = - \frac{2}{\pi} \bar{I}^{c}_{n2}$$

$$\bar{B}^{R}_{p0} = - J^{I}_{2}(q_4)$$

$$\bar{B}^{I}_{p0} = J^{R}_{2}(q_4)$$

$$\bar{C}^{R}_{pn} = \frac{2}{\pi} \left(\frac{c_{tm}}{\omega_p b}\right) \left[\bar{q}_4 \, \bar{I}^{s}_{n1} + \tilde{q}_4 \, \tilde{I}^{s}_{n1}\right]$$

$$\bar{C}^{I}_{pn} = \frac{2}{\pi} \left(\frac{c_{tm}}{\omega_p b}\right) \left[\bar{q}_4 \, \tilde{I}^{s}_{n1} - \tilde{q}_4 \, \bar{I}^{s}_{n1}\right]$$

$$\bar{D}^{R}_{pn} = \frac{2}{\pi} \left(\frac{c_{tm}}{\omega_p b}\right) \left[\bar{q}_4 \, \bar{I}^{c}_{n1} + \tilde{q}_4 \, \tilde{I}^{c}_{n1}\right]$$

$$\bar{D}^{I}_{pn} = \frac{2}{\pi} \left(\frac{c_{tm}}{\omega_p b}\right) \left[\bar{q}_4 \, \tilde{I}^{c}_{n1} - \tilde{q}_4 \, \bar{I}^{c}_{n1}\right]$$

$$\bar{D}^{R}_{p0} = - \left(\frac{c_{tm}}{\omega_p b}\right) \left[\bar{q}_4 \, J^{I}_{1}(q_4) - \tilde{q}_4 \, J^{R}_{1}(q_4)\right]$$

$$\bar{D}^{I}_{p0} = \left(\frac{c_{tm}}{\omega_p b}\right) \left[\bar{q}_4 \, J^{R}_{1}(q_4) + \tilde{q}_4 \, J^{I}_{1}(q_4)\right] ,$$

(B.17)

where the barred and tilde quantities, I^{s}_{n2}, I^{c}_{n2}, I^{c}_{n1}, are functions defined by Eqs. (B.13) and (B.14), with argument q_3 replaced by q_4.

157

DOCUMENT CONTROL DATA - R&D

(Security classification of title, body of abstract and indexing annotation must be entered when the overall report is classified)

1. ORIGINATING ACTIVITY *(Corporate author)*	2a. REPORT SECURITY CLASSIFICATION
Grumman Aircraft Engineering Corporation Bethpage, N. Y.	Unclassified
	2b. GROUP

3. REPORT TITLE

DYNAMIC STRESSES IN A THICK ELASTIC CYLINDER SUBJECT TO TRANSIENT PRESSURE LOADINGS
Volume I: Theoretical Analysis and Discussion of Results

4. DESCRIPTIVE NOTES *(Type of report and inclusive dates)*

1 June 1963 through 16 March 1965.

5. AUTHOR(S) *(Last name, first name, initial)*

Garnet, Hyman; Crouzet-Pascal, Jacques; Isakson, Gabriel; and Pifko, Allan.

6. REPORT DATE	7a. TOTAL NO. OF PAGES	7b. NO. OF REFS
September 1965	180	22

8a. CONTRACT OR GRANT NO. AF 29(601)-5993	9a. ORIGINATOR'S REPORT NUMBER(S)
b. PROJECT NO. 5710	AFWL-TR-65-20, Vol. I.
c. Subtask 13.148	9b. OTHER REPORT NO(S) *(Any other numbers that may be assigned this report)*
d.	

10. AVAILABILITY/LIMITATION NOTICES

Qualified users may obtain copies of this report from DDC.
Distribution is limited because of the technology discussed in this report.

11. SUPPLEMENTARY NOTES	12. SPONSORING MILITARY ACTIVITY
	Air Force Weapons Laboratory (WLDC) Kirtland Air Force Base, New Mexico

13. ABSTRACT

The response of a hollow circular cylindrical shell of arbitrary thickness, in either an elastic or a viscoelastic medium, to transient dilatational and shear waves (and their superposition) is presented. The solution is valid within the scope of the linear theory of elasticity or viscoelasticity. The technique for obtaining the solution relies upon 1) the construction of a train of incident pulses from steady-state components, where each pulse represents the time history of the transient stress in the incident wave, and 2) the existence of a physical mechanism that, between pulses, restores the disturbed particles of the cylinder and the surrounding medium to an unstrained state of rest.

The influence on the cylinder response of the following factors is discussed: liner thickness, cylinder-medium impedance mismatch, viscoelasticity in the medium, and incident wave form (step pulse, rectangular, triangular, linear rise-exponential decay).

DD FORM 1473

14 KEY WORDS	LINK A		LINK B		LINK C	
	ROLE	WT	ROLE	WT	ROLE	WT
Hollow circular cylindrical shell of arbitrary thickness						
Elastic and viscoelastic medium						
Transient dilatational and shear waves						
Liner displacements and stresses						
Underground structures - effects of blast						

INSTRUCTIONS

1. ORIGINATING ACTIVITY: Enter the name and address of the contractor, subcontractor, grantee, Department of Defense activity or other organization (corporate author) issuing the report.

2a. REPORT SECURITY CLASSIFICATION: Enter the overall security classification of the report. Indicate whether "Restricted Data" is included. Marking is to be in accordance with appropriate security regulations.

2b. GROUP: Automatic downgrading is specified in DoD Directive 5200.10 and Armed Forces Industrial Manual. Enter the group number. Also, when applicable, show that optional markings have been used for Group 3 and Group 4 as authorized.

3. REPORT TITLE: Enter the complete report title in all capital letters. Titles in all cases should be unclassified. If a meaningful title cannot be selected without classification, show title classification in all capitals in parenthesis immediately following the title.

4. DESCRIPTIVE NOTES: If appropriate, enter the type of report, e.g., interim, progress, summary, annual, or final. Give the inclusive dates when a specific reporting period is covered.

5. AUTHOR(S): Enter the name(s) of author(s) as shown on or in the report. Enter last name, first name, middle initial. If military, show rank and branch of service. The name of the principal author is an absolute minimum requirement.

6. REPORT DATE: Enter the date of the report as day, month, year; or month, year. If more than one date appears on the report, use date of publication.

7a. TOTAL NUMBER OF PAGES: The total page count should follow normal pagination procedures, i.e., enter the number of pages containing information.

7b. NUMBER OF REFERENCES: Enter the total number of references cited in the report.

8a. CONTRACT OR GRANT NUMBER: If appropriate, enter the applicable number of the contract or grant under which the report was written.

8b, 8c, & 8d. PROJECT NUMBER: Enter the appropriate military department identification, such as project number, subproject number, system numbers, task number, etc.

9a. ORIGINATOR'S REPORT NUMBER(S): Enter the official report number by which the document will be identified and controlled by the originating activity. This number must be unique to this report.

9b. OTHER REPORT NUMBER(S): If the report has been assigned any other report numbers (either by the originator or by the sponsor), also enter this number(s).

10. AVAILABILITY/LIMITATION NOTICES: Enter any limitations on further dissemination of the report, other than those

imposed by security classification, using standard statements such as:

(1) "Qualified requesters may obtain copies of this report from DDC."

(2) "Foreign announcement and dissemination of this report by DDC is not authorized."

(3) "U. S. Government agencies may obtain copies of this report directly from DDC. Other qualified DDC users shall request through

_____ ."

(4) "U. S. military agencies may obtain copies of this report directly from DDC. Other qualified users shall request through

_____ ."

(5) "All distribution of this report is controlled. Qualified DDC users shall request through

_____ ."

If the report has been furnished to the Office of Technical Services, Department of Commerce, for sale to the public, indicate this fact and enter the price, if known.

11. SUPPLEMENTARY NOTES: Use for additional explanatory notes.

12. SPONSORING MILITARY ACTIVITY: Enter the name of the departmental project office or laboratory sponsoring (paying for) the research and development. Include address.

13. ABSTRACT: Enter an abstract giving a brief and factual summary of the document indicative of the report, even though it may also appear elsewhere in the body of the technical report. If additional space is required, a continuation sheet shall be attached.

It is highly desirable that the abstract of classified reports be unclassified. Each paragraph of the abstract shall end with an indication of the military security classification of the information in the paragraph, represented as (TS), (S), (C), or (U)

There is no limitation on the length of the abstract. However, the suggested length is from 150 to 225 words.

14. KEY WORDS: Key words are technically meaningful terms or short phrases that characterize a report and may be used as index entries for cataloging the report. Key words must be selected so that no security classification is required. Identifiers, such as equipment model designation, trade name, military project code name, geographic location, may be used as key words but will be followed by an indication of technical context. The assignment of links, rules, and weights is optional.